
HYDRAULIC JUMPS IN TURBIDITY CURRENTS – FLUME EXPERIMENTS

*On the influence of sediment concentration and grain size
on flow dynamics and deposits in 1-phase and 2 phase turbidity currents
with and without occurrence of the hydraulic jump*

Jeffrey J. Walet

MSc thesis
August 2012

Contact: j.walet@gmail.com

Utrecht University, Faculty of Geosciences
Supervision: Dr. George Postma, Matthieu Cartigny

ABSTRACT

The focus of this innovative research is on the effects of grain size and various sediment concentrations on flow dynamics, hydraulic jump characteristics and sediment deposition of experimental turbidity currents. Of special interest is the origin of structureless graded sand beds (Bouma's Ta), supposed to be the result of an internal hydraulic jump of the high density traction carpet in a 2-phase turbidity current. In this experimental study turbidity currents of different sediment concentration and sediment grain size are created and observed in a flume at the Eurotank laboratory facility at Utrecht University. A hydraulic jump is triggered and flow dynamics and resultant deposits are analyzed. Froude numbers are calculated for 1-phase flows and partial Froude numbers for the bottom layer of 2-phase flows, to determine whether a hydraulic jump occurred. Interpretation of flow dynamics suggested the occurrence of hydraulic jumps, however measurements appeared inadequate to produce reliable Fr' numbers to support this observation. The supposed hydraulic jump did not produce structureless sand beds; deposits observed were plane bed lamination and low shear lamination (Bouma's Tb and Td, respectively).

ACKNOWLEDGEMENTS

I would like to thank George Postma for his supervision. The opportunity to perform turbidity current experiments in the Eurotank flume in combination with complementary field research on turbidite deposits in the Tabernas Basin in Spain (documented in a different report) is highly appreciated.

I would like to thank Matthieu Cartigny for his supervision, insightful discussions and help with the experiments.

I would like to thank Joris Eggenhuisen for his insightful discussions.

I would like to thank Joost Mulder for his help with the experiments, his insightful discussions and pleasant collaboration in the Eurotank facility.

I would like to thank Jochem Bijkerk en Jan de Vries their help with the experiments and insightful discussions.

I would like to thank Arie van Wettum for providing to this research his data logger and support.

I would like to thank Tony van der Gon Netcher for his help constructing and repairing the experiment setup in the Eurotank.

I would like to thank Henk van der Meer for his technical support in the Eurotank.

I would like to thank Lesley Walet for her textual suggestions to improve the readability of this thesis.

TABLE OF CONTENTS

Abstract.....	2
Acknowledgements.....	3
Table of contents.....	4
Introduction.....	7
Theoretical framework.....	9
Turbidity currents.....	9
Hydraulic jump and Froude number.....	9
Hydraulic jump at slope transition.....	10
Gravity transformation.....	10
Suspension fall-out.....	11
Traction carpets.....	11
1-phase and 2-phase turbidity currents.....	11
Deposition by turbidity currents.....	11
Depositional context and facies of the Bouma Ta unit.....	13
Methodology.....	15
Experimental setup – sediment supply.....	15
Experimental setup – flume.....	16
Experiments – test phase.....	16
Experiments – successful experiments.....	17
Measurements – grain sizes.....	17
Measurements – particle concentration.....	17
Measurements – imagery.....	17
Measurements – flow velocity.....	18
Measurements – data logger.....	18
Results.....	19
Description of the flow dynamics of each run.....	21
Backflow.....	21
Detachment zone (DZ).....	22
Hydraulic jump / rapidly upstream moving detachment zone.....	22
Overview of phenomena occurring in the runs.....	24
Low concentration runs.....	25
Run 1: Average concentration 4.7% and grain size (d_{50}) 120 μ	26
Run 2: Average concentration 6.7% and grain size (d_{50}) 120 μ	28
Run 6: Average concentration 4.4% and grain size (d_{50}) 313 μ	30
Run 7: Average concentration 7% and grain size (d_{50}) 313 μ	31

Run 11: Average concentration 5% and grain size (d_{50}) 570 μ	33
High concentration runs.....	36
Run 3: Average concentration 16.8% and grain size (d_{50}) 120 μ	37
Run 4: Average concentration 16.8% and grain size (d_{50}) 120 μ	41
Run 5: Average concentration 21.6% and grain size (d_{50}) 120 μ	43
Run 8: Average concentration 12.9% and grain size (d_{50}) 313 μ	46
Run 9: Average concentration 15% and grain size (d_{50}) 313 μ	47
Run 10: Average concentration 22.1% and grain size (d_{50}) 313 μ	49
Run 12: Average concentration 28.5% and grain size (d_{50}) 570 μ	50
Discussion	52
What influence does sediment concentration have on flow dynamics and deposits?	53
Low concentration runs.....	53
High concentration runs.....	54
Concentration profiles.....	54
What influence does grain size have on flow dynamics and deposits?.....	56
Influence of grain size in low concentration runs.....	56
Influence of grain size in high concentration runs	56
Which runs display a hydraulic jump?	57
Flow velocity measurements and corrections	57
Calculation of overall Froude numbers.....	61
Calculation of partial Fr' numbers.....	62
Which deposits can be related to the hydraulic jump?.....	66
Bedforms.....	66
Grain fabric.....	69
Limitation of the experiments and further research.....	70
Challenges with concentration and concentration measurement.....	70
Concentration measurement – Temperature bias.....	71
Concentration measurement – Conductivity influencing particles	71
Concentration measurement - Zero measurement.....	71
Conclusions.....	72
What are the effects of grain size and various sediment concentrations on flow dynamics, hydraulic jump characteristics and sediment deposition?	72
Flow dynamics.....	72
Hydraulic jump characteristics.....	72
Sediment deposition	72
References.....	74
Appendices	77
Appendix A1: Run 1, exp1_ : Measured data.....	77

Appendix A2: Run 2, exp4: Measured data.....	78
Appendix A3: Run 3, exp2_: Measured data.....	79
Appendix A4: Run 4, exp3: Measured data.....	80
Appendix A5: Run 5, exp5: Measured data.....	81
Appendix A6: Run 6, exp11: Measured data.....	82
Appendix A7: Run 7, exp9_: Measured data.....	83
Appendix A8: Run 8, exp7: Measured data.....	84
Appendix A9: Run 9, exp10: Measured data.....	85
Appendix A10: Run 10, exp8: Measured data.....	86
Appendix A11: Run 11, exp13: Measured data.....	87
Appendix A12: Run12, exp12: Measured data.....	88
Appendix B: MATLAB script for data retrieval and presentation.....	89

INTRODUCTION

Turbidity currents are sediment gravity currents, a class of flows in which there is movement because of differences in density between two fluids. The higher density in the turbidity currents of this research is created by sediment in suspension. Turbidity currents can flow in two states, supercritical or subcritical, influenced by flow velocity, flow height and density of the flow. When supercritical flow changes to subcritical flow, it goes through a hydraulic jump, after which the flow velocity is lower and flow height is larger. At the location of a hydraulic jump a large amount of energy is dissipated. The occurrence of a hydraulic jump is expected to leave an expression in the sediments.

The formation processes of coarse-tail graded structureless sand beds in turbidity current deposits (turbidites) are not yet clearly understood. The facies of these turbidite sand beds seem to be indicative of a low shear and low flow velocity depositional environment. Their position within contemporary models of turbidite sedimentation however, would suggest a high energy, high shear and high flow velocity depositional environment. Recent new insights suggest that internal hydraulic jumps of traction carpets within high density 2-phase turbidity currents could be responsible for the formation of these sand beds.

In order to examine this further, in this experimental study I attempt to create hydraulic jumps in 1-phase and 2-phase turbidity currents in a flume. I create turbidity currents with particle concentrations between 4.4% and 28.5% of volume and sediment grain sizes from 120 μm to 570 μm . Sediment-water mixtures are fed into a rectangular channel with gradually decreasing slope and the flows are forced to go through a hydraulic jump using a weir or dam in the flow. This experimental setup enables the investigation of the effects of grain size and various sediment concentrations on sediment deposition, flow dynamics and hydraulic jump characteristics.

The focus of this research is on the effects of grain size and various sediment concentrations on flow dynamics, hydraulic jump characteristics and sediment deposition. I expect these variables to have a considerable effect in the experiments. Since the hydraulic jump is the transition from supercritical to subcritical flow, I expect to see deposits resulting from both super- and subcritical flow, as well as hydraulic jump effects.

Insights in the structure and fabric of turbidity current deposits (turbidites) are of key importance in understanding their reservoir characteristics for hydrocarbon exploration. I hope the results of this thesis will add to the understanding of turbidite deposit characteristics at locations where a hydraulic jump is expected, such as canyon-fan transitions.

My main research question is: What are the effects of grain size and various sediment concentrations on flow dynamics, hydraulic jump characteristics and sediment deposition?

In order to interpret the experiments I measure flow velocity, sediment concentration and grain sizes of the input mixture. Froude numbers are calculated where possible to investigate the criticality of flows and to assess whether the hydraulic jump occurred. Flow dynamics and deposition are recorded and studied via high speed cameras.

To answer the main research question, I aim to answer the following sub questions:

- What influence does sediment concentration have on flow dynamics and deposits?
- What influence does grain size have on flow dynamics and deposits?
- Which runs display a hydraulic jump?
- Which deposits can be related to the hydraulic jump?

In this thesis, I will first provide an overview of the relevant concepts and theories in the theoretical framework. Second, the methodology of the experiments will be discussed. Third, in the result section, the different experiments will be elaborated on. These will be analyzed and discussed further in the discussion section, together with the limitations and challenges of this research. Last, in the conclusion I will discuss and answer the research questions as presented above.

THEORETICAL FRAMEWORK

This section provides a succinct elaboration and definition of the concepts that are considered to be relevant for the interpretation of my results. Furthermore, the theoretical debates concerning some of these concepts are discussed. First, the following concepts are concisely defined: turbidity currents, hydraulic jump and Froude number, hydraulic jump at slope transition, gravity transformation, suspension fall-out, traction carpets and 1-phase and 2-phase turbidity currents. Then, the deposition by turbidity currents is discussed in more detail. Last, I will discuss the different theories regarding the depositional context and facies of the Bouma Ta unit, in which this research is framed.

TURBIDITY CURRENTS

Turbidity currents are sediment gravity currents, a class of flows in which there is movement because of differences in density between two fluids. I.e. turbidity currents are currents which are driven by their higher density relative to the ambient fluid. Depending on the circumstances, differences in gravitational pull may create flows below, above or in between ambient fluids (with a different density). The higher density in the turbidity currents of this research is created by sediment in suspension, creating a 'bottom-hugging' flow.

Turbidity currents can flow in two states, supercritical or subcritical, influenced by flow velocity, flow height and density of the flow. When a supercritical turbidity current changes to subcritical, the flow goes through a hydraulic jump, after which the flow velocity is lower and flow height is larger. At the location of a hydraulic jump a large amount of energy is dissipated. The occurrence of a hydraulic jump is expected to leave an expression in the sediments.

HYDRAULIC JUMP AND FROUDE NUMBER

A hydraulic jump is a zone where the flow conditions change rather abruptly. It is the transition from a supercritical high-velocity flow upstream to a low velocity subcritical flow downstream. To describe whether a flow is super- or subcritical the Froude number is used:

$$Fr = U / \sqrt{g \cdot h} \quad \text{where}$$

U = flow velocity [m/s]
g = gravitational acceleration constant 9,81 [m/s²]
h = flow height [m]

It describes whether the velocity of flow is larger (supercritical, $Fr > 1$) or smaller (subcritical, $Fr < 1$) than the internal wave propagation velocity. It can be seen as the hydrodynamic equivalent of the Mach number used for objects moving through air. Figure 1 shows a schematic overview of a flow going through the hydraulic jump.

In my experiments I need to calculate the Froude number to investigate whether flows are supercritical. This will be used to assess the occurrence of a hydraulic jump in my experiments.

For turbidity current research the densimetric Froude number is used:

$$Fr' = U / \sqrt{g' \cdot h}$$

Where

$$g' = g ((\rho_{\text{mix}} - \rho_{\text{water}}) / \rho_{\text{water}})$$

where ρ_{mix} is the density or unit weight of the sediment-water mixture and ρ_{water} is the density or unit weight of the ambient water.

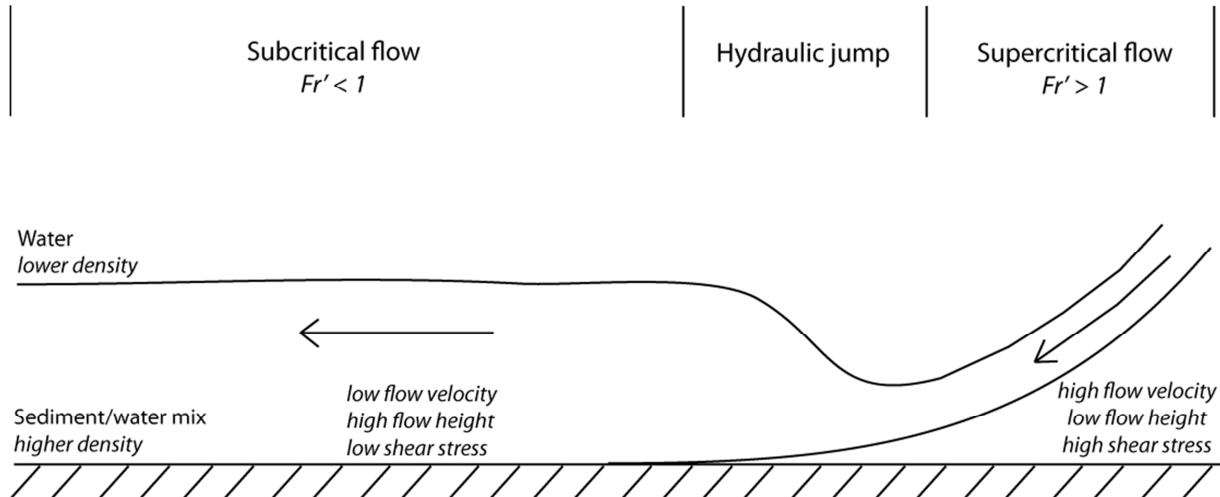


FIGURE 1: SCHEMATIC OVERVIEW OF A FLOW GOING THROUGH THE HYDRAULIC JUMP AT THE END OF A GRADUALLY DECLINING SLOPE. FLOW ENTERS IN SUPERCRITICAL STATE AT THE RIGHT HAND SIDE OF THE PICTURE.

HYDRAULIC JUMP AT SLOPE TRANSITION

In a natural environment, a location where turbidity currents occur is on the slope of submarine canyons at the edge of the continental shelf. Komar (1971) calculated that most turbidity currents in canyons are supercritical. The critical gradient is around 0.001 m/m. This implies most turbidity currents in canyons will be forced through a hydraulic jump when they decelerate as they leave the confinement of the canyon and/or when the slope is reduced. Both happen where the canyon ends and the depositional fan system begins; the canyon-fan transition.

To simulate turbidity current flow behavior near a canyon-fan transition Garcia & Parker (1989) performed experiments in a flume tank. As expected, turbidity currents flowing out of a relatively steep canyon onto a fan with a lower slope were observed to go through the hydraulic jump. This is also supported by the experiments of Garcia (1993), where hydraulic jumps at a slope transition were created with both saline and sediment laden turbidity currents. In the set of experiments in my research a gradually decreasing slope (horizontal at the end) with a weir is used to investigate the effects of deceleration of the flow.

GRAVITY TRANSFORMATION

Fisher (1983) introduced the term flow transformations for sediment gravity flows, marking changes in flow behavior between laminar and turbulent states. From the four types described in his article the gravity transformation is best suitable for interpretations in this research. Particle concentration, thickness of the flow and flow velocity influence whether gravitational segregation may take place, creating a highly concentrated lower part of the flow. Between the two parts of this flow a density interface exists, which also marks the difference in flow state (suppressed turbulence by grain-to-grain interactions or fully turbulent). The lower high density

layer is a traction carpet. This mechanism of gravity transformation enables the formation of 2-phase flows in my experiments.

SUSPENSION FALL-OUT

Lowe (1988) considers suspended-load fall-out rate as an important variable in the analysis of turbidity currents. He argues that turbidity currents with high concentrations will probably not derive their bedload layer concentration from erosion of the underlying substrate, but from the suspended sediment above. The sediment fall-out rate can be larger or smaller than the ability of the bedload layer to move infalling grains. This influences whether deposition will take place or not. The particle fall-out rate will also influence the speed at which gravity transformation (Fisher, 1983) will take place. With a low fallout rate more time (or distance) is needed for a flow to undergo gravity transformation than with a high fallout rate.

TRACTION CARPETS

Traction carpets are highly concentrated bedload layers that are developed beneath and driven by turbulent overlying flows with a 'convex-upwards' velocity profile. They consist of two regions, the lower frictional region and the upper collisional region. This frictional region has a concentration of 80% of the packed bed. The upper collisional region can have different particle concentrations. The thickness of traction carpet deposits depends on variations in applied shear stress, grain size, and downward sediment flux (after Sohn, 1997).

1-PHASE AND 2-PHASE TURBIDITY CURRENTS

In the interpretation of turbidity current deposits and flow dynamics a distinction can be made between 1-phase flows and 2-phase flows. A 1-phase flow does not have a high density traction carpet at its base, a 2-phase flow does. Since the Fr' number is a representation of the internal wave propagation velocity versus flow velocity, an interface is needed on which a wave can manifest itself. The location of this interface determines $[h]$ in the Fr' number equation. In a 1-phase turbidity current this is the interface between the sediment-water mix and the ambient water. In a 2-phase turbidity current an extra interface can be present between the high density layer and the low density layer. This interface is absent or graded if the concentration gradually increases downwards.

DEPOSITION BY TURBIDITY CURRENTS

Based on a study by Kuenen et al. (1957) and his own research, Bouma (1962) developed a common sequence found in turbidites later called the Bouma sequence. This classical model describes a turbidite sedimentation succession formed as result of a decelerating turbidity current.

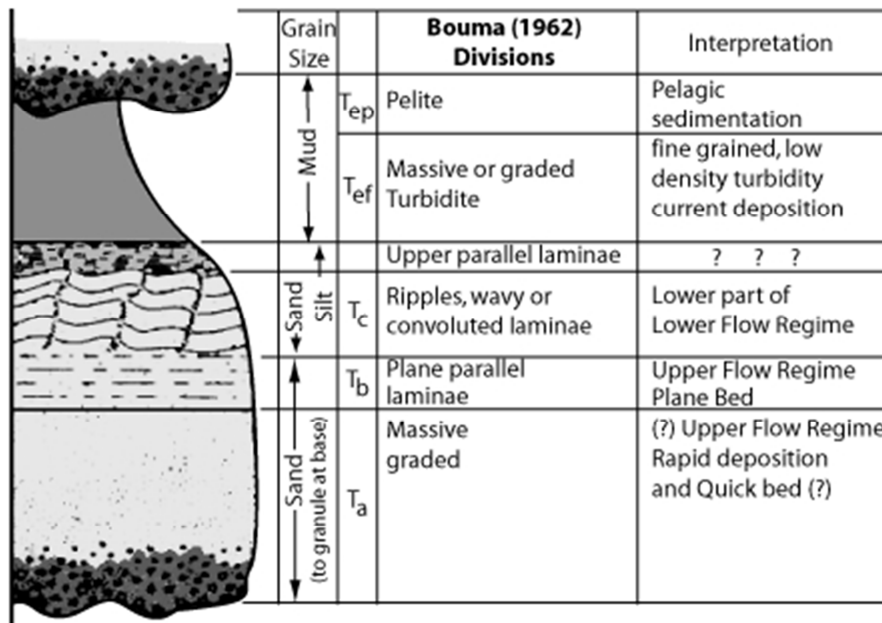


FIGURE 2: THE BOUMA SEQUENCE FOR TURBIDITE SEDIMENTATION.

The Bouma sequence recognizes 5 turbidite facies: Ta, Tb, Tc, Td and Te. Each depositional unit is the result of a specific depositional environment with specific hydraulic conditions of the decelerating turbidity current. It is important to realize that this is an idealized sequence. Depending on the circumstances only parts of the succession may have been deposited. As indicated in figure 2, Ta is a massive unsorted sand deposit. I will discuss the depositional conditions of this unit in more detail in the next paragraph. Tb consists of upper flow regime plane bed laminations in sand, deposited under a shearing flow. Tc consists of the sand and silt fraction, deposited as ripples or wavy laminae. Td consists of parallel laminae, formed in the presence of shear and suspension fallout. Te is a graded hemipelagic mud unit.

From further observations in turbidite deposits Lowe (1982) suggested to extend the Bouma sequence further down to coarser and higher energy deposits. Where Bouma's sequence is based primarily on field evidence, Lowe (1982) has broadened the view starting from different suspension- and transport mechanisms of grain size populations and particle concentrations.

In turbidity currents three particle size populations can be distinguished:

- 1) Clay, silt and fine-medium sand. Can be maintained in suspension by fluid turbulence alone.
- 2) Coarse sand to small pebbles. Can be maintained in suspension in concentrated suspensions with a large range of grain sizes by combined effects of turbulence, hindered settling (by own high concentration) and buoyant lift from interstitial mix of water and fine grained sediment.
- 3) Pebble and cobble-sized clasts. At concentrations larger than 10%-15% they are supported by clast collisions and buoyant lift from interstitial mix of water and fine grained sediment.

Population 2 and 3 will therefore only be transported in high concentration turbidity currents. Deposition from a turbidity current takes place as a series of sedimentation waves, induced by flow deceleration and the inherent loss of the different sediment suspension- and transport mechanisms. In figure 3 R₁, R₂ and R₃ represent population 3 grain deposition, S₁, S₂ and S₃ represent population 2 grain deposition. On top of that are Bouma's Tb-Te. Lowe's depositional unit S₃ is the same as Bouma's Ta. The three fases within R and S stand for 3 successive stages in the deposition:

(R,S)₁ - initial stage of traction sedimentation

(R,S)₂ - mixed frictional freezing and suspension sedimentation within traction carpets

(R,S)₃ - direct suspension sedimentation

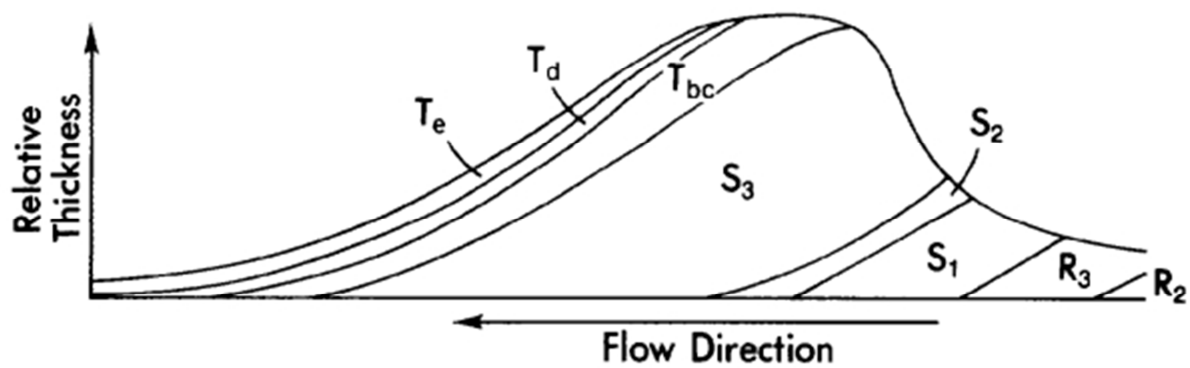


FIGURE 3: DEPOSITIONAL SEQUENCE AND THICKNESS OF LOWE'S R AND S UNITS, WITH BOUMA'S TB-TE UNITS ON TOP (FROM LOWE, 1982).

DEPOSITIONAL CONTEXT AND FACIES OF THE BOUMA TA UNIT

The position of Ta in the Bouma sequence or S₃ in Lowe's addition shows that this unit must be deposited under high energy flow conditions. However, the facies type of the Ta unit is a massive unsorted sand bed, indicative of rapid deposition with no or minimal shear stress. This seems a remarkable combination because a high energy depositional context may be intuitively associated with tractional features, laminations or depositional structures of some sort.

Different theories have been proposed to explain the occurrence of the massive unsorted sand bed at this position in turbidites:

It has been suggested that the massive unsorted sand bed is deposited in the antidune phase of upper the flow regime (Harms and Fahnestock, 1965; Walker, 1967), however other researchers noticed that antidune laminations would be preserved and visible in the deposits (Middleton, 1965; Hand, 1969, 1974).

Other depositional mechanisms proposed are:

- Quick deposition, possibly accompanied by interfacial waves which could rework laminations (Middleton, 1967).
- Deposition from grain flow, where just prior to deposition dispersion is maintained by inertial interaction of grains (Stauffer, 1967; using Bagnold, 1954, 1956).
- Deposition from a modified grain flow, maintained by high concentration interstitial suspension, excess pore-fluid pressure or shear stress of the overriding flow (Lowe, 1976; Mullins and van Buren, 1979; Hiscott and Middleton, 1980).
- Suppression of lamination formation as result of high fallout rate (Middleton, 1970; Collinson and Thompson, 1982; Allen, 1984; tested with experiments by Arnott and Hand, 1989). However, a high fallout and aggradation rate alone is not enough to explain this facies. LeClair and Arnott (2005) investigated deposition by sustained turbidites with a high concentration of 20% to 35% and high fallout rates. With a bed aggradation rate of 4 mm s⁻¹ parallel lamination was formed in each run. They conclude that suppression of lamination formation by a high fallout rate as investigated by Arnott and Hand (1989) cannot explain the facies of Bouma's Ta.
- Very rapid deceleration of a turbidity current, where at high fallout and aggradation rates the sequential collapse of laminar sheared layers produces the poorly graded poorly sorted structureless sand bed (Sumner et al, 2008). However, Baas (2004) has performed numerical modeling concluding that neither rapid deceleration of the flow

nor high fallout rate can develop Bouma's Ta unit, because tractional features would form within seconds.

The summary above illustrates the controversy or lack of understanding about the formation process(es) of the massive unsorted sand bed. Postma et al (2009) have provided a new insight as to which depositional context can be attributed to the massive unsorted sand bed. They postulate that in and beneath a hydraulic jump within the traction carpet of a 2-phase turbidity current the right conditions (low shear and high fallout) are present to form a Ta deposit. Changes in density and flow velocity rapidly change the position of the hydraulic jump, developing a sheet-like Ta unit. This was observed in their experiments and used to explain the formation processes of several field outcrops of structureless sand beds.

My Master's thesis and experiments are framed in this context. I aim to produce turbidity currents with different flow characteristics (1-phase flow, 2-phase flow, occurrence or absence of hydraulic jump) in order to investigate which of the theories can best explain the deposits and flow dynamics.

METHODOLOGY

In this experimental study turbidity currents of different sediment concentration and sediment grain size are created and observed in a flume at the Eurotank laboratory facility at Utrecht University. In this section I will discuss the the experimental setup, the experiments and measurement methods.

The experiments entail the creation of 1-phase and 2-phase turbidity currents with particle concentrations between 4.4% and 28.5% of volume and sediment grain sizes from 120 μm to 570 μm . Sediment-water mixtures are fed into a rectangular channel with gradually decreasing slope and the flows are forced to go through a hydraulic jump using a weir or dam in the flow.

The effects of grain size and various sediment concentrations on sediment deposition, flow dynamics and hydraulic jump characteristics are studied from high speed motion pictures.

To be able to draw conclusions and order the data I measure flow velocity, sediment concentration and grain sizes of the input mixture. Froude numbers are calculated where possible to investigate the criticality of flows.

Limitations of and problems with this setup are discussed in the Discussion section.

EXPERIMENTAL SETUP – SEDIMENT SUPPLY

In order to produce turbidity currents of specific density (particle concentration), the following experimental setup was constructed in the Eurotank facility:

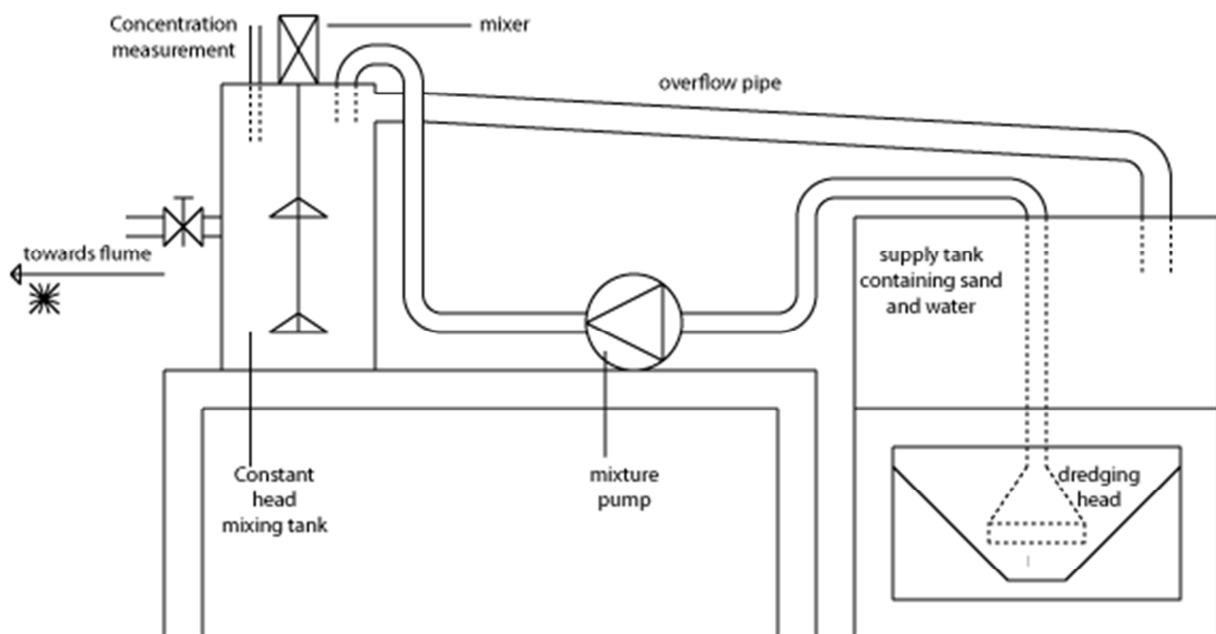


FIGURE 4: SEDIMENT-WATER MIX PUMPING SYSTEM, PART OF THE EXPERIMENTAL SETUP OF THE 13 EXPERIMENTS. THE STAR AT THE LEFT MARKS THE OUTPUT TOWARDS THE FLUME.

The experimental setup is schematized in figure 4, including the terms used in the following description. The setup works as follows:

- The supply tank is filled with sand and water.

- Turning on the mixture pump feeds a sand/water mixture to the constant head mixing tank.
- Within the constant head mixing tank, the sand/water mixture is kept fully in suspension. Within this constant head mixing tank, the concentration is measured. Overflow can take place towards the supply tank.
- From the constant head mixing tank the mixture can be released into the flume. At the inlet into the flume the speed is measured.
- The turbidity current within the flume is filmed using two high speed cameras (figure 5).

EXPERIMENTAL SETUP – FLUME

The Eurotank 4 meter long tilting flume was used with a few adaptations. The width of the flume was reduced to 5 centimeters using panels 1 meter long. A slope was constructed with gradually decreasing steepness, ending horizontally. The bottom of the whole flume including the slope was covered with sanding paper to mimic the roughness and structure of a sand bed. Height of the weir (named obstruction in figure 5) was 22.5 centimeters, except for run 1, where weir height was 26.5 centimeters.

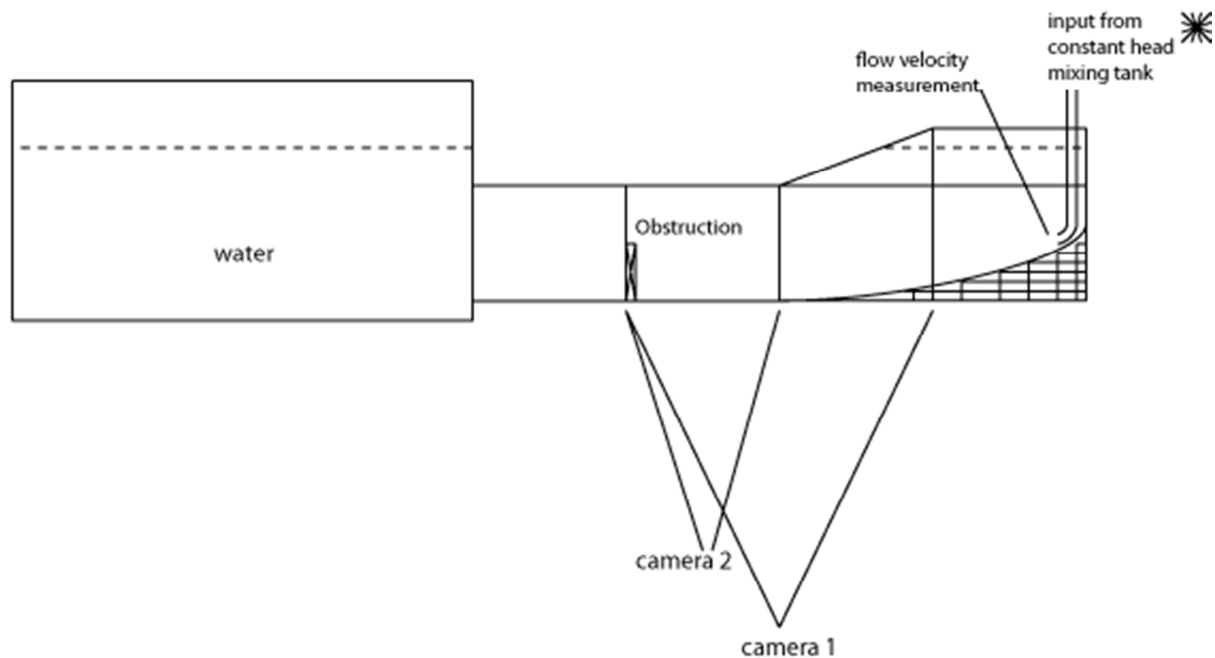


FIGURE 5: THE FLUME PART OF THE EXPERIMENTAL SETUP. THE STAR AT THE RIGHT OF THE PICTURE MARKS THE INPUT COMING FROM THE MIXING APPARATUS. TWO HIGH SPEED CAMERAS FILM THE TURBIDITY CURRENT AND OCCURRING HYDRAULIC PHENOMENA. FLUME LENGTH IS 4 METERS.

EXPERIMENTS – TEST PHASE

The construction of the experimental setup took several months, during which test experiments were performed. Unfortunately, these test experiments lack reliable concentration data as the concentration measurement was, in most cases, the reason of construction adjustments. However, some results from the test runs, such as the motion pictures obtained from the cameras and deposit pictures, were used in the analysis and discussion of the successful experiments. Furthermore, these test experiments provided insight into which adjustments had to be made in the sediment supply and flume design.

EXPERIMENTS – SUCCESSFUL EXPERIMENTS

Thirteen successful experiments were conducted using three different grain sizes and different concentrations. For each experiment, a sediment-water mix was created with approximately the desired concentration. The sediment-water mix was then released into the flume, where it created a turbidity current. Input concentration was measured before and during the experiments. The turbidity current was filmed using high speed cameras and the flow velocity at the inlet was measured using an EMS sensor.

MEASUREMENTS – GRAIN SIZES

Three different sands were used. For all three, a grain size distribution analysis was performed using the Malvern Particle Sizer: fine sand with d_{50} of $120\mu\text{m}$, medium sand with a d_{50} of $313\mu\text{m}$ and coarse sand with a d_{50} of $570\mu\text{m}$ were used (see table 1).

	d_{10}	d_{50}	d_{90}
Fine sand	53	119	217
Medium sand	187	313	500
Coarse sand	310	570	2000

TABLE 1: GRAIN SIZE DISTRIBUTIONS OF THE SANDS USED IN THE EXPERIMENTS.

MEASUREMENTS – PARTICLE CONCENTRATION

Concentrations were chosen between 0% and 30% of volume. Concentration was influenced by adjusting the height of the mouth in the dredging head above the sediment, and by the amount of sand in the supply tank. Before every run, a sample was taken to give an indication of the concentration in the mixing tank. This sample was obtained by filling a 1 liter jar using the output/input hose (indicated with a large * in the figures). This measurement was indicative only, used to determine whether the right concentration was reached to start the experiment.

During the experiment concentration was measured using CCM conductivity concentration meters (see figure 6). Acquiring correct results proved to be very problematic, as described below and in the Discussion section.

The time averaged concentration of the total experiment was measured using a centrifuge and a hose pump (see figure 6). A tube was placed in the mixing tank, at the exact height of the outflow hose. From this location the hose pump took a continuous sample during the whole run. This sample was put through a centrifuge, so the water in the mixture could be measured with a second CCM, as a zero measurement, see further. At the end of every experiment, the average concentration could be determined using the sample from the hose pump. The centrifuged sediment and water were put together again to give the time averaged concentration of the whole experiment. This average concentration was used when describing and organizing the results because this proved to be the most reliable measurement.

MEASUREMENTS – IMAGERY

High speed cameras were used to record flow dynamics. Camera 1 from figure 5 is a Basler Scout camera (659px * 494px, 70 fps), camera 2 is a Basler Pilot (648px * 488px, 210 fps).

The Basler Scout camera was used to capture a 2.5 meter wide part of the flume, approximately from the inlet to the weir. The Basler Pilot camera was used to focus on specific areas of interest.

A synchronization trigger was used to start recording of the two cameras at the exact same moment.

MEASUREMENTS – FLOW VELOCITY

Flow velocity was measured using an EMS sensor. The EMS sensor was placed directly at the end of the inlet tube so overall input flow speed could be measured before any flow changes had occurred. A correction was applied to the measured data, as described in the Discussion section.

MEASUREMENTS – DATA LOGGER

Using a data logger the EMS sensor and CCM data was recorded at resolutions up to 20 data points per second. For clear representation in the graphs the data was fed into a specially programmed moving median filter script. This script takes each data point and replaces it with the median of the 6 data points surrounding it. The advantages of a moving median filter script over a moving average smoothing script: extreme or out of range data points are automatically discarded and the position of true peaks in data is not changed.

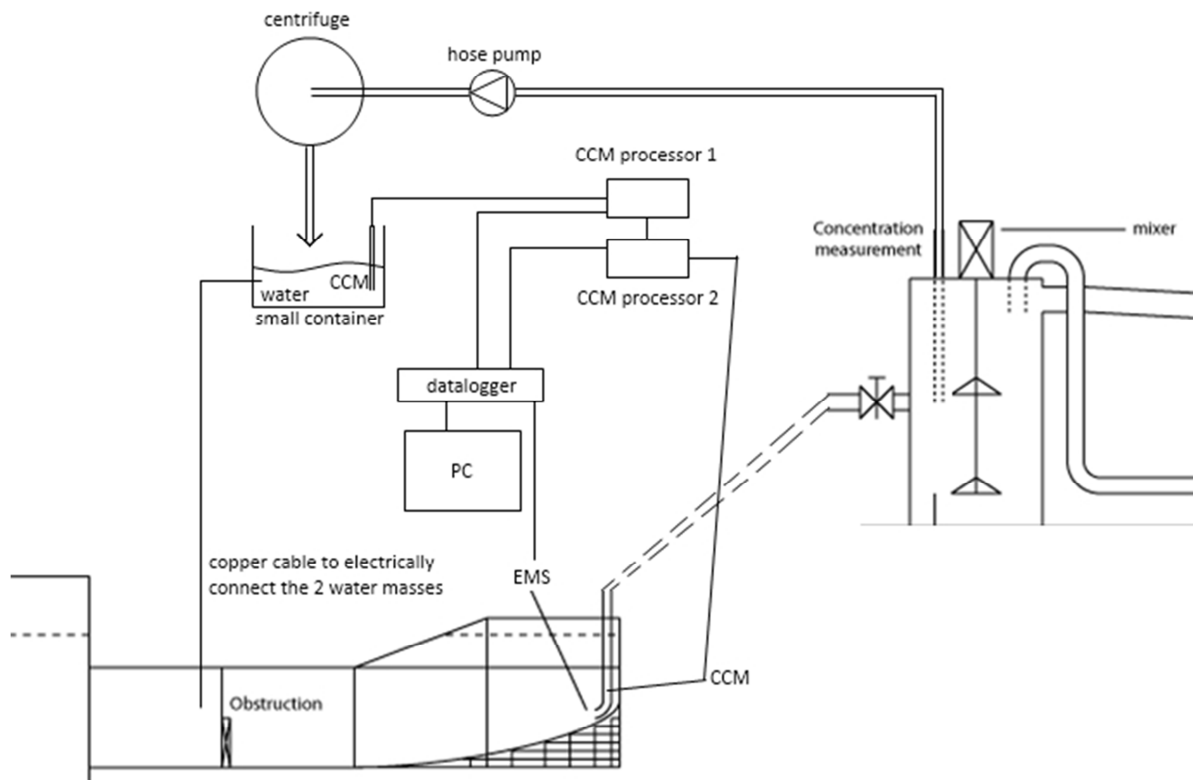


FIGURE 6: SCHEMATIC OVERVIEW OF THE MEASUREMENT INSTALLATION WITH THE TWO CCMS, EMS SENSOR AND DATA LOGGER.

RESULTS

In this section the results and measurements are presented. Also, it is clarified which corrections are made to the measured data in order to achieve the correct results. The following order will be used to present the results:

- Overviews of the experiment runs performed
- Description of the flow dynamics of each run

Actual plots of the input velocity and input concentration measurements during the experiments are included in this thesis as Appendix A1 to A12. Trends in the results are discussed in the Discussion section.

Table 2 shows the 12 successful runs sorted by low or high sediment concentration. Grain sizes used are 120 μm , 313 μm and 570 μm (d_{50}). Averaged input concentrations range between 4.4% and 28.5% by volume. Runs below 9% concentration are considered low concentration turbidity currents, runs with a concentration higher than 9% are considered high concentration turbidity currents. This distinction is based on suspension mechanism theory and experiment results (differences in flow dynamics), as will be elaborated later on in this section.

Run	Name	d_{50}	h_{weir}	$U_{\text{avg at inlet}}$	C_{avg}
<i>Low concentration runs</i>					
1	exp1_	120	26.5	1.58	4.7%
2	exp4	120	22.5	1.98	6.7%
6	exp11	313	22.5	1.33	4.4%
7	exp9_	313	22.5	1.23	7.0%
11	exp13	570	22.5	1.50	4.3%
<i>High concentration runs</i>					
3	exp2_	120	22.5	1.93	16.8%
4	exp3	120	22.5	1.80	16.8%
5	exp5	120	22.5	1.31	21.6%
8	exp7	313	22.5	1.49	12.9%
9	exp10	313	22.5	1.44	15.0%
10	exp8	313	22.5	1.39	22.1%
12	exp12	570	22.5	1.32	28.5%
	exp6	313	22.5	1.36	23.5%

TABLE 2: EXPERIMENT CHARACTERISTICS. UNFORTUNATELY, IMAGERY OF EXPERIMENT EXP6 WAS NOT CAPTURED SUCCESSFULLY, AND IS THEREFORE NOT FURTHER CONSIDERED. SOME EXPERIMENTS HAD TO BE REPEATED, FOR CORRECT REFERENCE THE SECOND RUN'S NAME ENDS WITH AN UNDERSCORE.

Figure 7 on the next page shows an overview of the experiments in a matrix with grain size on the horizontal axis and concentration on the vertical axis.

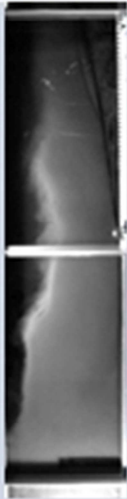

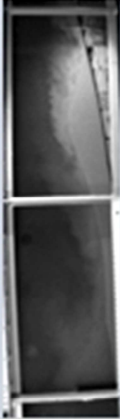
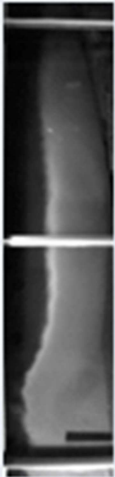


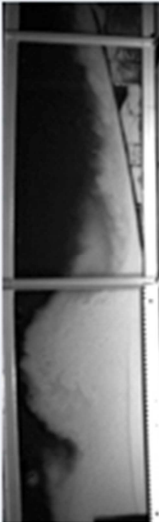
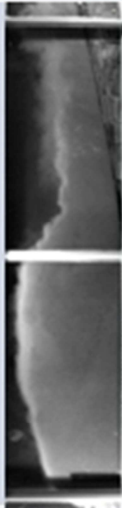
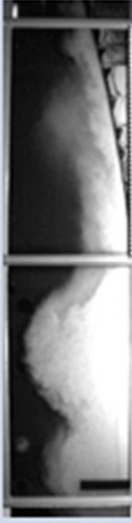

	120 μ	300 μ	570 μ
5%			
7%			Not done
12%	Not successful		Not done
17%			Not done
22%			

FIGURE 7: OVERVIEW OF THE EXPERIMENTS CONDUCTED.

DESCRIPTION OF THE FLOW DYNAMICS OF EACH RUN

First, three terms I use to describe the flow dynamics are clarified:

Backflow, detachment zone and hydraulic jump/rapidly upstream moving detachment zone.

BACKFLOW

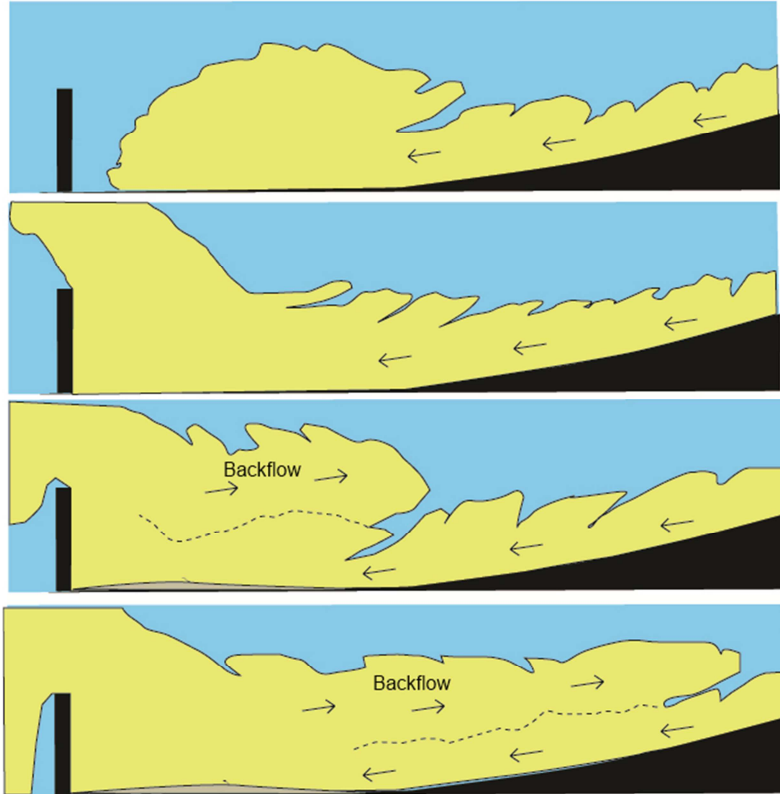


FIGURE 8: ILLUSTRATION EXPLAINING THE TERM BACKFLOW.

When the head of the turbidity current reaches the weir (upper two panel in figure 8), part of the head does not pass over the weir but folds back to travel on top of the inflowing turbidity current, in upstream direction (lower two pictures). This is called a backflow. This backflow is re-entrained in the inflowing turbidity current and could remain in place during the whole experiment or disappear, depending on flow dynamics.

In all the fine grain size runs the backflow remains present throughout the duration of the run. In the low concentration medium grain size and both coarse grain size runs the backflow is swept away downstream with the incoming turbidity current. In the medium grain size run of high concentration the hydraulic jump forms a backflow which remains present because it is constantly 'refilled' with sediment.

The backflow does not have a great influence on the flow dynamics but does reduce visibility of the upper flow edge of the incoming flow.

DETACHMENT ZONE (DZ)

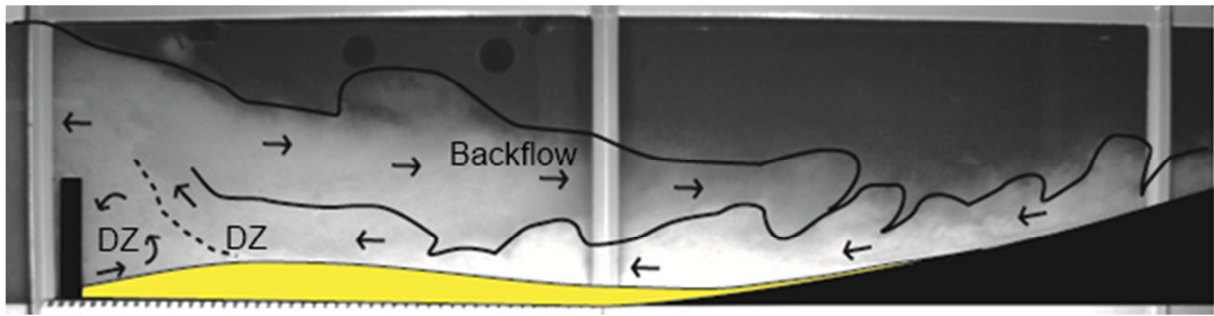


FIGURE 9: ILLUSTRATION SHOWING THE POSITION AND FLOW DYNAMICS OF THE DETACHMENT ZONE.

The term detachment zone (DZ) (figure 9) is used to name the location where the 'bottom-hugging' flow detaches from the flume floor or sand bed as result of an obstacle in the flow (the weir). Between the detachment zone and the weir a slowly circulating cell forms, over which the turbidity current passes the obstacle. This feature is present in all the runs.

HYDRAULIC JUMP / RAPIDLY UPSTREAM MOVING DETACHMENT ZONE

Local flow directions were studied to understand the flow dynamics related to hydraulic jump / rapidly upstream moving detachment zone in the runs. Figure 10 shows these flow directions.

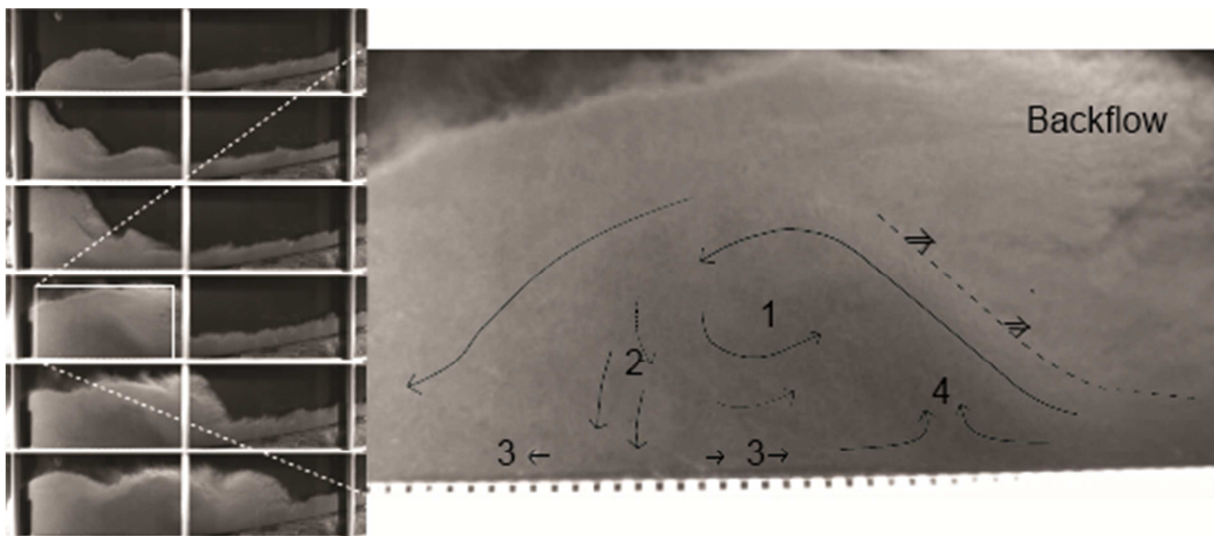


FIGURE 10: LOCAL FLOW DIRECTION AT THE LOCATION WHERE THE LOWER LAYER OF THIS 2-PHASE TURBIDITY CURRENT GOES THROUGH A HYDRAULIC JUMP, OBTAINED BY FOLLOWING MOVEMENT OF LIGHT AND DARK SPOTS. DASHED LINE INDICATES THE UPPER BORDER OF THE HIGHER DENSITY TRACTION CARPET. ABOVE IT A BACKWARDS FLOWING SEDIMENT CLOUD CAN BE OBSERVED STEMMING FROM THE TURBIDITY CURRENT'S HEAD. SCALE: CENTIMETRES ARE INDICATED IN BOTTOM PART OF THE PICTURE BY DOTS. ARROWS INDICATE FLOW DIRECTION ONLY, NOT SPEED.

Figure 10 demonstrates a high concentration fine grain size flow (run 5) going through a hydraulic jump expanding to a flow height approximately four times larger in the subcritical part (left in figure) than in the supercritical part. Immediately downstream of this expansion, part of the flow re-circulates towards the jump location, going in upstream direction [1]. This recirculation creates a downward movement approximately 20 centimeters downstream of the jump [2]. Here, the sediment is flowing down onto the bed. The sand undergoing this movement is deflected away from that point in both up and downstream direction [3]. Where the re-

circulating flow meets the 'incoming' sediment of the supercritical part of the turbidity current, the local flow direction is upwards [4]. The whole structure rapidly moves upstream [double arrows].

Location 4 is where deposition can take place without shear, in the middle of a high energy environment. Wherever possible, I try to find the path that location 4 in the hydraulic jump has followed through the deposit. I then describe the resulting deposits.

The hydraulic jump as described here is present in runs 3, 4, 5, 8, 9 and 10, which are the high concentration runs of fine and medium grain size.

OVERVIEW OF PHENOMENA OCCURRING IN THE RUNS

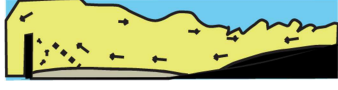


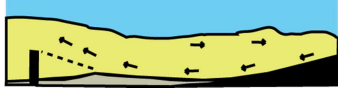







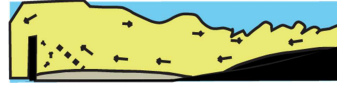
Concentration	Grain size 120 μ	Grain size 313 μ	Grain size 570 μ
Low ~5%	<u>Run 1, exp1</u> Backflow 1-phase flow DZ stays close to weir 	<u>Run 6, exp11</u> Backflow 1-phase flow DZ stays close to weir 	<u>Run 11, exp13</u> Backflow 1-phase flow DZ stays close to weir 
Low ~7%	<u>Run 2, exp4</u> Backflow 1-phase flow DZ stays close to weir 	<u>Run 7, exp9</u> Backflow 1-phase flow DZ stays close to weir 	Not done
High ~12%	Not successful, exp6	<u>Run 8, exp7</u> Backflow 2-phase flow (?) DZ rapidly moving upstream hydraulic jump 	Not done
High ~17%	<u>Run 3, exp2; Run 4, exp3</u> Backflow 2-phase flow (?) DZ rapidly moving upstream hydraulic jump 	<u>Run 9, exp10</u> Backflow 2-phase flow (?) DZ rapidly moving upstream hydraulic jump 	Not done
High <22%	<u>Run 5, exp5</u> Backflow 2-phase flow (?) DZ rapidly moving upstream hydraulic jump 	<u>Run 10, exp8</u> Backflow 2-phase flow (?) DZ rapidly moving upstream hydraulic jump 	<u>Run 12, exp12</u> Backflow 1-phase flow DZ stays close to weir 

TABLE 3: OVERVIEW OF PHENOMENA OCCURRING IN THE RUNS.

LOW CONCENTRATION RUNS

In this subsection the low input concentration runs (between 4.4% and 7.0%) are described:

run 1: input concentration 4.7%; grain size 120 μ



run 2: input concentration 6.7%; grain size 120 μ



run 6: input concentration 4.4%; grain size 313 μ



run 7: input concentration 7.0%; grain size 313 μ



run 11: input concentration 5.0%; grain size 570 μ



Common characteristics of the low concentration runs are a stationary detachment zone near the weir. Here, a circulating cell forms over which the turbidity current flows over the weir. This mechanism creates a depression in deposits in front of the weir and shears some sediment in a counter-flow direction.

When grain size increases, the location of thickest deposits is more upstream. The largest grain size population is deposited first, resulting in a fining of the deposits downstream. All deposits are laminated throughout. In some runs, buildup of deposits alters the flow in such manner that previous layers are scoured.

All low concentration runs demonstrated a backflow and 1-phase flow. Backflow remained present throughout the fine grain size runs and disappeared in the medium and coarse grain size runs.

Froude numbers are calculated to be below 1, except for run 6 ($Fr = 1.03$). The calculation and discussion of Fr' numbers is in the Discussion section.

Next, the characteristics of the low concentration runs are described separately in more detail.

RUN 1: AVERAGE CONCENTRATION 4.7% AND GRAIN SIZE (D_{50}) 120μ .

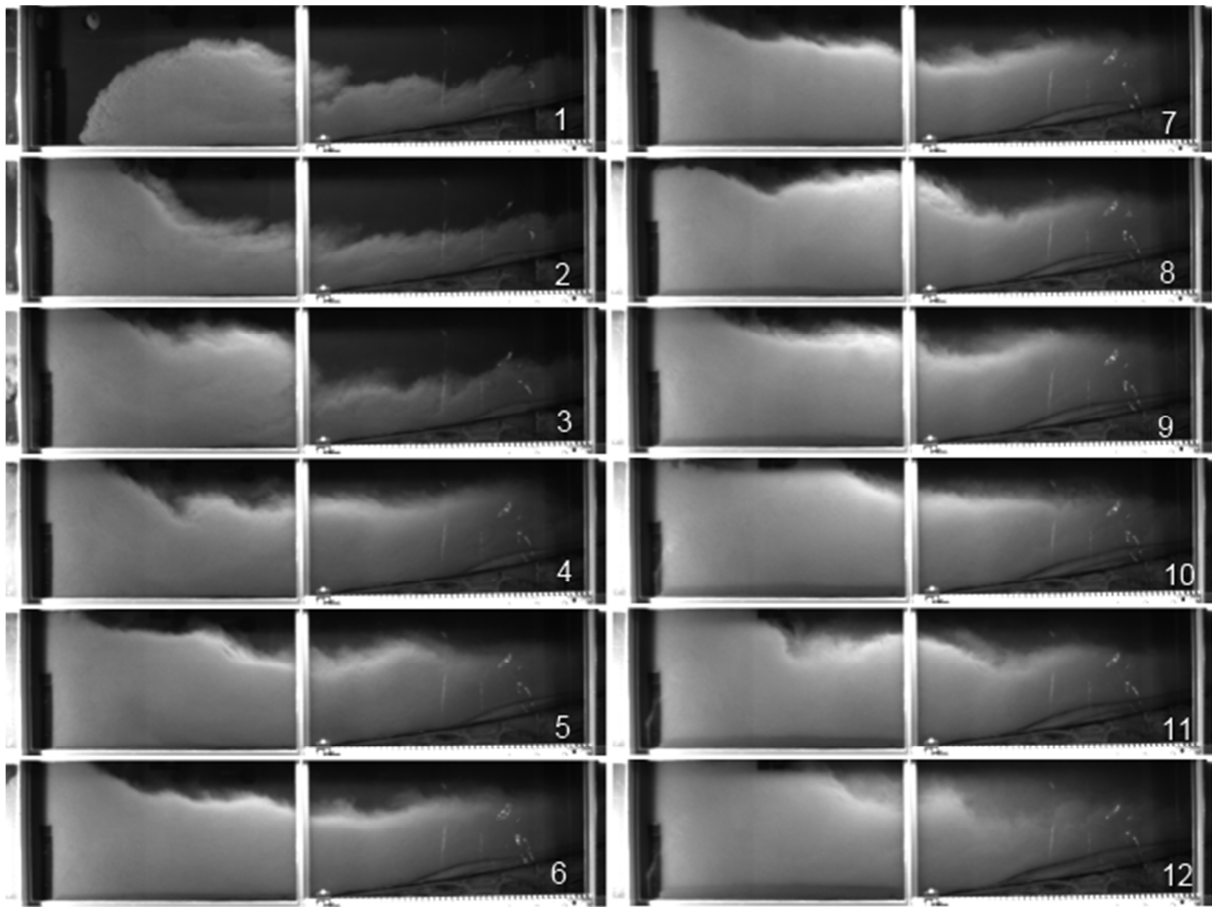


FIGURE 11: STILLS FROM THE VIDEO IMAGERY OF RUN 1.

Run 1 was performed with a low concentration of 4.7% and fine grain size of 120μ . The measured data of run 1 is included as Appendix A1.

A small disturbance of the flow was present because the sanding paper on the flume floor came loose (visible in the panels 1 to 12 in figure 11; on the slope, right part of the flume).

When this turbidity current hits the weir (in the left corner of the pictures) part of the head folds back to form a backflow (panel 2), which overrides the turbidity current in an upstream direction (panels 2 to 12). Because this backflow is directly on top of the incoming turbidity current, entrainment of the backflow into the body of turbidity current takes place.

The flow detaches from the bottom near the weir as described in paragraph 'Detachment zone (DZ)'. This detachment feature moves back and forward over the last 50cms of the flume floor, fed by surges in the flow. A surge with higher flow velocity pushes the detachment zone downstream. In between surges the detachment zone moves slightly upstream.

Deposition takes place between the end of the slope and the weir, with the thickest deposit underneath the detachment feature. Because of the movement of the DZ this highest point migrates back and forth, leaving a bed of fairly equal height. The whole bed is lightly laminated throughout (see figure 12).

Upstream of the DZ the depositing flow shears the bottom leaving laminations in the deposits. Downstream of the DZ the main deposition mechanism seems to be suspension fallout, and these

loose deposits are slightly sheared in upstream direction by a small overriding flow of the DZ circulation cell (as described in paragraph 'Detachment zone (DZ)'. This mechanism creates fainter laminations downstream of the detachment zone. Unfortunately, there was no picture taken to support this observation.

The deposit is laminated throughout giving it the characteristics of Bouma's Tb (see figure 12). No structureless beds were observed. On top of the deposits are ripples (bouma's Tc) and a silt/mud drape. These are not considered part of the experiment since they are deposited when the input flow was stopped.

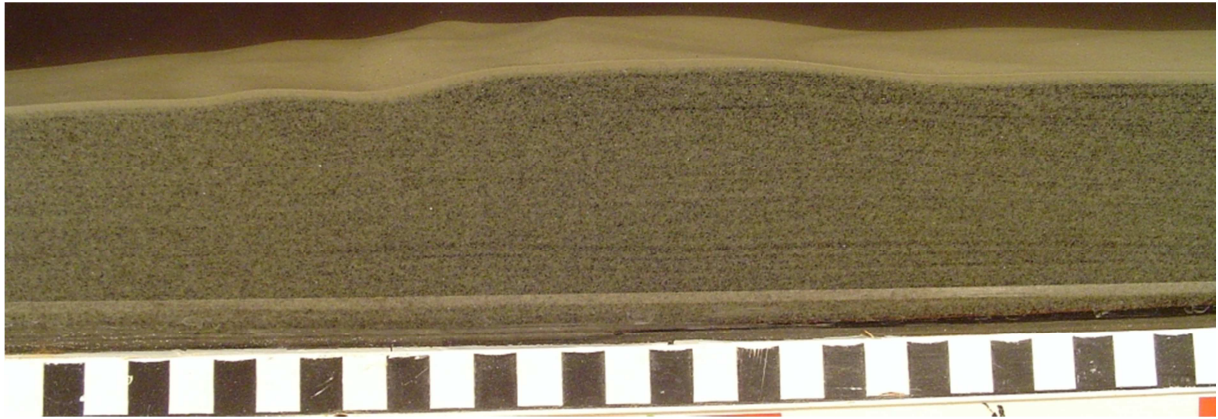


FIGURE 12: PHOTOGRAPH OF THE DEPOSITS OF RUN 1 WITH SCALE IN CMS. THE DEPOSIT IS LAMINATED THROUGHOUT. RIPPLES AND A MUD DRAPE WERE DEPOSITED ON TOP, WHEN INPUT WAS STOPPED.

RUN 2: AVERAGE CONCENTRATION 6.7% AND GRAIN SIZE (D_{50}) 120μ .

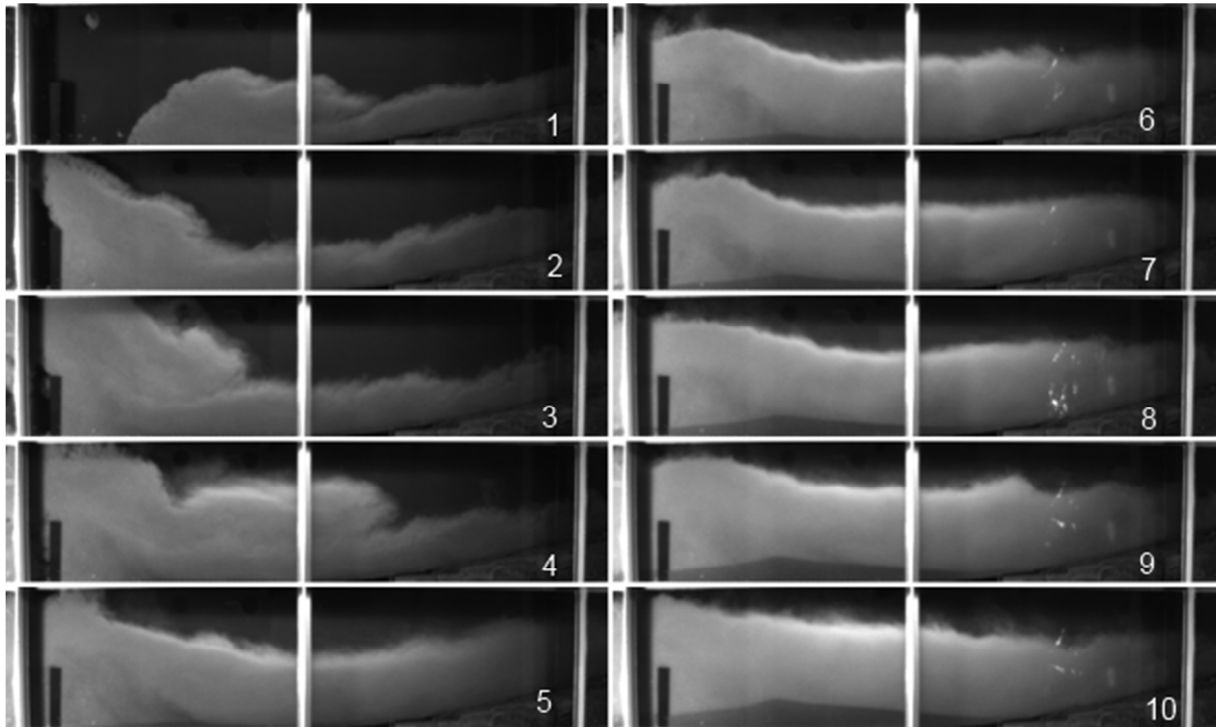


FIGURE 13: STILLS FROM THE VIDEO IMAGERY OF RUN 2.

Run 2 was performed with a low average concentration of 6.7% and fine grain size (120μ). The measured data of run 2 is included as Appendix A2.

Run 2 shows the same sequence of events as run 1 and is therefore described in less detail, however in run 2 the DZ does not shift up- and downstream but migrates towards a stationary position (panel 5 and onwards in figure 13).

When the flow hits the weir, part of the head flows back (panel 2 to 4, and onwards). This is further clarified in figure 14 below:

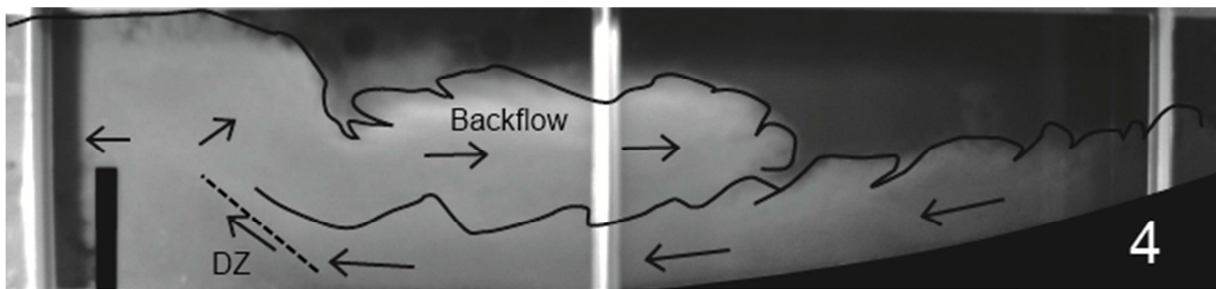


FIGURE 14: LOCATION OF THE DETACHMENT ZONE AND BACKFLOW IN RUN 2.

This backflow is again entrained in the incoming flow. Flow detachment starts at the weir location and migrates upstream (panels 3, 4 and 5) towards a stationary position in the middle of the left panel, or approx. 40 cm upstream of the weir (panel 5 to 10).

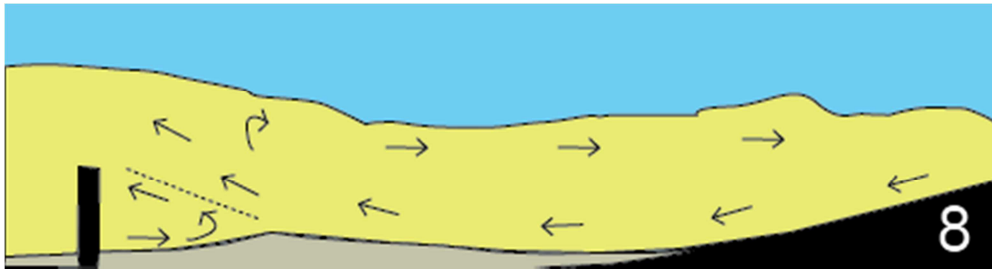


FIGURE 15: FLOW DYNAMICS AT THE END OF RUN 2.

Deposition starts between the end of slope and the weir. The buildup of a sand body moves the first location of sediment deposition more and more upslope. The detachment location is where the thickest deposits are formed, as a result of the flow dynamics as described in the description of the DZ in the beginning of this chapter. Direction of shear upstream of the DZ was in flow direction, direction of shear downstream of the DZ was in counter-flow direction (as indicated by flow direction arrows in figure 15).

The whole deposit is laminated throughout (also in the DZ region) giving it the characteristics of Bouma's Tb (see figure 16). No structureless beds were observed.

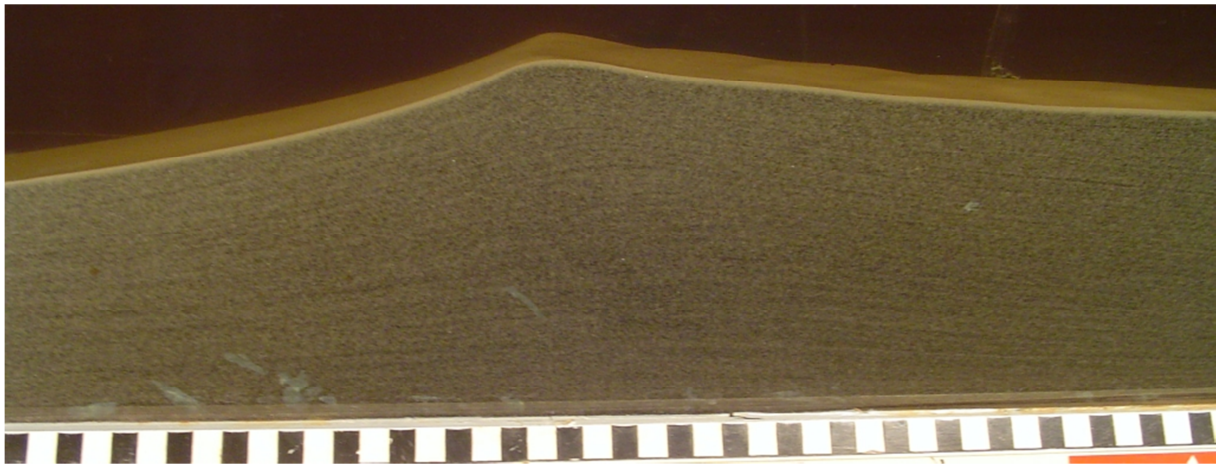


FIGURE 16: PHOTOGRAPH OF THE DEPOSITS OF RUN 2 WITH SCALE IN CMS. LOCATION OF THE PHOTOGRAPH IS JUST UPSTREAM OF THE WEIR. THE DEPOSIT IS LAMINATED THROUGHOUT. A MUD DRAPE WAS DEPOSITED ON TOP, WHEN INPUT WAS STOPPED.

RUN 6: AVERAGE CONCENTRATION 4.4% AND GRAIN SIZE (D_{50}) 313μ .



FIGURE 17: STILLS FROM THE VIDEO IMAGERY OF RUN 6.

Run 6 was performed with a low average concentration of 4.4% and medium grain size of 313μ . The measured data of run 6 is included as Appendix A6.

The results of run 6 are very similar to run 7, to which I therefore refer. Also included in the description of run 7 is a visualization of flow directions (figure 19).

RUN 7: AVERAGE CONCENTRATION 7% AND GRAIN SIZE (D_{50}) 313μ .



FIGURE 18: STILLs FROM THE VIDEO IMAGERY OF RUN 7.

Run 7 was performed with a low average concentration of 7% and medium grain size of 313μ . The measured data of run 7 is included as Appendix A7.

To support flow dynamics descriptions, a visualization of flow directions is included as figure 19 on the next page.

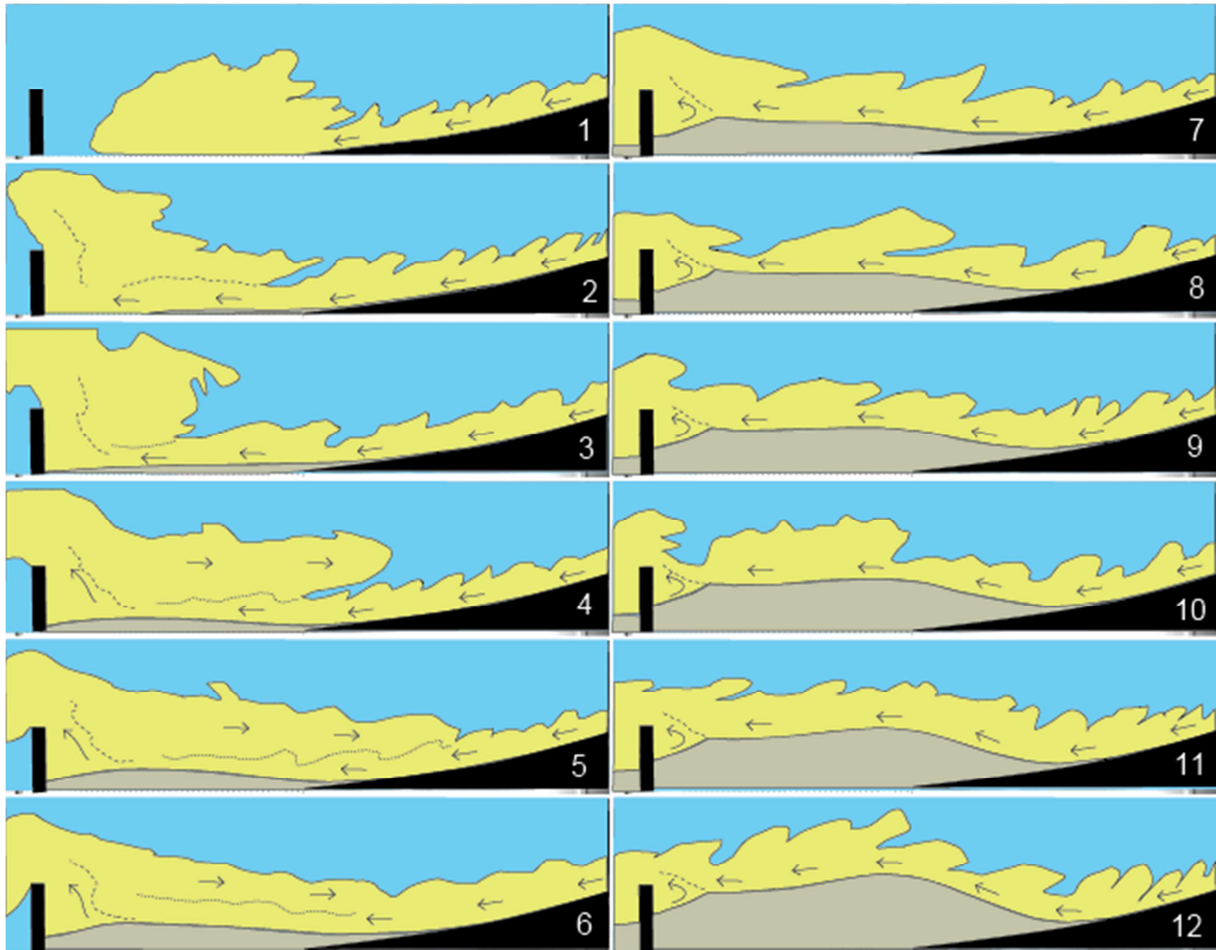


FIGURE 19: VISUALISATION OF FLOW DYNAMICS OVERDRAWING STILL FROM THE VIDEO IMAGERY OF RUN 7.

The low concentration turbidity current meets the weir (panels 1 to 3 in figures 18 and 19) and a small backflow forms (panels 4 to 6). Since this backflow is kept totally in suspension while flow velocity was low, it is assumed that only the smaller sized particles are present in this backflow. A detachment zone seems to form (panel 3 and onwards) but it does not migrate upstream. Instead, near the weir a slowly stationary circulating cell formed with a relatively high sediment concentration, effectively creating an upward ramp over which the remaining flow could pass the weir (panel 6 and onwards). As the run continued, the concentration of the input mixture decreased which also caused the visibly higher density in this cell to drop.

The deposits clearly show the location of the detachment zone, about 20 cm upstream of the weir. Deposition starts immediately downstream of the input location, still on the slope. The highest bulge of sediment forms at the end of slope (panel 7 to 12). This position maintains itself, because the growing sediment bulge creates an upward slope where flow velocity decreases.

This high sediment fall-out rate makes that before the flow reaches the weir, concentration has dropped. A downstream fining of the deposits was observed.

The whole deposit is laminated throughout, giving it the characteristics of Bouma's Tb. No structureless beds were observed. This visual observation made at the end of the experiment cannot be supported by a picture. It could only just be observed by eye and is not visible on photographs. This is caused by the uniform color of the sand. When the flume was emptied and a dry sand bed remained, the laminations were clearly present.

RUN 11: AVERAGE CONCENTRATION 5% AND GRAIN SIZE (D_{50}) 570μ .



FIGURE 20: STILLS FROM THE VIDEO IMAGERY OF RUN 11.

Run 11 was performed with a low concentration of about 5% and large grain size of 570μ . The measured data of run 11 is included as Appendix A11.

To support flow dynamics descriptions, a visualization of flow directions is included as figure 21 on the next page.

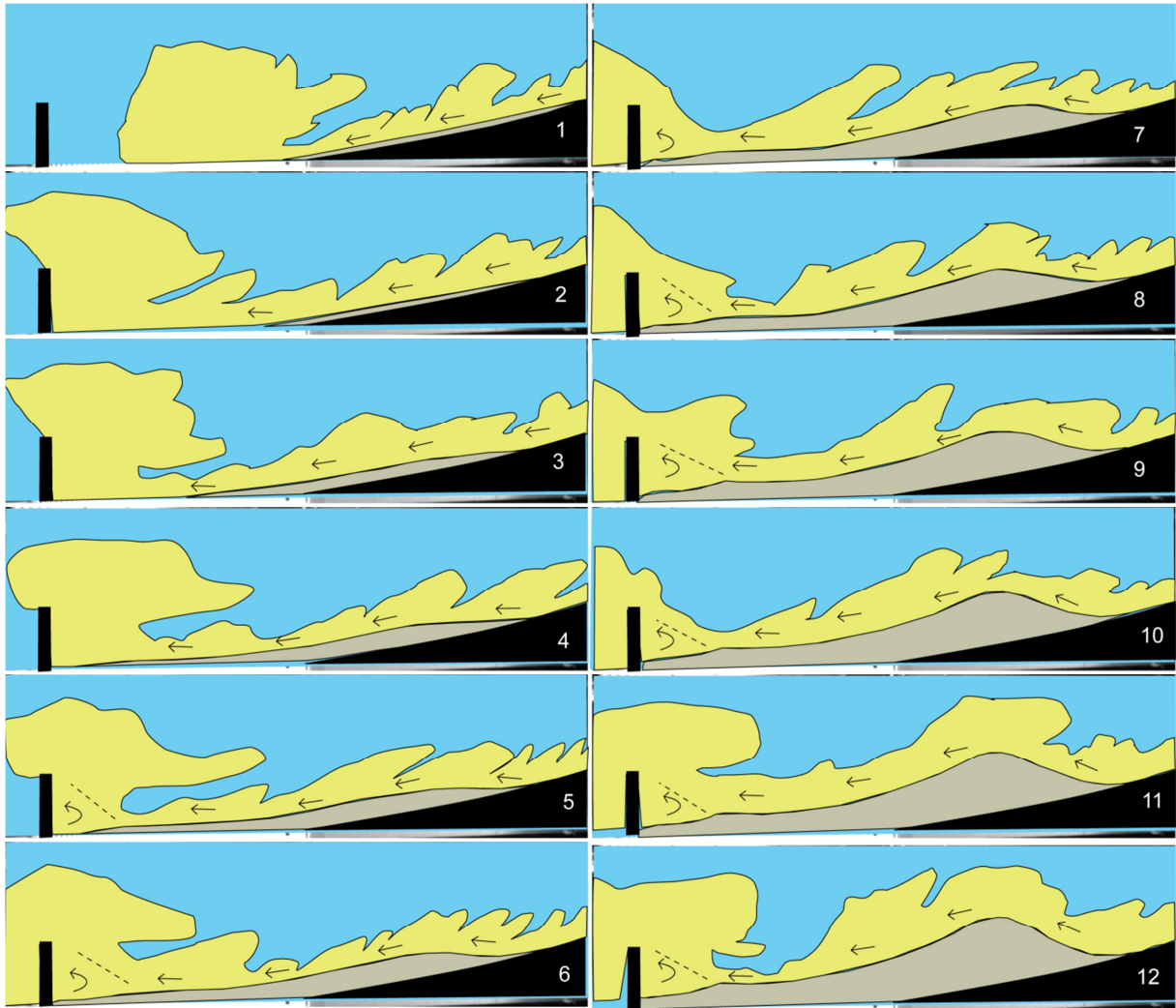


FIGURE 21: VISUALISATION OF FLOW DYNAMICS OVERDRAWING STILL FROM THE VIDEO IMAGERY OF RUN 11.

It is observed that already on the slope, the large grain population is not kept in suspension and falls out (all panels in figure 20 and 21). The sediment fallout rate and deposition rate is high, and a bulge of coarse grained sediment is formed at the proximal part of the flume. The remaining mix contains finer grained sand but the concentration of this remaining mix has become very low (visual observation). This low concentration remaining mix forms its own 'ramp' in the form of a stationary circulating cell at the flow detachment zone, over which it passes the obstruction (panel 5 and onwards).

This combination of events made the fine grained sand bypass sedimentation in this location. Overall there is a rough sorting in grain size of the deposits in a longitudinal direction, fining downstream.

The deposit is laminated throughout, giving it the characteristics of Bouma's Tb (see figure 22). No structureless beds were observed.

A remarkable sorting of grains occurs below the detachment zone near the weir. Large grains are not deposited downstream of the DZ. The mechanism by which this happens is as follows: the largest grains are transported as bedload, rolling downstream sheared by the overriding turbidity current. At the detachment zone the flow detaches from the bed, no longer enabling

this form of transport. The large grains are not in suspension and do therefore not pass the detachment zone (visible in figure 22).

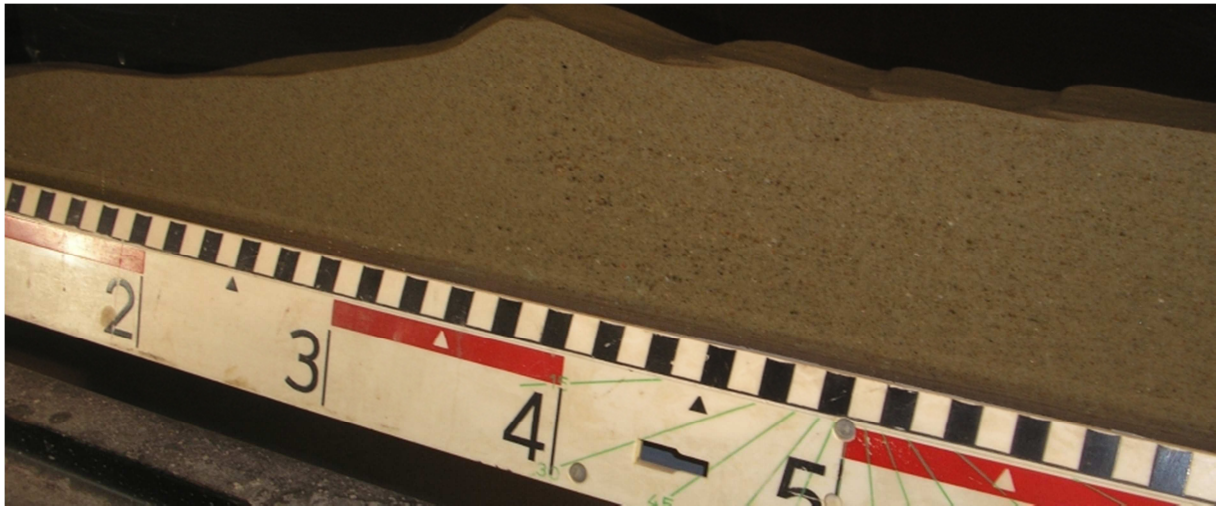


FIGURE 22: PHOTOGRAPH OF THE DEPOSITS OF RUN 11. THE BED IS LAMINATED THROUGHOUT. AT THE DETACHMENT ZONE LARGE BED-LOAD TRANSPORTED GRAINS ARE DEPOSITED WHEREAS SMALLER SUSPENDED GRAINS CONTINUE WITHIN THE FLOW.

HIGH CONCENTRATION RUNS

In this subsection the high input concentration runs (between 12.9% and 28.5%) are described:

run 3: input concentration 16.8%; grain size 120 μ



run 4: input concentration 16.8%; grain size 120 μ



run 5: input concentration 21.6%; grain size 120 μ



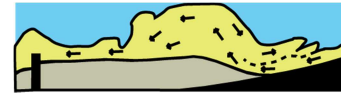
run 8: input concentration 12.9%; grain size 313 μ



run 9: input concentration 15.0%; grain size 313 μ



run 10: input concentration 22.1%; grain size 313 μ



run 12: input concentration 28.5%; grain size 570 μ



Common characteristics of the high concentration runs are a rapidly upstream moving detachment zone. Judging by flow dynamics only, this structure is the hydraulic jump. In the Discussion section I will discuss, using calculated Fr' numbers, whether this observation is supported by measurements.

The high concentration runs also show a circulating cell near the weir.

A difference in flow dynamics and deposition rate is observed between the runs with fine grain size and the runs with medium grain size.

All deposits are laminated throughout.

Run 12, in spite of having a high input concentration, displays the flow dynamics of a low concentration run. It is observed that deposition rate is so high, that the remaining flow over the deposits is of low concentration.

All high concentration runs except run 12 demonstrated a backflow and possibly 2-phase flow.

Next, the characteristics of the high concentration runs are described separately in more detail.

RUN 3: AVERAGE CONCENTRATION 16.8% AND GRAIN SIZE (D_{50}) 120 μ .

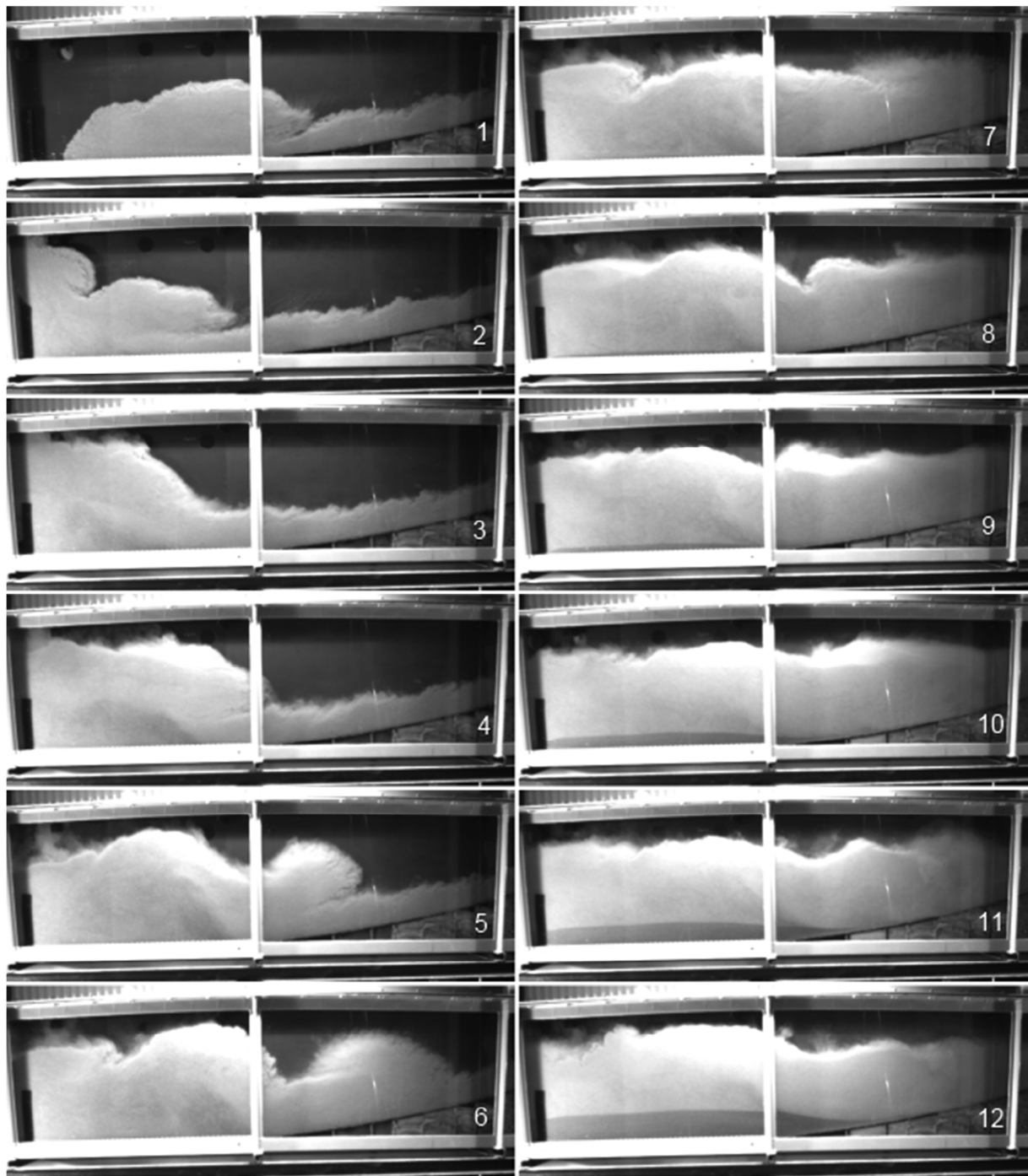


FIGURE 23: STILLS FROM THE VIDEO IMAGERY OF RUN 3.

Run 3 was performed with a high average concentration of 16.8% and fine grain size of 120 μ . The measured data of run 3 is included as Appendix A3.

To support flow dynamics descriptions, a visualization of flow directions is included as figure 24 on the next page.

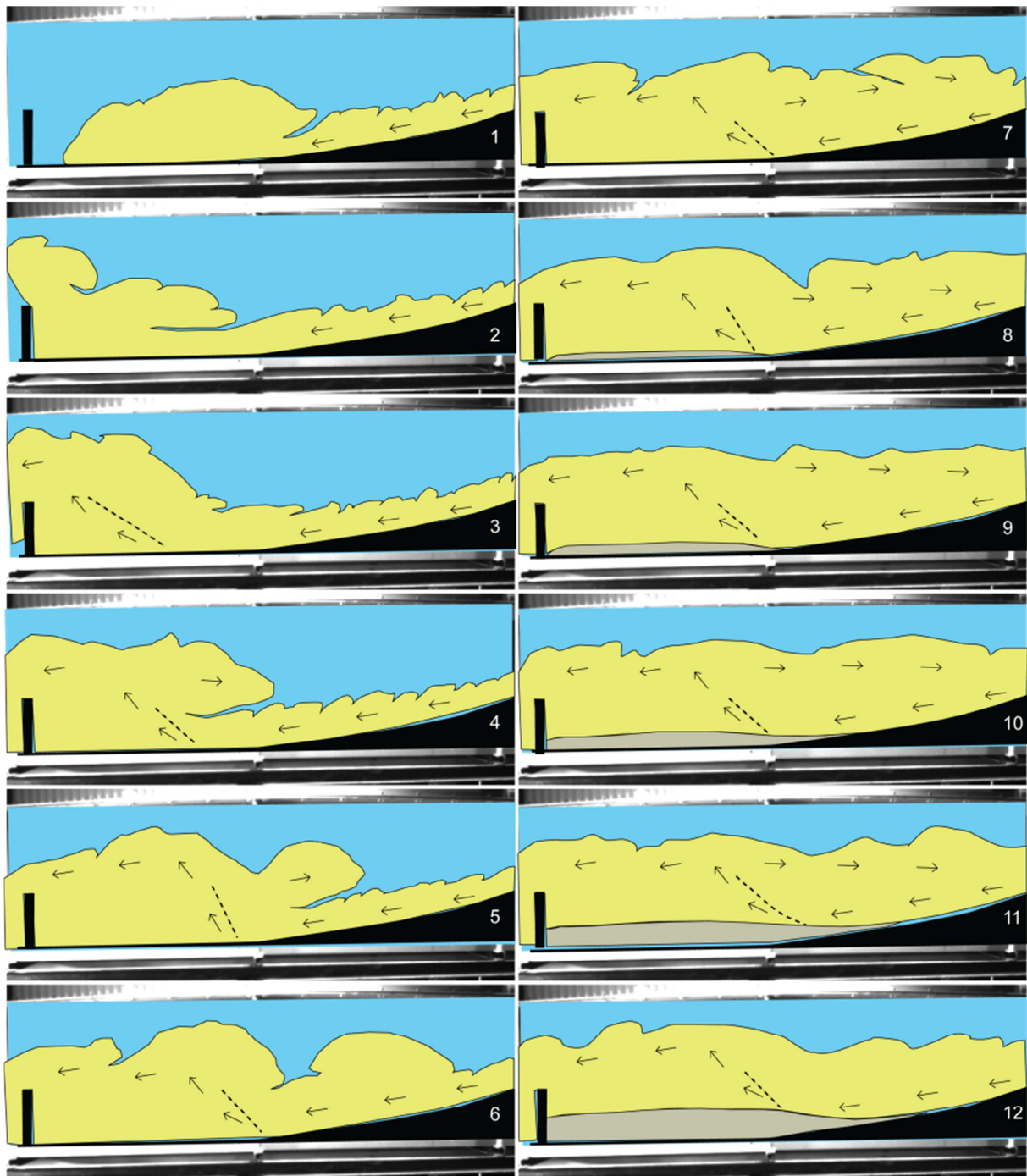


FIGURE 24: VISUALISATION OF FLOW DYNAMICS OVERDRAWING STILL FROM THE VIDEO IMAGERY OF RUN 11.

This high concentration run displays a low flow height of the head and body of the turbidity current (panels 1 to 5 in figures 23 and 24). When the current meets the weir, a backflow forms (panel 3 and 4), immediately followed by a rapidly upstream moving hydraulic jump/detachment zone (panel 3 to 5). Also see figure 25 on the next page.

The hydraulic jump / detachment zone maintains a stationary position near the end of slope (panels 6 to 12). This stationary position reinforces itself because the flow has to move more and more upslope, meeting previous deposits.

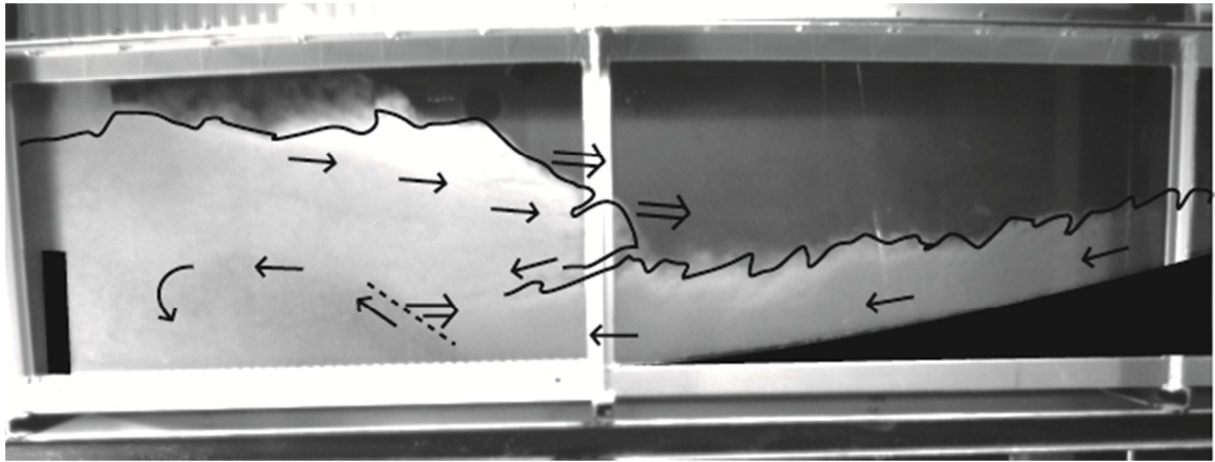


FIGURE 25: TURBIDITY CURRENT SHOWING A BACKFLOW AND HYDRAULIC JUMP / FLOW DETACHMENT MOVING UPSTREAM (INDICATED WITH DASHED LINE). MOVEMENT OF A STRUCTURE IS INDICATED WITH DOUBLE ARROW, DIRECTION OF FLOW WITH A SINGLE ARROW.

Between the hydraulic jump / DZ location and the weir, sediment remains mainly suspended and turbulent; fall-out rate is low as compared to the larger grained runs.

Deposits are laminated throughout giving it the characteristics of Bouma's Tb or Td (see figure 26). No structureless beds were observed.

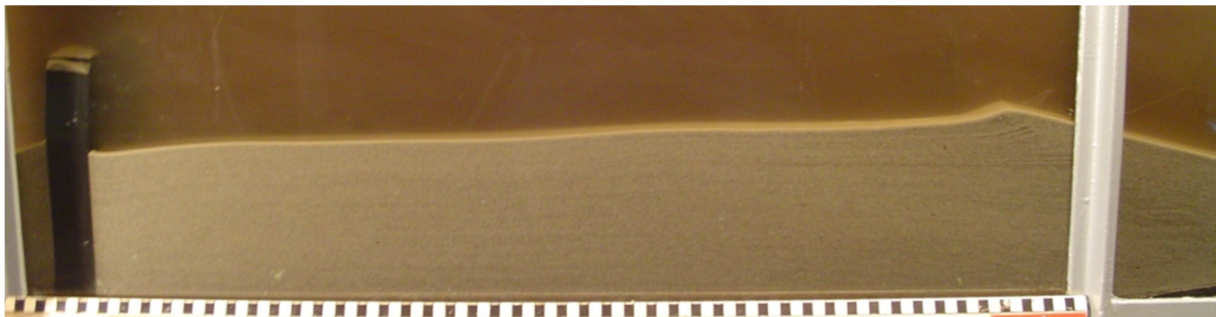


FIGURE 26: PHOTOGRAPH OF THE DEPOSITS OF RUN 3 WITH SCALE IN CMS. THE DEPOSIT IS LAMINATED THROUGHOUT. A MUD DRAPE WAS DEPOSITED ON TOP, WHEN INPUT WAS STOPPED.

At the hydraulic jump location, a small climbing ripple-like feature is left in the sediments (see figure 27). This feature is created by the mechanism described in the paragraph 'Hydraulic jump / rapidly moving detachment zone'.



FIGURE 27: PHOTOGRAPH OF A DETAIL OF THE DEPOSITS OF RUN 3, SHOWING LAMINATIONS THROUGHOUT THE DEPOSIT AND THE RIPPLE-LIKE FEATURE WHICH FORMED AT THE HYDRAULIC JUMP LOCATION.

RUN 4: AVERAGE CONCENTRATION 16.8% AND GRAIN SIZE (D_{50}) 120 μ .

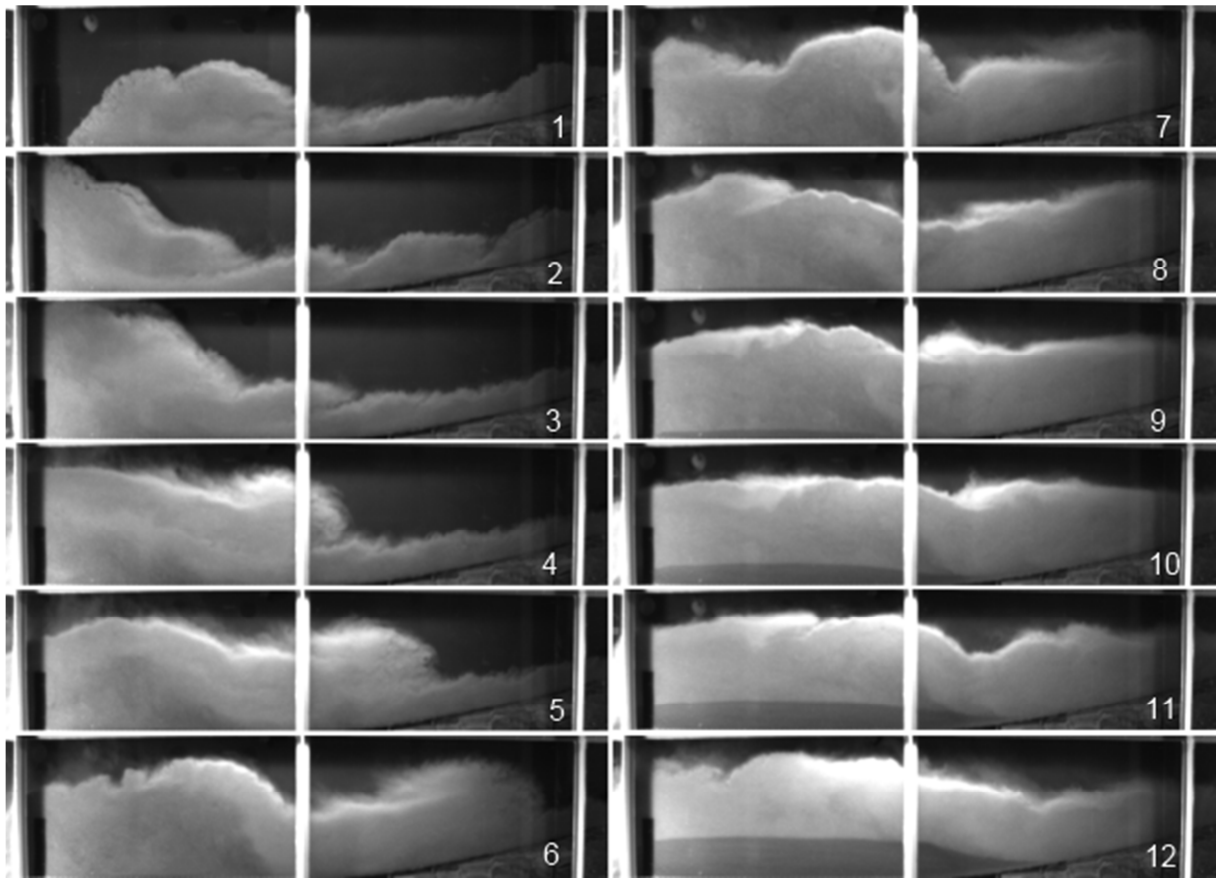


FIGURE 28: STILL FROM THE VIDEO IMAGERY OF RUN 4.

Run 4 was performed with a high average concentration of 16.8% and fine grain size of 120 μ . The measured data of run 4 is included as Appendix A4.

The actual input concentration could not be regulated completely, and it was only after the run was done that it was found that the input characteristics were the same as run 3 (exp2_).

This turbidity current follows the same sequence of events as run 3 which is a good replica of results. It produced a backflow (panel 3 to 5 and onwards in figure 28) and an upstream migrating hydraulic jump / detachment zone (panels 4 to 10). This hydraulic jump / DZ moves upstream towards a stationary position (panels 10 to 12).

Sedimentation takes place underneath the jump / DZ onwards to the weir. The bed is laminated throughout, giving it the characteristics of Bouma's Tb or Td (see figure 29). No structureless beds were observed.

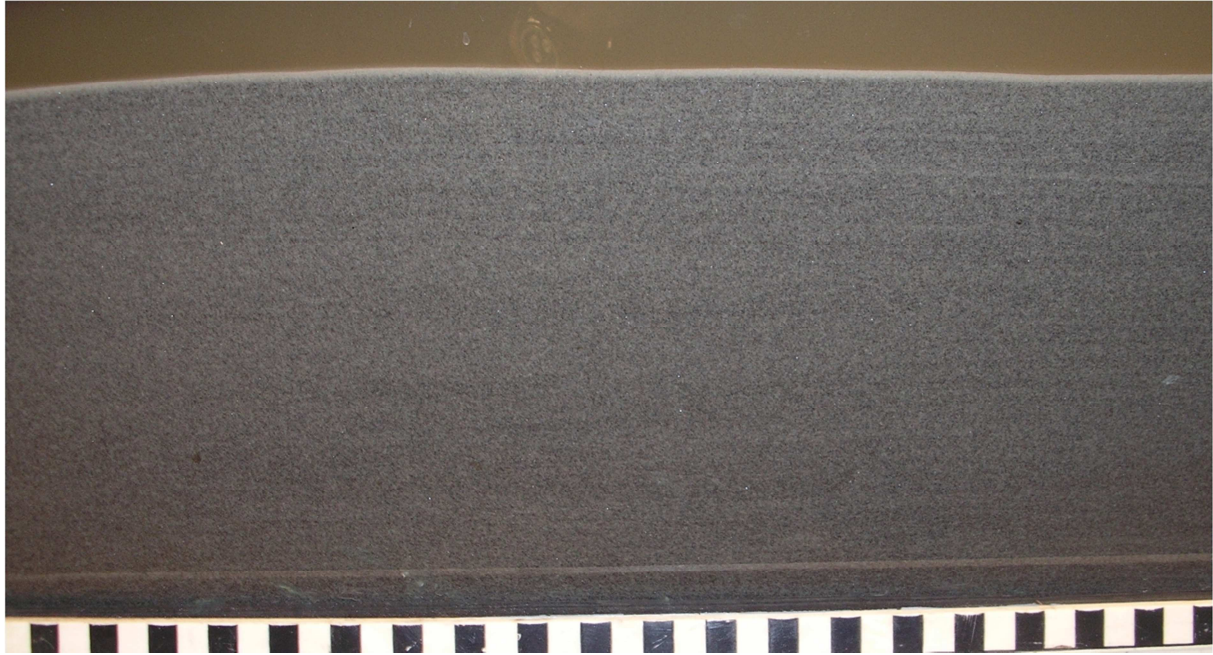


FIGURE 29: PHOTOGRAPH OF THE DEPOSITS OF RUN 4 WITH SCALE IN CMS. THE DEPOSIT IS LAMINATED THROUGHOUT. A MUD DRAPE WAS DEPOSITED ON TOP, WHEN INPUT WAS STOPPED.

At the hydraulic jump location, the only trace left in the deposits is a small climbing ripple-like feature. The formation mechanism of this feature is the local counter-directional shear direction, as described in the paragraph 'hydraulic jump / rapidly upstream moving DZ'.

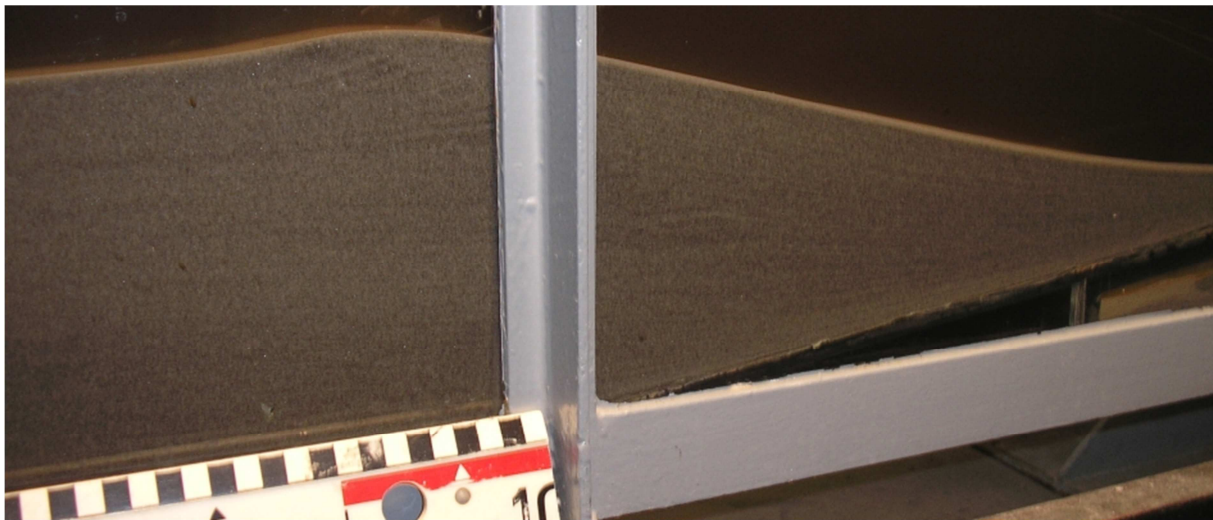


FIGURE 30: PHOTOGRAPH OF THE DEPOSITS OF RUN 4 WITH SCALE IN CMS. THE DEPOSIT IS LAMINATED THROUGHOUT. AT THE LOCATION OF THE STATIONARY HYDRAULIC JUMP A CLIMBING RIPPLE-LIKE FEATURE WAS LEFT IN THE DEPOSITS.

RUN 5: AVERAGE CONCENTRATION 21.6% AND GRAIN SIZE (D_{50}) 120 μ .

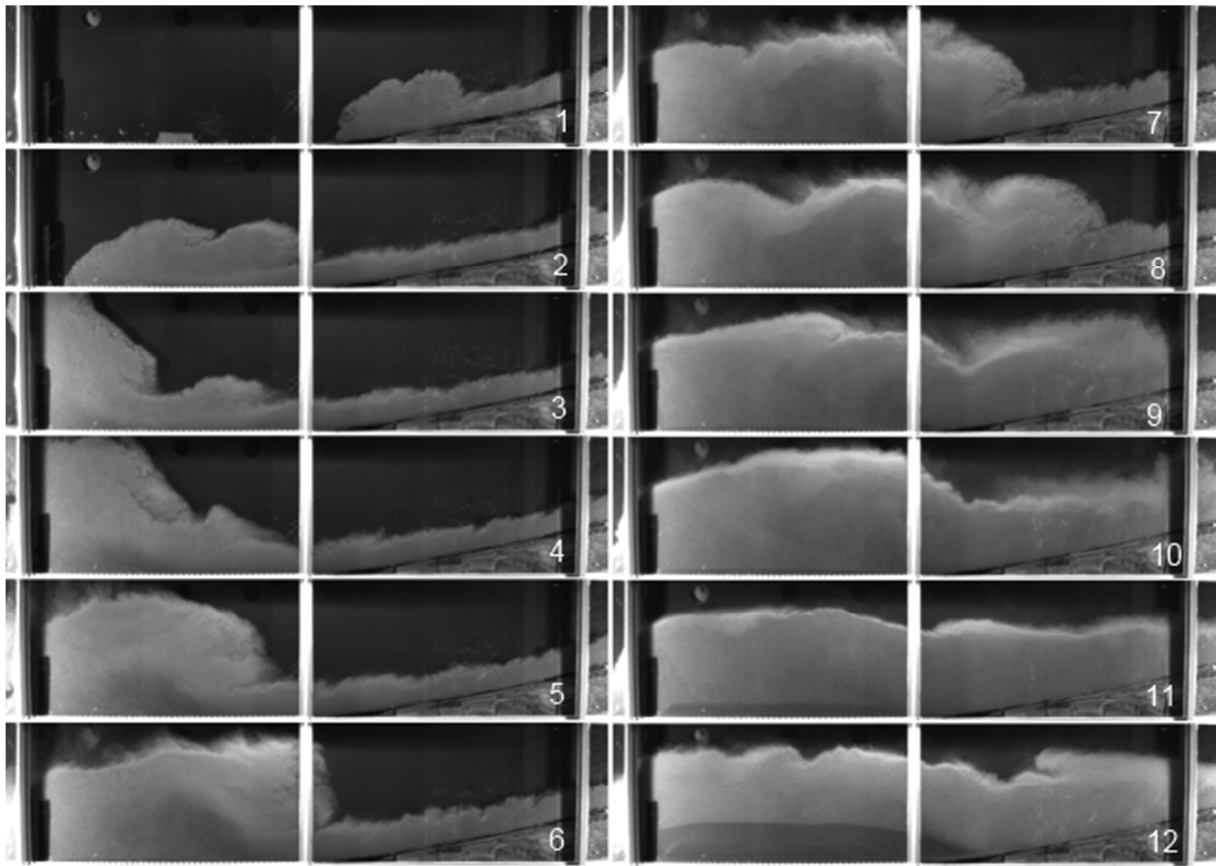


FIGURE 31: STILLS FROM THE VIDEO IMAGERY OF RUN 5.

Run 5 was performed with a high average concentration of 21.6% and fine grain size of 120 μ . The measured data of run 5 is included as Appendix A5.

This high-concentration turbidity current has a small head and low flow height (panel 1 in figure 31). When the head passes the break of slope, the head seems to form a partition into 2 parts (panel 2). The mixture meets the obstruction (panel 3) and a backflow forms (panel 5 and onwards). A hydraulic jump / DZ forms, which migrates upstream directly under the backflow (panels 4-10). The hydraulic jump / detachment zone then moves towards a stationary position (panels 11 and 12).

Deposition takes place in the same manner as in run 3 and run 4 (16,8%), starting underneath and just upstream of the detachment location. Maximum deposition is between the end of the detachment zone and the weir. The sediment bulge at the end of slope again maintains and reinforces the stationary position of the hydraulic jump / detachment zone.

The deposit is laminated throughout, giving it the characteristics of Bouma's Tb or Td (see figure 32). No structureless beds were observed.

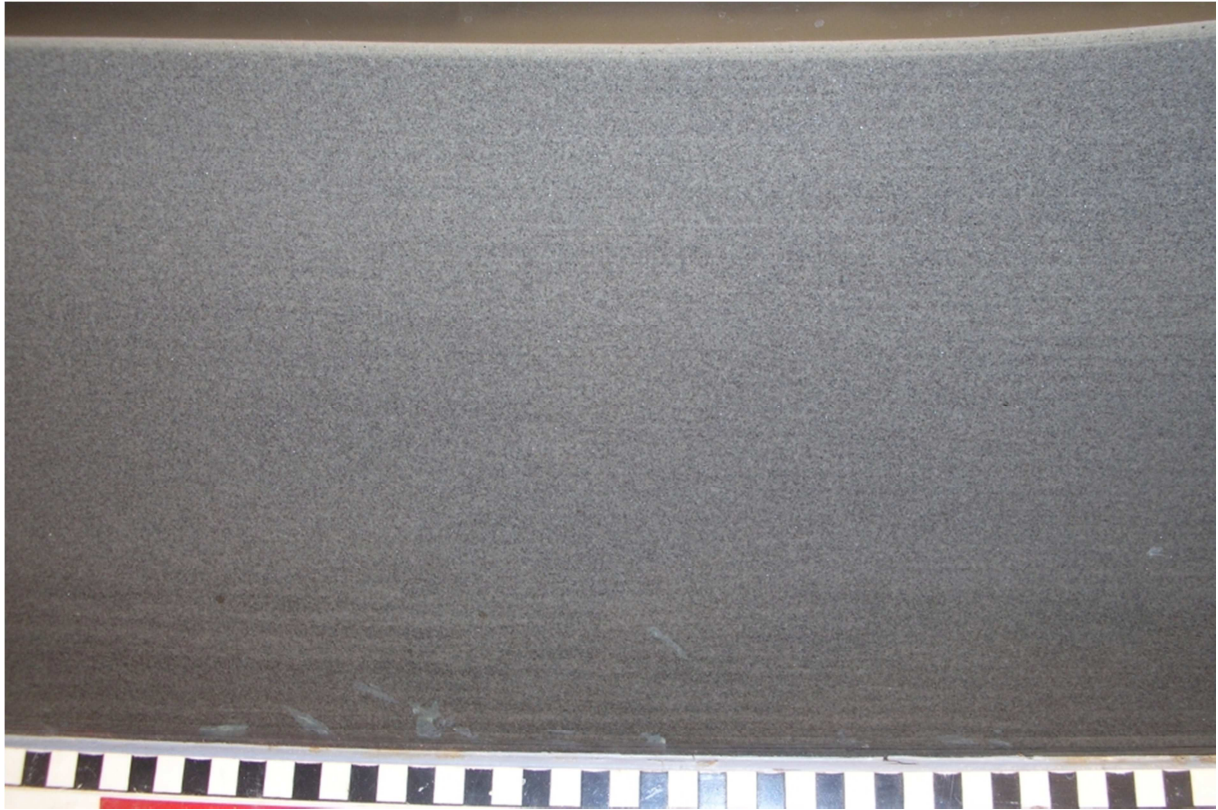


FIGURE 32: PHOTOGRAPH OF THE DEPOSITS OF RUN 5 WITH SCALE IN CMS. THE DEPOSIT IS LAMINATED THROUGHOUT.

At the hydraulic jump location, the climbing ripple-like feature in the deposit is not very pronounced in this run (figure 33).

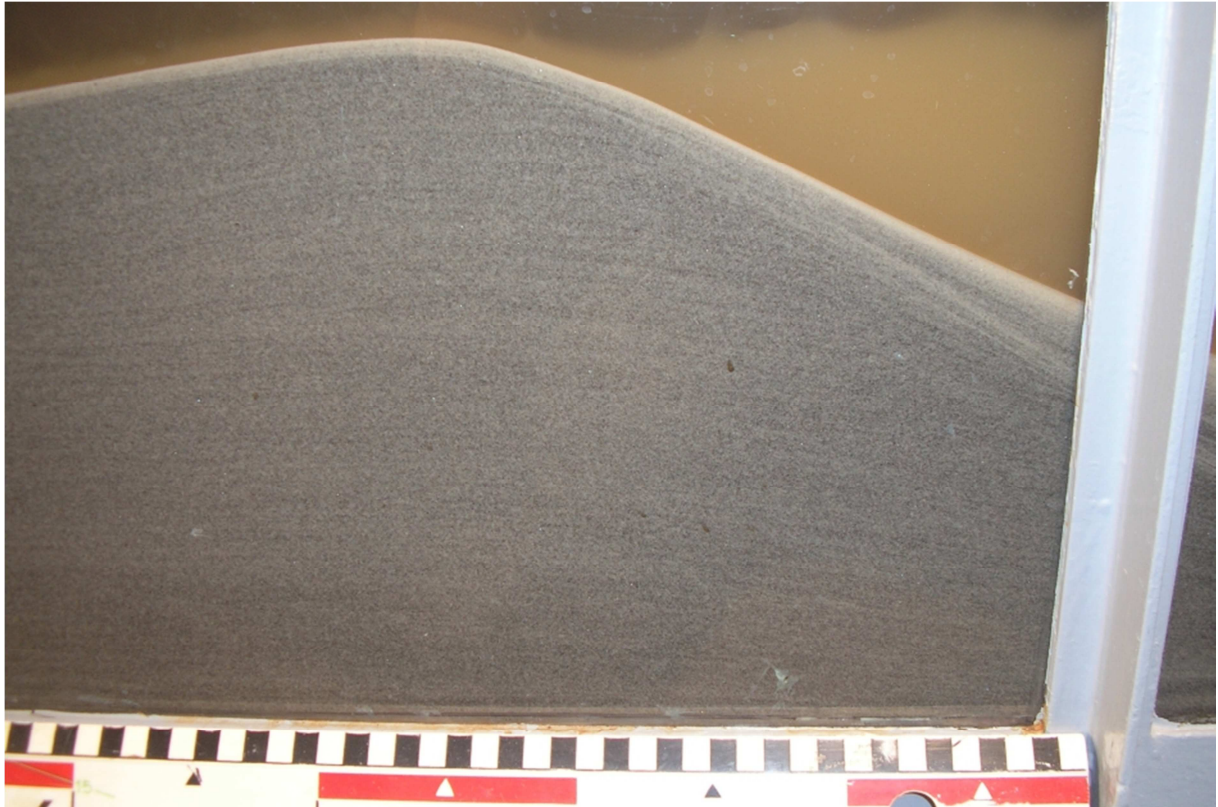


FIGURE 33: PHOTOGRAPH OF A DETAIL OF THE DEPOSITS OF RUN 5 WITH SCALE IN CMS. THE DEPOSIT IS LAMINATED THROUGHOUT. THE CLIMBING RIPPLE-LIKE FEATURE AT THE HYDRAULIC JUMP LOCATION IS NOT VERY PRONOUNCED IN THIS RUN. THE TOP 1-2 CMS IN THE RIGHT OF THE PHOTOGRAPH ARE A RESULT OF THE STOPPING OF THE FLOW AND ARE NOT TO BE INTERPRETED.

RUN 8: AVERAGE CONCENTRATION 12.9% AND GRAIN SIZE (D_{50}) 313μ .

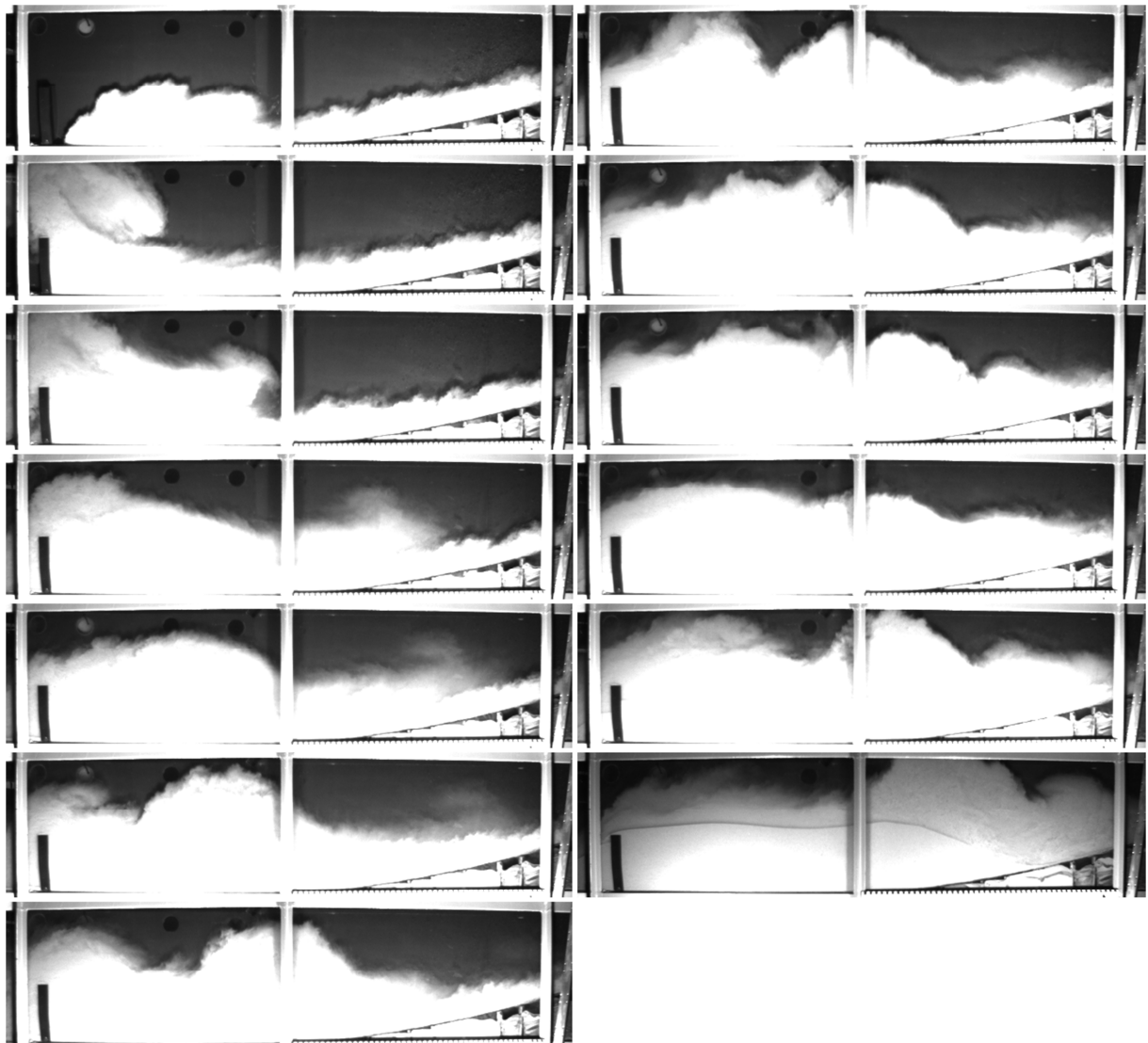


FIGURE 34: STILLS FROM THE VIDEO IMAGERY OF RUN 8.

Run 8 was performed with a medium average concentration of 12.9% and medium grain size of 313μ . The measured data of run 8 is included as Appendix A8.

Unfortunately, the lighting of this run was not done properly and the video was overexposed.

The outline of the top of the turbidity current shows the sequence of events similar to run 9 (exp10) described on the next page. A backflow and a hydraulic jump / detachment zone migrating upstream to a stationary location can be observed. In the end of the run the lighting was adjusted (see last picture) showing a stationary hydraulic jump / detachment zone and a large bulge of deposited sediment.

RUN 9: AVERAGE CONCENTRATION 15% AND GRAIN SIZE (D_{50}) 313μ .



FIGURE 35: STILLs FROM THE VIDEO IMAGERY OF RUN 9.

Run 9 was performed with medium concentration of 15% and medium grain size of 313μ . The measured data of run 9 is included as Appendix A9.

To support flow dynamics descriptions, a visualization of flow directions is included as figure 36 on the next page.

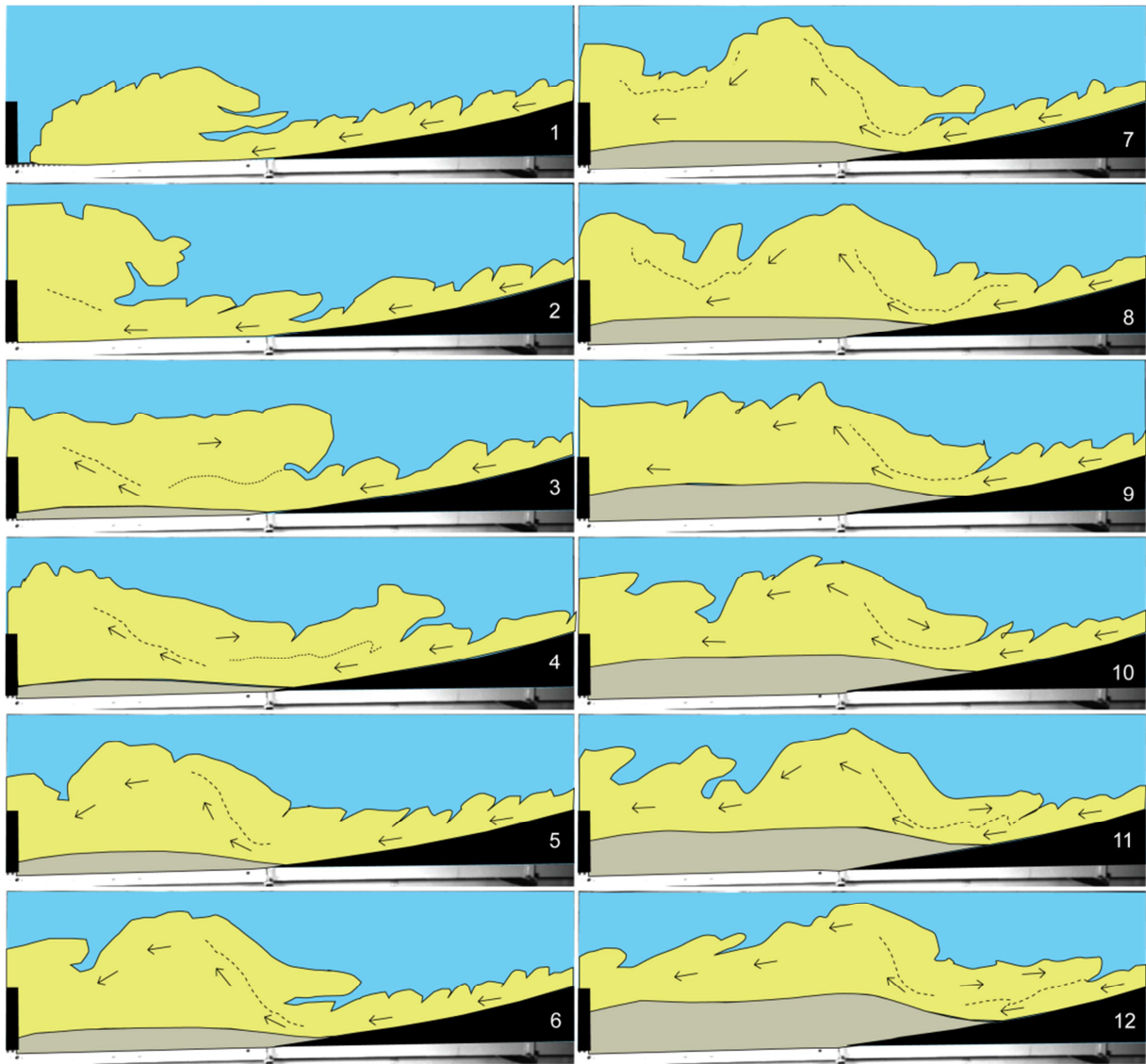


FIGURE 36: VISUALISATION OF FLOW DYNAMICS OVERDRAWING STILL FROM THE VIDEO IMAGERY OF RUN 9.

When the flow meets the weir a backflow forms (panels 1 to 4 in figures 35 and 36). A hydraulic jump / rapidly upstream moving flow detachment is observed (panels 3 to 7). This structure migrates upstream towards a stationary position (panels 8 to 12) and forms its own backflow (panels 8 to 12).

Downstream of the hydraulic jump / DZ, flow velocity increases and flow height decreases again. In other words, the Froude number is increasing again after the detachment zone / hydraulic jump. Sedimentation rate is higher than in the fine grain size runs. This is a difference in flow dynamics from the fine grain size runs where in between the jump location / DZ and the weir, flow velocity remains low, flow height high and sediment in turbulent suspension.

Deposition takes place from the slope to the weir, starting below and just upstream of the hydraulic jump / detachment zone. The thickest deposits are located below the hydraulic jump / detachment zone location. The deposit is laminated throughout, giving it the characteristics of Bouma's Tb. No structureless beds were observed. This visual observation could not be supported by a picture. It could only just be observed by eye and is not visible on photographs. This is caused by the uniform color of the sand.

RUN 10: AVERAGE CONCENTRATION 22.1% AND GRAIN SIZE (D_{50}) 313 μ .



FIGURE 37: STILLS FROM THE VIDEO IMAGERY OF RUN 10.

Run 10 was performed with a high concentration of 22.1% and medium grain size of 313 μ . The measured data of run 10 is included as Appendix A10.

Run 10 displays a succession of events similar to the other high concentration runs, like run 9:

- Arrival of the head near the weir (panel 1 and 2 in figure 37).
- part of the head 'folds' back to form a backflow (panel 2 to 4).
- a hydraulic jump / flow detachment zone forms near the weir (panel 2 to 4).
- the hydraulic jump /flow detachment zone migrates upstream (panel 3 to 7).
- hydraulic jump / flow detachment zone finds equilibrium location (panel 7 to 12).

For a more detailed description of flow dynamics and deposits I refer to description of run 9.

RUN 12: AVERAGE CONCENTRATION 28.5% AND GRAIN SIZE (D_{50}) 570 μ .



FIGURE 38: STILLS FROM THE VIDEO IMAGERY OF RUN 12.

Run 12 was performed with a high average concentration of 28.5% by volume and a coarse grain size of 570 μ . The measured data of run 12 is included as Appendix A12.

Sedimentation rate is high and deposition takes place already at the slope (panel 1 and onwards in figure 38). In a short amount of time sediment of large grain population is deposited from the inlet to the weir. The finer grained sediment population has formed a turbidity current on top of the deposits and has mostly bypassed deposition before the weir.

The deposit is laminated throughout, giving it the characteristics of Bouma's Tb (figure 39). No structureless beds were observed.



FIGURE 39: PHOTOGRAPH OF THE DEPOSITS OF RUN 12 WITH SCALE IN CMS. THE DEPOSIT IS LAMINATED THROUGHOUT.

DISCUSSION

In this section trends in the dataset are analyzed and the research topics are discussed:

- What influence does sediment concentration have on flow dynamics and deposits?
- What influence does grain size have on flow dynamics and deposits?
- Which runs displayed a hydraulic jump?
- Which deposits can be related to the hydraulic jump?
- Limitations of the experiments
- Further research recommendations

WHAT INFLUENCE DOES SEDIMENT CONCENTRATION HAVE ON FLOW DYNAMICS AND DEPOSITS?

Concentration appears to influence the turbidity current and its deposits in multiple ways.

It is assumed that the distinction between low and high concentration runs is to be made at 9% concentration because there, different support mechanisms of the sediment-water mix meet (Bagnold, 1954). Fully turbulent mixtures are considered to have a maximum concentration of 9%, and in mixtures with a concentration higher than 9%, grain-to-grain interactions become important (Bagnold, 1954). Above 9% concentration the flow is able to form a high density 'traction carpet' at the base of the flow (Sohn, 1997).

In my experiments, it is indeed observed that the turbidity currents with concentrations lower than 9% (between 4.0% and 7.0%) displayed significantly different flow dynamics from the turbidity currents with concentrations higher than 9% (between 12.9% and 30%).

LOW CONCENTRATION RUNS

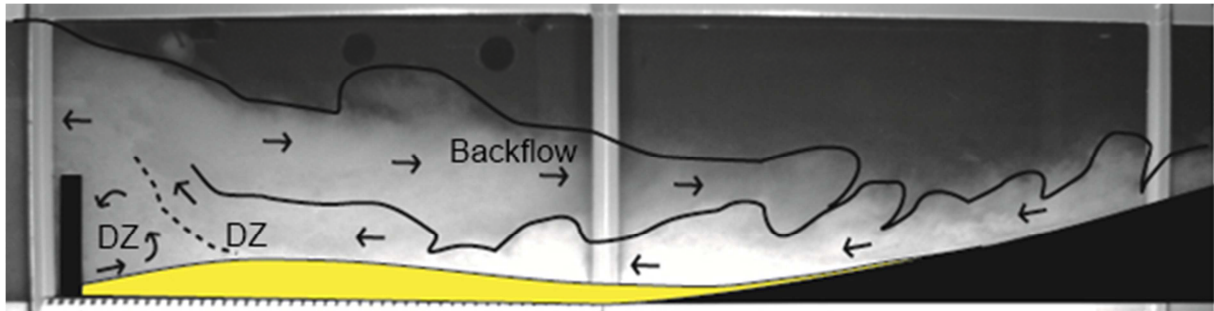


FIGURE 40: DEPICTION OF FLOW DYNAMICS AND PHENOMENA IN A LOW CONCENTRATION RUN.

The turbidity currents with low concentrations do not show a clear hydraulic jump near the obstruction. The low concentration turbidity currents initially create a small flow detachment zone near the obstruction. Here, a small stationary turbulence vortex-like circulation pattern develops. The rest of the flow can move over this stationary circulating cell and the obstruction (figure 40).

Sedimentation takes place by fall-out under the turbidity current, exerting some shear on the fresh deposits. The deposits are laminated throughout and interpreted as Bouma's Tb. No structureless beds were observed in the low concentration runs.

HIGH CONCENTRATION RUNS

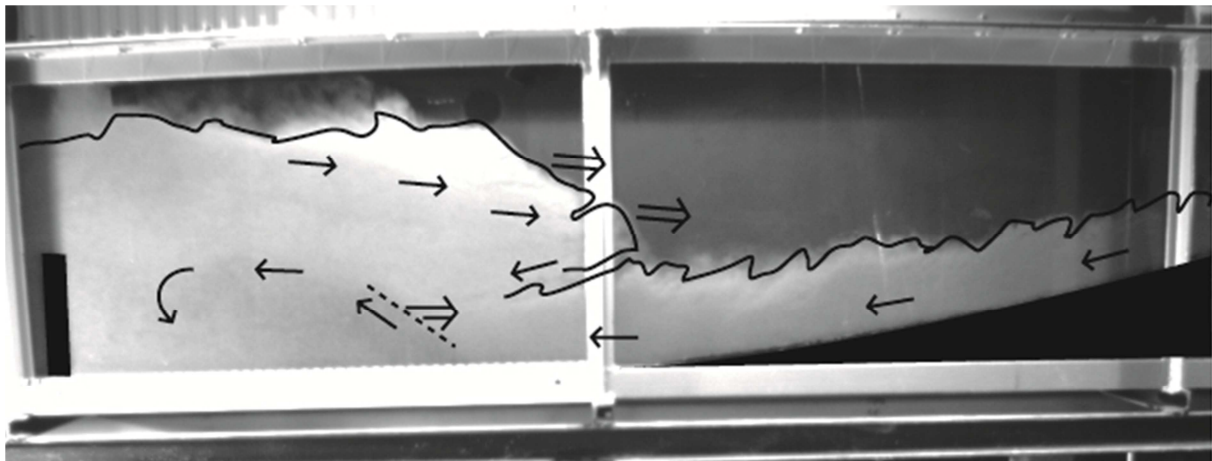


FIGURE 41: FLOW DYNAMICS AND PHENOMENA IN A HIGH CONCENTRATION RUN.

The turbidity currents with high concentrations show, judging by flow dynamics only, a clear hydraulic jump, which starts where the flow meets the weir (figure 41). The hydraulic jump is observed to migrate upstream in all high concentration experiments, except for run 12.

The occurrence of a hydraulic jump causes a difference in depositional environment. The low concentration runs deposit sediment underneath a stable flowing turbidity current. The high concentration runs show more energetic flow dynamics at the jump location (as shown in figure 10). Even though there are different depositional mechanisms, there is almost no difference visible the fabric of the deposits between low and high concentration runs.

At the hydraulic jump location, some high concentration runs show a climbing-ripple like feature, a result from the low shear location where flow is locally counter-directional.

Because of high concentration and large grain size run 12 deposited all of its sediment in a very short time after which it behaved as a low concentration run.

CONCENTRATION PROFILES

The segregation of high density turbidity currents into two different layers creates a difference in concentration in the two layers. The bottom layer has a higher sediment concentration and density. Unfortunately, this concentration/density profile could not be measured in these experiments. An upgrade in the experimental setup is needed to provide for this kind of measurements. At first instance, the video data could not positively determine the existence of 2-phase flow.

Closer examination of the imagery enabled me to create velocity profiles for a few, but not all, runs. In order to obtain the velocity profiles it was necessary to follow individual grains in frames of the filmed experiments. This proved to be unsuccessful for the fine grained runs. In the medium grained runs it was possible for run 7 (exp9, 7%), run 9 (exp10, 15%) and 10 (exp8, 22%). The concentration profiles that were constructed show that the bottom layer is moving faster than the top layer (figures 42 and 43). The bottom layer was also observed to flow less turbulently than the top layer.

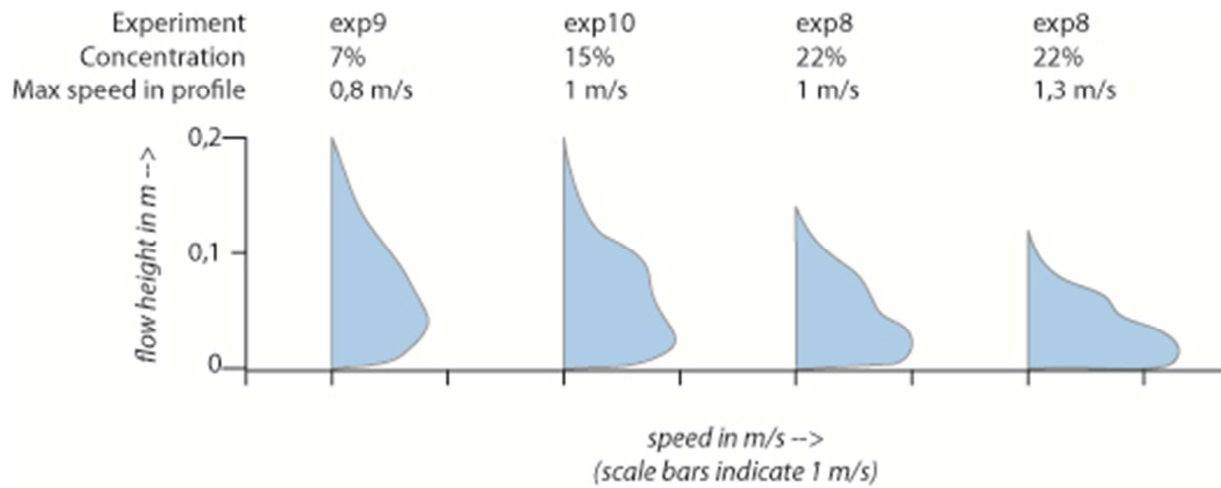


FIGURE 42: VELOCITY PROFILES IN TURBIDITY CURRENTS AS CAPTURED FROM STILLS OF HIGH-SPEED MOVIES OF THE TURBIDITY CURRENT EXPERIMENTS. HIGH CONCENTRATION RUNS DEVELOPED A HIGH DENSITY BOTTOM LAYER TRAVELLING FASTER THAN THE HIGHER LOWER DENSITY PART.

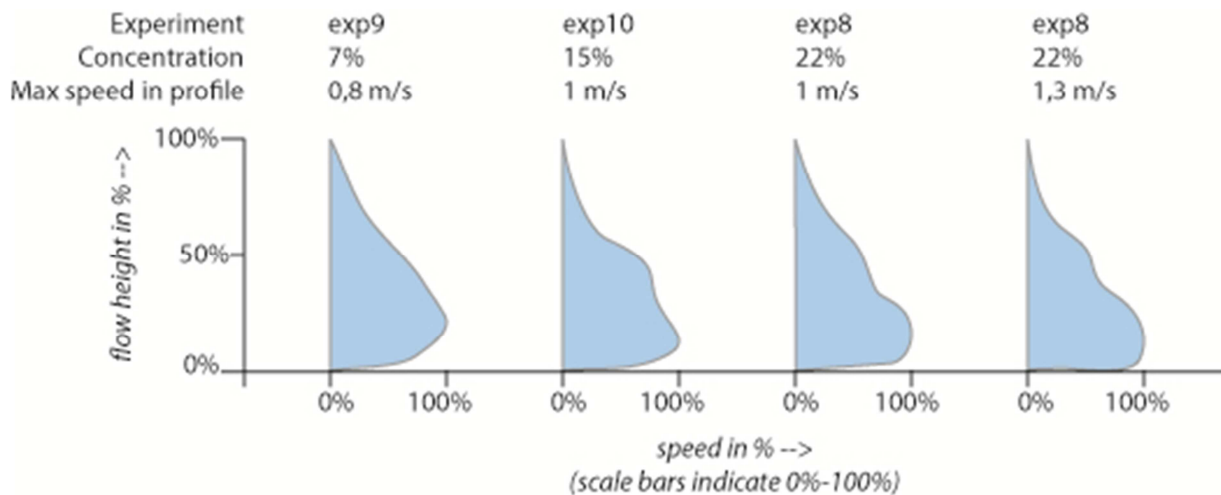


FIGURE 43: NORMALIZED VELOCITY PROFILES IN TURBIDITY CURRENTS AS CAPTURED FROM STILLS OF HIGH-SPEED MOVIES OF THE TURBIDITY CURRENT EXPERIMENTS. HIGH CONCENTRATION RUNS DEVELOPED A HIGH DENSITY BOTTOM LAYER TRAVELLING FASTER THAN THE HIGHER LOWER DENSITY PART.

WHAT INFLUENCE DOES GRAIN SIZE HAVE ON FLOW DYNAMICS AND DEPOSITS?

INFLUENCE OF GRAIN SIZE IN LOW CONCENTRATION RUNS

The low concentration runs are all intercomparable with respect to flow dynamics. Small grain sizes accommodated for the backflow to remain present throughout the run. The fine grained sediment was maintained in suspension longer than the medium and coarse grained sediment. Larger grain sizes caused a higher sedimentation rate and thus thicker deposits. The location of thickest deposits is more upstream for larger grain size runs. Deposits with all three grain sizes are laminated throughout, giving it the characteristics of Bouma's Tb. No structureless sand beds were observed.

INFLUENCE OF GRAIN SIZE IN HIGH CONCENTRATION RUNS

The fine grain size runs (120μ) show a large low-velocity suspended sediment volume between the jump location and the weir. Deposition downstream of the jump with the fine grained runs consists mainly of suspension fallout with a relatively low settling velocity or fall-out rate. This argues for an interpretation of the deposits as Bouma's Td.

The medium grain size runs (313μ) show a supposed hydraulic jump moving upstream without this growing downstream zone of suspended sediment. In fact, downstream of the jump, the flow is seen to increase in speed and decrease in flow height thus increasing its Fr' number.

Deposition downstream of the jump is less influenced by suspension fallout and relatively more by the movement this 'new' turbidity current. This argues for an interpretation of the deposits of Bouma's Tb.

The experiments with the coarsest grain size (570μ) did not produce a hydraulic jump. In fact, the sediment fall-out rate of this sand was so high, that the largest part of the fully suspended mix was deposited on the ramp in the flume. The turbidity current that remained consisted of the finer fraction of the sand and was low in concentration. No jump was observed in this low-concentration turbidity current.

Deposits with all three grain sizes are laminated throughout, giving it the characteristics of Bouma's Tb or in some fine grained runs as Td. No structureless sand beds were observed.

WHICH RUNS DISPLAY A HYDRAULIC JUMP?

Observation of the flow characteristics shows what appears to be a hydraulic jump in runs 3, 4, 5, 8, 9 and 10. These are the high concentration runs with fine and medium grain size.

To determine whether these runs indeed displayed a hydraulic jump, the Fr' numbers of the flow in the upstream part of the flume need to be higher than 1, indicating supercritical flow state.

Two methods were used to calculate Fr' numbers (as elaborated below). The first method is to calculate overall Fr' numbers, using measurements in the upstream part of the turbidity current. This method does not account for Fr' differences in the two layers of 2-phase flows and is therefore considered not sufficient for the runs 3, 4, 5, 8, 9 and 10. The second method is calculation of partial Fr' numbers of the bottom layer of a 2-phase flow.

The data used for these calculations are:

- Time averaged input concentration (centrifuged samples) to determine density (ρ_{mix} in formula)
- Height averaged flow velocity (corrected EMS measurement) (U_{avg} in formula)
Here, a correction was needed to transform the measured in-pipe flow velocity into average in-flume flow velocity. I elaborate on this correction below.
- Flow height approximately 0.4 m downstream of the input location, from imagery (h in formula)
Flow height could best be correctly measured when fairly steady (i.e. no surges) and with a distinguishable interface between the flow and the ambient water. This was the case for the high concentration runs 3, 4 and 5, (fine grain size) and runs 8, 9 and 10 (medium grain size).
- Velocity profiles are used to obtain partial flow velocities and partial flow heights for the 2-phase flow partial Fr' number calculation. Unfortunately, velocity profiles could only be constructed for run 7 (exp9), run 9 (exp10) and run 10 (exp8).

FLOW VELOCITY MEASUREMENTS AND CORRECTIONS

Flow velocity is not measured in the flow itself, but directly at the point where the sediment-water mix leaves the inlet tube. This measurement thus represents the velocity in the tube, instead of in the flume. Therefore flow velocity needs to be recalculated.

Assuming an equal discharge in the tube and in the most upstream part of the flume, the measured flow velocity can be corrected:

Assumption: $Q_{input} = Q_{flow}$ or $A_{input} * U_{input} = A_{flow} * U_{flow}$ gives

$$U_{flow} = Q_{input} / A_{flow}$$

Two things are important for this correction:

- Velocity profile within the tube, wall effect.
Is measured flow velocity U equally distributed in the tube?
- Measuring location and spreading of the flow outside the tube.
Is the surface area A at measuring location equal to the surface area of the inside of the tube?

These two questions are answered below so that U_{flow} can be calculated.

- Is measured flow velocity U equally distributed in the tube?

The velocity profile within the tube is related to the Reynolds number of the flow. The Reynolds number describes the ratio of inertial forces to viscous forces in the flow. Using this number, the flow can be characterized as laminar or turbulent. At a low Reynolds number, viscous forces are dominant and laminar flow occurs. At high Reynolds numbers, inertia forces are dominant and a turbulent flow occurs.

Here, the following equations for Reynolds number for flow in a pipe will be used:

$$Re = \rho U D / \mu \quad \text{where}$$

ρ = density of the fluid	[kg/m ³]
U = mean velocity	[m/s]
D = diameter of the pipe or tube	[m]
μ = dynamic viscosity	[Pa.s] or [N.s/m ²] or [kg/m.s]

In the experiments of this research densities are between 1070 and 1470 kg/m³, mean velocities are between 1.2 and 2 m/s. The inside diameter of the tube is 0.032 m.

The dynamic viscosity depends on particle concentration and needs to be calculated using empirical formulae. This was done by entering the highest concentration 28.5% into 3 empiric relations for dynamic viscosity of sand-water mixtures also used in Völtz et al, 2000.

$$\frac{\mu_2}{\mu_1} = \mu_r = \left(1 - \frac{\phi}{\phi_{\max}}\right)^{-2.5\phi_{\max}} \quad \text{with } \phi_{\max} = 0.63 ,$$

$$\frac{\mu_2}{\mu_1} = \mu_r = \left(1 + \frac{0.75}{(\phi_{\max}/\phi) - 1}\right)^2 \quad \text{with } \phi_{\max} = 0.605 ,$$

$$\frac{\mu_2}{\mu_1} = \mu_r = \frac{1}{[1 - (\phi/\phi_{\max})^{1/3}]} \quad \text{with } \phi_{\max} = 0.625$$

The three empirical formulae are from Krieger & Dougherty, 1959; Chong et al, 1971; Frankel & Acrivos, 1967. In this formulae μ_2 = dynamic viscosity index of the mix, μ_1 = dynamic viscosity index of water and Φ = packing density or volumetric concentration of the sand. So if the result of the formula equals 2.0 the mix has a dynamic viscosity of 2.0 that of water. Dynamic viscosity of water is approximately 0.001 Pas at 20 degrees Celsius. Results of the three formulae for 28.5% volumetric concentration are 2.58, 2.78 and 1.22 respectively. The highest value is used.

This means that Reynolds numbers were between

$$Re = \{[1070-1470] * [1.2-2] * 0.032 / [0.00278-0.001]\} = 1.5 * 10^4 \text{ and } 9.4 * 10^4$$

$$Re = \{[\text{density range}] * [\text{velocity range}] * \text{diameter} / [\text{dynamic viscosity range}]\}$$

which means that in all experiments flow through the tube was fully turbulent. The velocity profile within the tube is therefore most similar to velocity profile 3 in figure 44. As a result, the measured flow velocity v equals the average flow velocity within the tube and does not need to be corrected for wall effect in the discharge Q calculations.

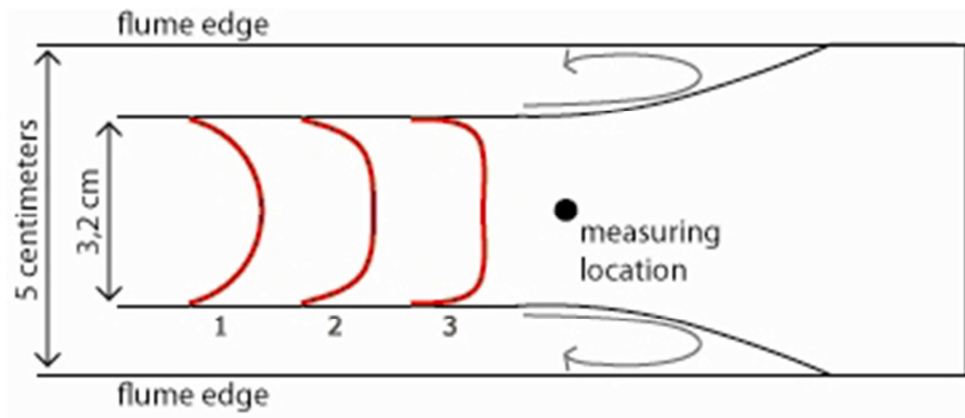


FIGURE 44: FLOW VELOCITY PROFILES WITHIN A TUBE. 1 SHOWS A MORE LAMINAR FLOW PATTERN, 3 SHOW THE MOST TURBULENT FLOW PATTERN.

- Is the surface area A at measuring location equal to the surface area of the inside of the tube?

The measurement point of the EMS is located less than 1 cm outside the tube (see figure 45). The surface area A within the tube is 804 mm², minus the surface blocked by the measurement device is 724 mm². Assuming an expansion of the flow of ~10%, the surface area A to work with is 800mm².

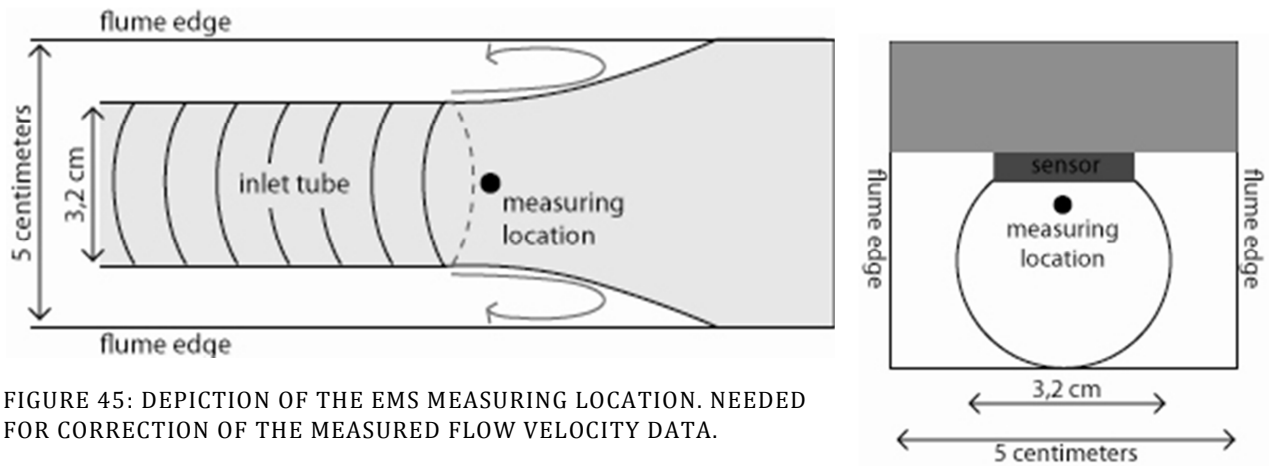


FIGURE 45: DEPICTION OF THE EMS MEASURING LOCATION. NEEDED FOR CORRECTION OF THE MEASURED FLOW VELOCITY DATA.

Having answered these two questions gives the following equation for calculation of flow velocity within the flume:

$$U_{\text{flow}} = Q_{\text{input}} / A_{\text{flow}}$$

$$U_{\text{flow}} = [0.0008 * U_{\text{input}}] / [0.05 * h]$$

This equation is used to obtain the Fr' numbers in table 4 on the next page.

CALCULATION OF OVERALL FROUDE NUMBERS

Knowing flow height, density (via concentration) and overall flow velocity, overall Fr' can be calculated. No entrainment of ambient fluid is considered in these results.

Run nr.	Name	Discharge Q in m ³ /s	Flow height h in m	Average corrected flow velocity U in m/s	Average concentration by volume	Fr'
<i>Low concentration runs</i>						
1	exp1_	0.001264	0.155	0.163	4.7%	0.47
2	exp4	0.001584	0.122	0.260	6.7%	0.72
6	exp11	0.001064	0.084	0.253	4.4%	1.03
7	exp9_	0.000984	0.101	0.195	7.0%	0.58
11	exp12	0.001056	0.055	0.384	4.3%	0.76
<i>High concentration runs</i>						
3	exp2_	0.001544	0.119	0.259	16.8%	0.46
4	exp3	0.001440	0.095	0.303	16.8%	0.60
5	exp5	0.001048	0.085	0.247	21.6%	0.45
8	exp7	0.001192	0.123	0.194	12.9%	0.38
9	exp10	0.001152	0.109	0.265	15.0%	0.41
10	exp8	0.001112	0.084	0.211	22.1%	0.48
12	exp13	0.001199	0.106	0.226	28.5%	0.83

TABLE 4: CALCULATED OVERALL FR' NUMBERS FOR ALL THE RUNS.

The overall Fr' numbers that were calculated indicate that flow states were all subcritical, except for run 6 where calculated Fr' number is 1.03.

However, analysis of the flow dynamics in the Results section indicates that the high concentration runs (3, 4, 5, 8, 9 and 10) did go through the hydraulic jump. These were the 2-phase turbidity currents. The measured velocity profiles and visible concentration layers indicate that there is an interface between the two layers, theoretically enabling the two layers have different Froude numbers. Calculation of one Froude number for a 2-phase flow is concluded to be inadequate. For the 2-phase runs partial Fr' numbers of the bottom layer are calculated in the next paragraph.

CALCULATION OF PARTIAL FR' NUMBERS

The results show a clear difference in flow dynamics between (supposedly 1-phase) low concentration runs and (supposedly 2-phase) high concentration runs 3, 4, 5, 8, 9 and 10. The reconstructed flow velocity profiles of runs 9 and 10 show different flow velocities for the two layers. If a distinction can be made between the two layers, partial Fr' numbers can be calculated. These partial Fr' numbers are better fit to explain the observed flow dynamics, as the overall Fr' numbers do not account for different flow velocities and densities in the two layers. Therefore, the overall Fr' numbers represent a skewed view of the criticality of the 2-phase flows. It is expected that the partial Fr' numbers will indicate supercriticality of the lower layer, which would better explain the observed flow dynamics, i.e. hydraulic jumps that seem to occur in the mentioned runs.

A difficulty in calculating the Fr' numbers of the bottom layer of a 2-phase flow will be that it depends on the density of the upper layer, as

$$Fr' = U / \sqrt{(g' * h)}$$

because

$$g' = g * ((\rho_{mix} - \rho_{ambient}) / \rho_{ambient}).$$

With a partial Fr' calculation for the bottom layer only, $\rho_{ambient}$ is no longer the density of the ambient water, but the density of the ambient overriding low density upper flow layer.

The exact concentrations within the flow are not measured but are needed for the calculation. Trying to solve this problem, I make three assumptions, using the 9% criterion of Bagnold (1954).

Assumption 1): The upper layer has a total particle concentration not higher than 9%.

Assumption 2): The base of the upper layer has a concentration of 9%, the top 0%. Assuming a linear concentration profile the average concentration of the upper layer is therefore 4.5%.

Assumption 3): The bottom layer has a particle concentration not lower than 9%.

Below, partial Fr' numbers are calculated step by step for the lower layer of the 2-phase flow in run 10 (exp8). Using the same calculation the partial Fr' number for the lower layer of run 9 is obtained.

Unfortunately, these were the only runs where experiment results allowed these calculations. Concentration profiles could not be constructed for all runs because of unfit measurements. The velocity profiles had to be constructed by visual analysis of grains. Image resolution was not adequate to do so for the fine grain size runs of interest (run 3, 4 and 5). The high speed video of the third medium grain size run of interest (run 8) was overexposed, making it unusable.

Calculation of partial Fr' number for run 10 (exp8):

Input variables

total concentration:	22%	[%]	<i>measured</i>
averaged concentration upper layer:	4,5%	[%]	<i>assumption 2</i>
concentration at base upper layer:	9%	[%]	<i>assumption 2</i>
flow height upper layer:	0,04 to 0,08 (wavy)	[m]	<i>measured from imagery</i>
flow height lower layer:	0,04	[m]	<i>measured from imagery</i>
flow velocity upper layer:	0,4	[ms ⁻¹]	<i>measured from imagery</i>
flow velocity lower layer:	1,16	[ms ⁻¹]	<i>measured from imagery</i>
density sand:	2650	[kgm ⁻³]	
density water:	1000	[kgm ⁻³]	

Derived variables

relative flow velocity of bottom layer:	0.76	[ms ⁻¹]	<i>U_{lower} minus U_{upper}</i>
sediment concentration lower layer:	39.5% to 57%	[%]	<i>see step 1 below</i>
ρ_{ambient} :	1148.5	[kgm ⁻³]	<i>see step 2 below</i>
ρ_{mix} :	1651.75 to 1940.5	[kgm ⁻³]	<i>see step 3 below</i>
g' :	4.299 to 6.765	[ms ²]	<i>see step 4 below</i>

Step 1: calculating concentration in the lower layer C_{lower}

Using mass conservation and the 3 assumptions the distribution of sediment through the two layers can be calculated.

[total flow height * average concentration] must equal [height of the lower layer * concentration of the lower layer] + [height of the upper layer * concentration of the upper layer].

Rewriting this equation:

$$H_{total} * C_{avg} = h_{lower} * C_{lower} + h_{upper} * C_{upper}$$

$$C_{lower} * h_{lower} = H_{total} * C_{avg} - h_{upper} * C_{upper}$$

$$C_{lower} = (H_{total} * C_{avg} - h_{upper} * C_{upper}) / h_{lower}$$

Since flow height of the upper layer is measured to be 0,04m to 0,08m, a minimum and maximum concentration can be calculated:

$$C_{lower-min} = (0.08 * 22\% - 0.04 * 4.5\%) / 0.04 = 39.5\%$$

$$C_{lower-max} = (0.12 * 22\% - 0.08 * 4.5\%) / 0.04 = 57\%$$

Step 2: calculating $\rho_{ambient}$

assuming a concentration of the maximum 9% at the bottom of the upper layer, $\rho_{ambient}$ can be calculated:

$$\rho = \%sand * density\ sand + \%water * density\ water$$

$$\rho_{ambient} = 0.09 * 2.65 + 0.91 * 1 = 1.1485$$

Step 3: calculating ρ_{mix}

$$\rho = \%sand * density\ sand + \%water * density\ water$$

$$\rho_{mix-Clowermin} = 0.395 * 2.65 + 0.605 * 1 = 1.65175$$

$$\rho_{mix-Clowermax} = 0.57 * 2.65 + 0.43 * 1 = 1.9405$$

Step 4: calculating g'

$$g'_{Clowermin} = 9.81 * ((1.65175 - 1.1485) / 1.1485) = 4.299$$

$$g'_{Clowermax} = 9.81 * ((1.9405 - 1.1485) / 1.1485) = 6.765$$

Using these values the partial Fr' number for the lower layer can be calculated:

$$Fr' = U / \sqrt{g' * h} \quad \text{where} \quad g' = g * ((\rho_{\text{mix}} - \rho_{\text{ambient}}) / \rho_{\text{ambient}})$$

$$\text{Run 10 partial } Fr'_{C_{\text{min}}} = 0.76 / \sqrt{4.299 * 0.04} = 1.83$$

$$\text{Run 10 partial } Fr'_{C_{\text{max}}} = 0.76 / \sqrt{6.829 * 0.04} = 1.45$$

This calculation assumes an equal flow height for the lower layer in both cases. Entrainment in any layer is not considered in these calculations.

This indicates a range of Fr'-numbers of the lower layer in run 10 between 1.45 and 1.83 or slightly supercritical.

If instead of a sediment concentration of 9% in the top layer, the average 4.5% is taken to calculate ρ_{ambient} , then Fr'-numbers of the bottom layer are between 1.35 and 1.65.

In the same manner the partial Fr' number can be calculated using the two other velocity profiles, which are a second measurement of run 10 (exp8, 22%) and one of run 9 (exp10, 15%).

Following the same steps as described above:

$$\text{Run 10, second measurement: Partial } Fr' = 0.6 / \sqrt{6.27 * 0.05} = 1.07 \quad [\text{with } C=53,5\%]$$

$$\text{Run 9: Partial } Fr' = 0.6 / \sqrt{3.918 * 0.065} = 1.19 \quad [\text{with } C=36,8\%]$$

In conclusion, the calculated overall Fr' numbers indicate subcritical flow in almost all of the runs. However, observation of the flow dynamics indicates the occurrence of a hydraulic jump (and therefore supercritical flow) in the fine and medium sand runs of high concentration (runs 3, 4, 5, 8, 9 and 10). Calculation of partial Fr' numbers for the bottom layer of runs 9 and 10 support this observation by indicating supercritical flow.

However, one should realize that there is a high uncertainty in the concentration and velocity measurements. The surging nature of turbidity current flow complicates the measurement of flow height and velocity profiles with the limited sensors available. The concentration measurement is only an average of the input throughout the duration of the run. Actual input concentration decreased from the beginning of the runs. Concentration profiles could not be measured.

This leaves my determination of Fr' numbers inconclusive.

WHICH DEPOSITS CAN BE RELATED TO THE HYDRAULIC JUMP?

BEDFORMS

In their study, Postma et al (2009) have constructed a 3-dimensional bed form stability diagram including 1-phase and 2-phase turbidity currents (see Figure 46). This bed form stability diagram will be used interpreting deposits of the experiments.

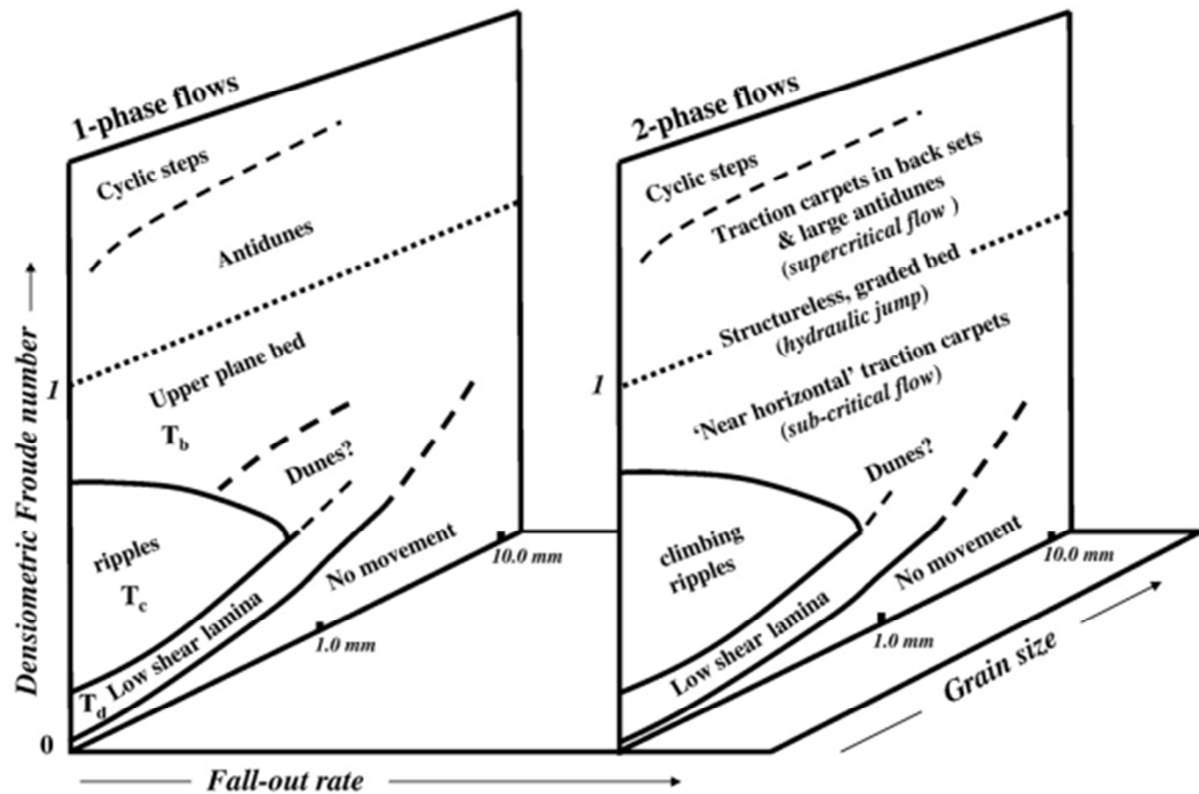


FIGURE 46: THREE-DIMENSIONAL BED FORM STABILITY DIAGRAM FROM POSTMA ET AL (2009). OF SPECIAL INTEREST IS THE POSITION OF THE STRUCTURELESS GRADED BED, AT THE HYDRAULIC JUMP LOCATION IN A 2-PHASE TURBIDITY CURRENT.

If the deposits of my experiments were to be placed within this diagram, they would all be placed near the subcritical, 1-phase flow part of the diagram (upper plane bed / T_b for all runs except 3, 4 and 5; low shear laminae for runs 3, 4 and 5). No traction carpet deposits, or structureless graded beds, characteristic for 2-phase flows, were observed.

The experiments did not produce flames or rip-up clasts as described in Postma et al. (2009). In fact, the only interaction with previous deposits was scouring.

Jopling and Richardson (1966) have conducted experiments with a stationary hydraulic jump setting (under air), investigating the resultant bedforms (see figure 47). They find backset bedding at the hydraulic jump location, and no deposition in the supercritical part of the flow.

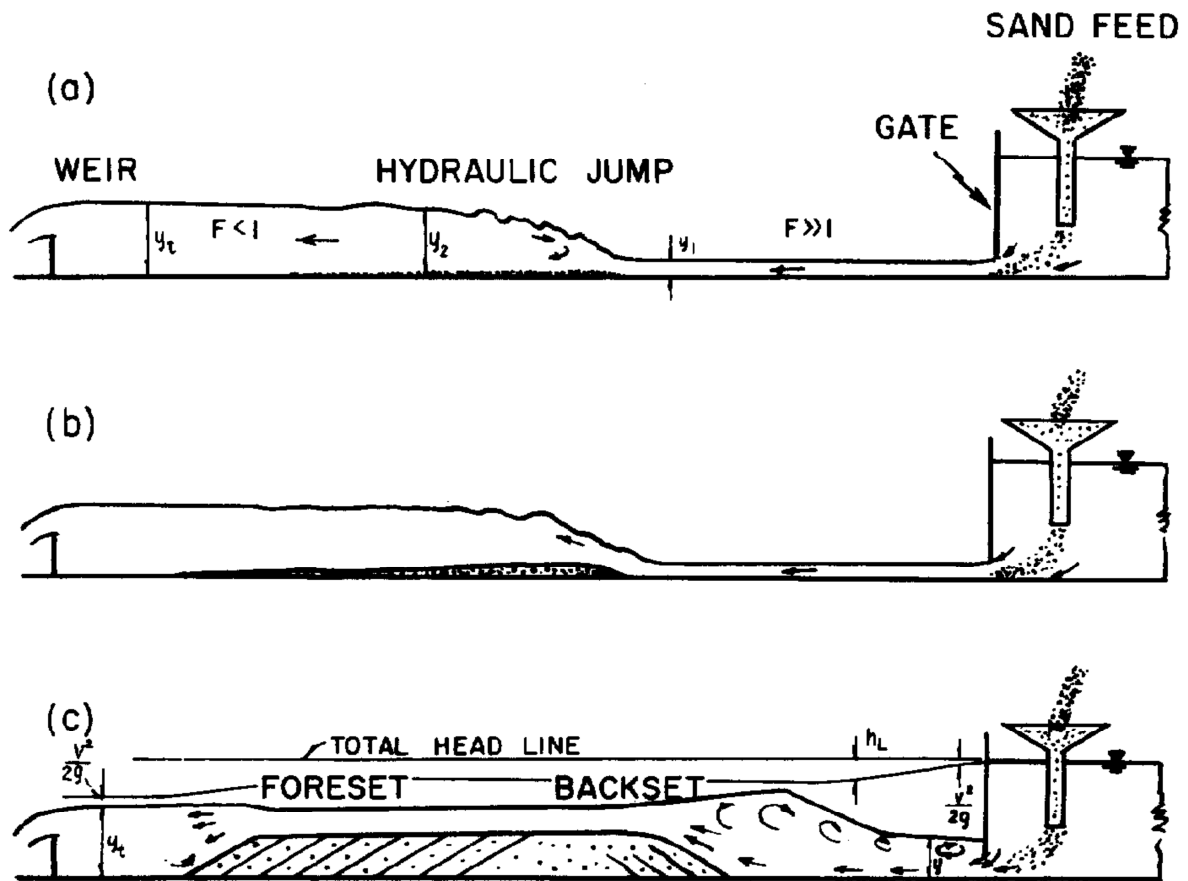


FIGURE 47: DEPOSITS IN EXPERIMENTS FROM JOPLING AND RICHARDSON (1966): BACKSET BEDDING AT THE HYDRAULIC JUMP LOCATION, AND NO DEPOSITION IN THE SUPERCRITICAL PART OF THE FLOW

In contrast to the backsets and foresets that are identified in that study, deposits created in my experiments were, at first, continuous laminae from hydraulic jump location to the weir. Later stages can scour into previous laminae, giving them the appearance of backsets (figure 48).

In my experiments the hydraulic jump migrates upstream and then maintains its own position. With a fairly constant input (concentration and discharge) an equilibrium position is maintained. The deposition of sediment in the subcritical part and the slope of the upstream side keeps the jump location fixed.

Parallel lamination occurs upstream, underneath and downstream of the hydraulic jump location, as a result of suspension fall-out in runs 3, 4 and 5 and as sheared deposition under the turbidity current in the other runs. Figure 48 shows the buildup of sediments and internal laminations in a fine + medium grained run from the test phase. At all locations, deposited loose beds experience some measure of shear as the effect of overriding flow. At low grain size + high concentrations this suspension fall-out experiences hindered settling (between the equilibrium jump location and the weir), also creating parallel (horizontal) lamination.

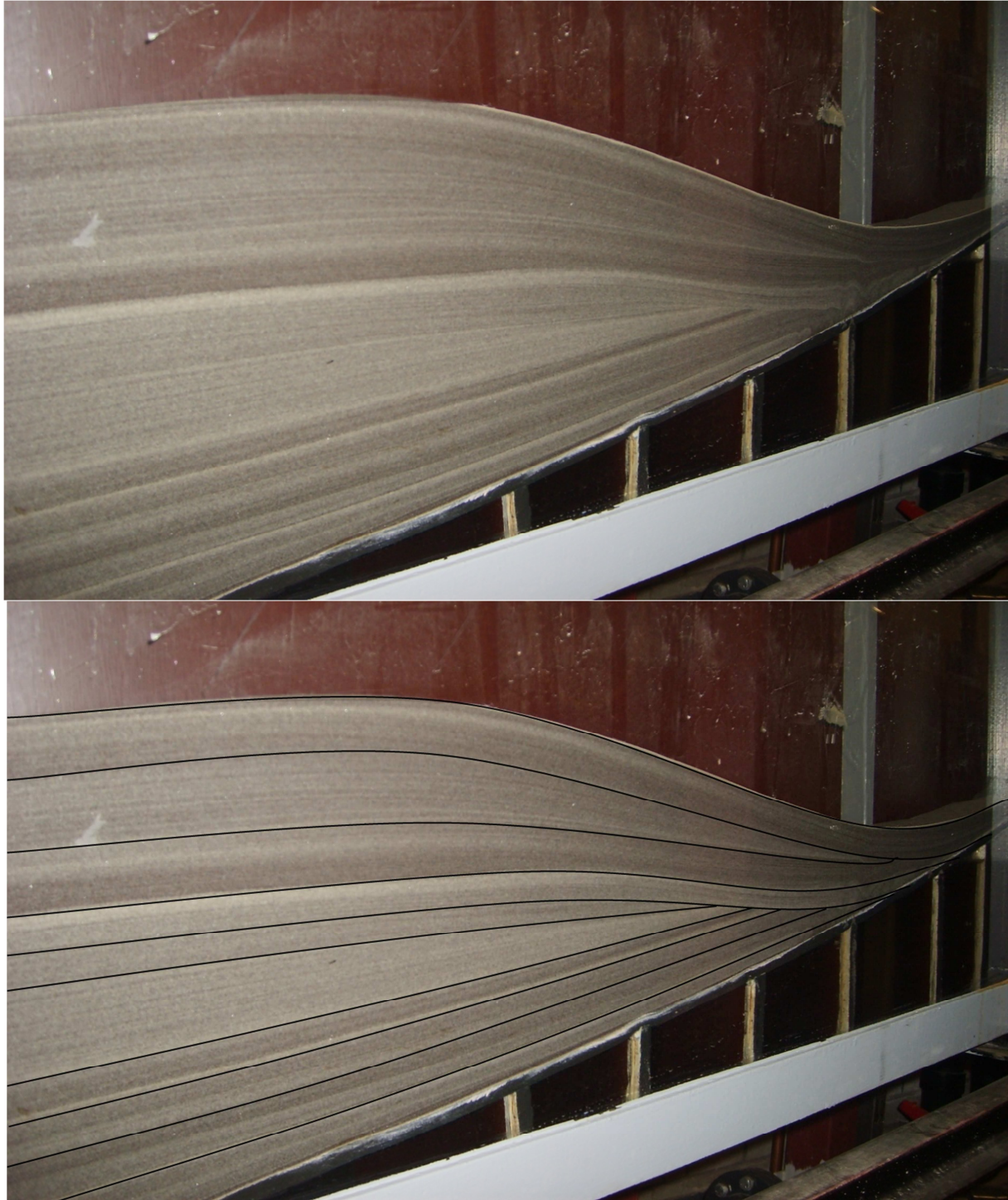


FIGURE 48: THIS PICTURE SHOWS THE EVOLVING SHAPE OF DEPOSITS. IT CONSISTS OF PARALLEL LAMINATED LAYERS, SCOURING INTO PREVIOUS LAYERS AS THE SHAPE OF THE BED BUILDS UP.

GRAIN FABRIC

Kostic & Parker (2004) have done numerical modeling to investigate the hydraulic jump and its influence on how and where sediments were deposited. They hypothesized that the fast decline in bed shear stress which results from the jump would leave a clear signature in the deposited sediments. This is similar to the results of the experiments of Garcia (1993) where a reduction in shear stress was observed immediately after the jump.

Figure 10 shows the flow patterns within a hydraulic jump. The downward flux of sediment creates a bottom layer with movements upstream at the upstream end of the jump and movement downstream at the downstream end of the jump. The upstream migration of the jump makes that the last movement of a grain is in a downstream direction. Shear is present here between the bed grains and the downstream flowing grains. Therefore, with upstream migrating jumps, the grains are assumed to show an imbrication dipping upstream along backset laminae. Grain movement mechanism is either in suspension or bed load transport, so long axes of deposited grains are expected to be perpendicular to flow direction due to the rolling movement of grains.

Unfortunately, the high water content of the deposits and their high sensitivity to liquefaction did not allow sampling of the grain orientations. After the experiment was done, any movement or slight vibration made the internal structure of the deposits collapse, releasing the excess water. It is expected that this mechanism can create dewatering structures in situations where multiple hydraulic jumps occur, especially in fine to very fine sand. The vibrations caused by a hydraulic jump may then dewater the underlying deposits.

Postma et al. (2009) concluded that turbidity currents that formed a traction carpet before the hydraulic jump produce a structureless bed at the hydraulic jump in combination with flame structures and rip-up clasts characteristic for Bouma Ta. The experiments in this thesis-research did not produce structureless beds; all deposits showed laminations (Tb or Td). This was the case for deposits with and without the occurrence of a hydraulic jump and for high and low concentration flows.

The formation mechanism of a structureless bed as proposed by Postma et al (2009), a hydraulic jump rapidly moving upstream, was observed in the high concentration runs, but there was no reworking of the underlying bed, only aggradation as a result of new sedimentation. There is however a location within the hydraulic jump (nr 4 in figure 10) where sediment can be deposited at almost no shear.

A rapid movement of the hydraulic jump (and the no-shear deposition location) did not form a structureless sand bed in my experiments. It produced other laminae. One could argue that if local deposition rate is much higher than the lateral movement a structureless sand bed will form at this location. Observation of the local flow directions within a hydraulic jump show that when the jump passes

LIMITATION OF THE EXPERIMENTS AND FURTHER RESEARCH

The first and most profound difficulty was the inability to properly determine criticality of the flow. Froude numbers could not be adequately calculated using the measured flow velocity and sediment concentration data. Without Froude numbers it is not possible to positively identify flow dynamic structures as a hydraulic jump. I believe that a few changes in the experimental setup would significantly improve results. In a best-case scenario, the experimental setup would facilitate non-disturbing through-flow high-resolution (in time and space) velocity and concentration measurement.

This study gives a limited insight into the hydraulic jump flow dynamics and its depositional signature. However, it is important to realize that the 2-dimensional characteristics of the flume may have influenced deposition and created artifacts in the results. For instance the high-angle slope created by the sediment bulge marking and fixing the location of the hydraulic jump is not expected to form with the same steepness in natural environments. The containment of the narrow flume may force the turbidity current to flow straight forward up a 'too steep slope', where in a natural environment it may diverge its path to a different flow direction.

Another limitation of these experiments is scale. Most of the experiments just deposited horizontal lamination. If these experiments can be performed on a larger scale, it is expected that many more features can be studied. A large turbidity current will for instance have a larger shear stress to exert on previous deposits. The hydraulic jump on a larger scale is expected to be more energetic and capable of more interaction with previous beds, lifting up and ripping up parts at the location of upward flow. A longer flow will allow for more time for flow transformation into a 2-phase flow.

Observation of the experiment imagery could not confirm whether the backflow that was produced in most runs was created by the limited height of the flume (thus being an artifact of the experimental setup), or that this was in fact a true phenomenon with this type of flow blocking.

CHALLENGES WITH CONCENTRATION AND CONCENTRATION MEASUREMENT

As can be seen in the appendices of the data logger results, the concentration of the sediment-water mix decreased in all experiments during the run. This is caused by the experimental design. The small constant head tank is filled with sediment and water from the supply tank. The overflow of this constant head tank is located on the top, so a mixture with a relatively low concentration flows back in the supply tank. Over time this can create a high density mixture in the constant head tank. However, as soon as the run starts, this high concentration mixture is used for the turbidity current, and the lower concentration mix from the supply tank is added, gradually decreasing the concentration. To improve this situation and allow for stable concentration runs, it is suggested that the constant head tank is a large reservoir containing all the sediment-water mix needed for the experiment. Large mixers are needed to keep the sediment in this large reservoir fully suspended.

The concentration meters that were used function by measuring the conductivity of the water/sediment mixture. The sensors had to be calibrated so that an output value of 0 volts corresponds with a concentration of 0% and an output of 10 volts with the concentration of the bed (set to 100%). By doing so, the sensor is calibrated for external factors which influence conductivity but are not of importance for the concentration determination. Two of these factors are the temperature difference between water masses in the experimental setup and the concentration of conductive particles in the water.

CONCENTRATION MEASUREMENT – TEMPERATURE BIAS

The temperature is not always the same at all places in the experimental setup. Water in the flume and water added to the supply tank had different sources, and therefore different temperatures. The sand in the supply tank had the temperature of the Eurotank lab, water in the flume had a lower temperature because of its underground source (outside of the Eurotank lab). Expected sources of added temperature are the mixture pump and the mixer in the constant head mixing tank.

CONCENTRATION MEASUREMENT – CONDUCTIVITY INFLUENCING PARTICLES

Within the sand different particles can be present that make the water more conductive. Positive and negative ions present in the fine fraction of the sand influence the measurement in a non-constant manner. To test this, a subset of experiments was done in which sensors were calibrated in a small reservoir with a sand bed. After stirring the sand, the water in the reservoir was more conductive and the calibration was no longer valid. It is expected that the stirring of the sand bed releases charged ions which make the water more conductive. The dredging head in the supply tank violently stirs the sand, so conductivity of the water in the supply tank was influenced by that.

CONCENTRATION MEASUREMENT - ZERO MEASUREMENT

To account for the differences in temperature and concentration of conductive particles within experiments a zero measurement was added to the experimental setup. To do this zero measurement, three parts were added to the experimental setup: a hose pump, a centrifugal machine and a second CCM concentration sensor (see figure 6). The hose pump takes a small sample from the constant head mixing tank which goes through the centrifugal machine. After this step, the water sample can be measured to provide the zero measurement. It was found that the two water masses in which the two CCMs were placed had to be connected electrically to obtain correct results.

CONCLUSIONS

WHAT ARE THE EFFECTS OF GRAIN SIZE AND VARIOUS SEDIMENT CONCENTRATIONS ON FLOW DYNAMICS, HYDRAULIC JUMP CHARACTERISTICS AND SEDIMENT DEPOSITION?

FLOW DYNAMICS

Results seem to suggest the occurrence of 1-phase flows and 2-phase flows. This is influenced by the input concentration of the turbidity current. The segregation of high density turbidity currents into two different layers creates a difference in concentration and flow velocity. The bottom layer has a higher sediment concentration and density. This concentration/density profile was not measured in these experiments. In these experiments, the bottom layer travels faster than the top layer down slope. It is left inconclusive whether this lower layer was a supercritical traction carpet which went through the hydraulic jump.

HYDRAULIC JUMP CHARACTERISTICS

The calculated overall Fr' numbers that are displayed in the results section indicate subcritical flow in all the experiments. Observation of the flow dynamics indicate a hydraulic jump occurring (and therefore supercritical flow) in the fine and medium sand runs of high concentration. The overall Froude number is therefore not considered adequate to assess the occurrence of a hydraulic jump in this case. Calculation of partial Fr' numbers for the bottom layer seem to support the observation of the occurrence of hydraulic jumps. However, large uncertainties in the measurements leave inconclusive whether flows were supercritical and if in fact a hydraulic jump occurred.

SEDIMENT DEPOSITION

Horizontal laminations were present in all the deposits, with and without the supposed hydraulic jump. In the fine grained high concentration runs this laminations were produced mainly by suspension fallout (downstream of the jump), so these deposits should be interpreted as Bouma's Td. The other runs show deposition under the shearing flow. These deposits should be interpreted as Bouma's Tb.

Underneath the hydraulic jump there is a location where sediment is deposited at almost no shear and direction. This would be a viable location for the formation of structureless graded sands. These were however not observed in my experiments. The upstream movement of the hydraulic jump created another lamina. It is possible that on a larger scale this 'lamina' is in fact a structureless sand bed. However the amount of sediment deposited in my experiment could not conclude whether this is the case.

The buildup of a sediment bulge at the end of slope (underneath the hydraulic jump but also in 'non-jump' runs) causes scouring into previous layers. The inclined laminations may be interpreted as backsets.

Postma et al. (2009) concluded that turbidity currents that formed a traction carpet before the hydraulic jump produce a structureless bed at the hydraulic jump location in combination with flame structures and rip-up clasts characteristic for Bouma Ta. The experiments in this thesis-research did not produce structureless beds; all deposits showed laminations, giving it the characteristics of Bouma's Tb or even Td in the fine grained runs. This was the case for deposits with and without the (supposed) occurrence of a hydraulic jump and for high and low concentration flows.

This thesis-research can neither prove nor disprove their statement, since I am unsure whether the 2-phase flows in fact contained traction carpets and whether flow states were supercritical or not.

REFERENCES

- Allen, J. R. L.**, 1984, *Sedimentary Structures – Their character and physical basis*; Elsevier, Amsterdam, 593 p.
- Arnott, R. W. C. and Hand, B. M.**, 1989, Bed forms, primary structures and grain fabric in the presence of suspended sediment rain; *Journal of Sedimentary Petrology*, v. 59, p. 1062-1069.
- Baas, J. H.**, 2004, Conditions for formation of massive turbidite sandstones by primary depositional processes; *Sedimentary Geology* 166, 293-310.
- Bagnold, R.A.**, 1954, Experiments on a gravity-free dispersion of large solid spheres in a Newtonian fluid under shear; *Proceedings of the Royal Society of London, Series A*, v. 225, p. 49-63.
- Bagnold, R.A.**, 1956, The flow of cohesionless grains in fluids; *Philosophical Transactions of the Royal Society, Series A*, v. 249, p. 235-297.
- Bouma, A. H.**, 1962, *Sedimentology of some flysch deposits: a graphic approach to facies interpretation*; Elsevier, Amsterdam, 168 p.
- Chong, J. S., Christiansen, E. B. and Baer, A. D.**, 1971, Rheology of concentrated suspensions; *Journal of Applied Polymer Science*, v. 15, p. 2007-2021
- Collinson, J. D. and Thompson, D. B.**, 1982, *Sedimentary Structures*; Allen and Unwin, Boston, 194 p.
- Fisher, R. V.**, 1983, Flow transformations in sediment gravity flows; *Geology*, v. 11, p. 273-274.
- Frankel, N.A., Acrivos, A.**, 1967, On the viscosity of a concentrated suspension of solid spheres; *Chemical Engineering Science*, v. 22, p 847-853.
- Garcia, M. H.**, 1993, Hydraulic jumps in sediment-driven bottom currents; *Journal of Hydraulic Engineering*, v. 119, p. 1094-1117.
- Garcia, M. H. and Parker, G.**, 1989, Experiments on hydraulic jumps in turbidity currents near a canyon-fan transition; *Science*, v. 245, p. 393-396.
- Garcia, M. H. and Parker, G.**, 1991, Entrainment of bed into suspension; *Journal of Hydraulic Engineering*, v. 117(4), p. 414-435.
- Hand, B. M.**, 1969, Antidunes as trochoidal waves; *Journal of Sedimentary Petrology*, v. 39, p. 1302-1309.
- Hand, B. M.**, 1974, Supercritical flow in density currents; *Journal of Sedimentary Petrology*, v. 44, p. 637-648.
- Harms, J. C. and Fahnestock, R. K.**, 1965, Stratification, bedforms, and flow phenomena (with an example from the Rio Grande), in Middleton, G. V., (ed.) *Primary sedimentary structures and their hydrodynamic interpretation*; *SEPM Spec. Pub.* 12, p. 84-115.
- Hiscott, R. N. and Middleton, G. V.**, 1980, Fabric of coarse deepwater sandstones, Tourelle Formation, Quebec, Canada; *Journal of Sedimentary Petrology*, v. 50, p. 703-722.
- Komar, P. D.**, 1971, Hydraulic jumps in turbidity currents; *GSA Bulletin*, v. 82, p. 1477-1488.

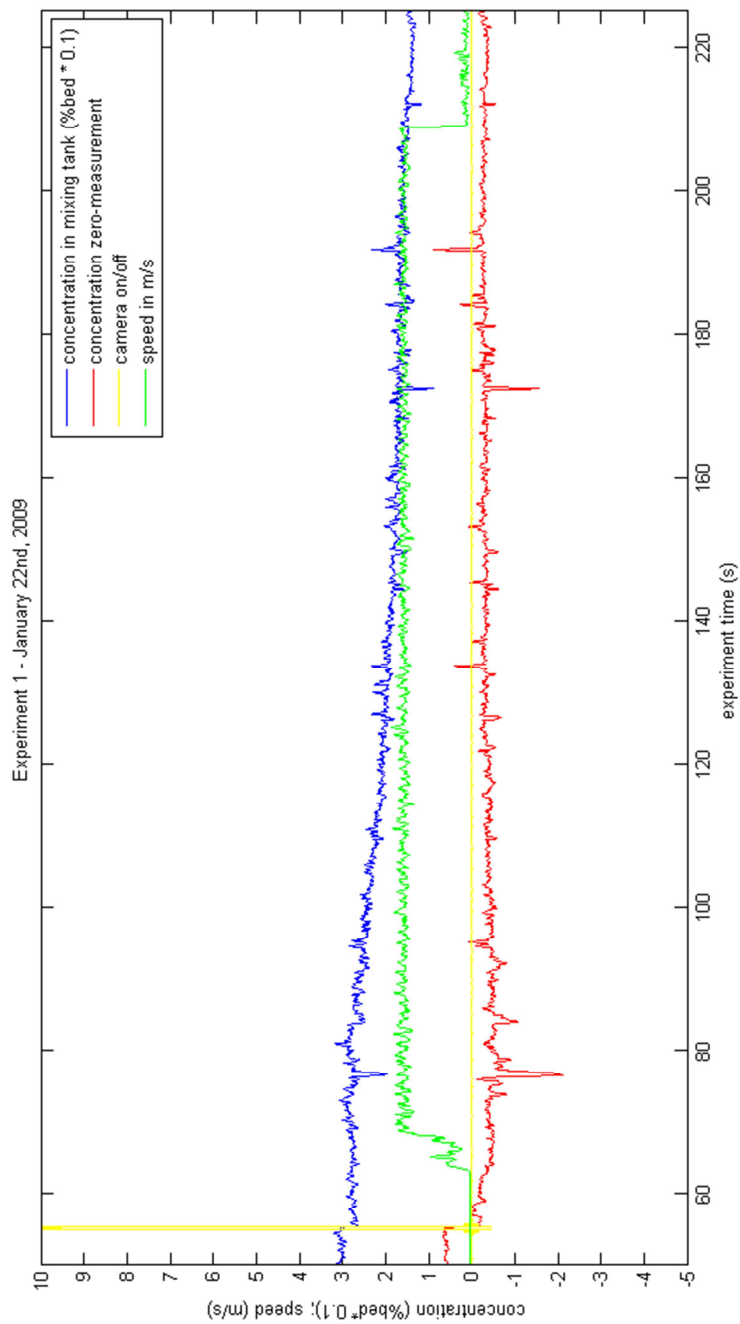
- Komar, P. D.**, 1985, The hydraulic interpretation of turbidites from their grain sizes and sedimentary structures; *Sedimentology*, v. 32, p. 395-407.
- Kostic, S. and Parker, G.**, 2004, Can an internal hydraulic jump be inferred from the depositional record of the turbidity current?; *Proceedings, RiverFlow 2004 International Conference on Fluvial Hydraulics, Napoli, Italy, June 23-25*, 9 p.
- Kuenen, P.H., Faure-Muret, A., Lanteaume, M., Fallot, P.**, 1957, Observations sur les flyschs des Alpes-Maritimes françaises et italiennes; *Bulletin Société Géologique de France*, v. 7, p. 4-26.
- Krieger, I.M. and Dougherty, T.J.**, 1959, Concentration dependence of the viscosity of suspensions. v. 3, p. 137-152.
- LeClair, S. and Arnott, R. W. C.**, 2005, Parallel lamination formed by high-density turbidity currents; *Journal of Sedimentary Research*, v. 75, p. 1-5.
- Lowe, D. R.**, 1976, Grain flow and grain flow deposits; *Journal of Sedimentary Petrology*, v. 46, p. 188-199.
- Lowe, D. R.**, 1982, Sediment gravity flows: II. Depositional models with special reference to the deposits of high-density turbidity currents; *Journal of Sedimentary Petrology*, v. 52, p. 279-297.
- Lowe, D.R.**, 1988, Suspended-load fallout rate as an independent variable in the analysis of current structures; *Sedimentology*, v. 35, p. 765-776.
- Middleton, G. V.**, 1965, Antidune cross-bedding in a large flume; *Journal of Sedimentary Petrology*, v. 35, p. 922-927.
- Middleton, G. V.**, 1967, Experiments on density and turbidity currents. III. Deposition of sediment; *Canadian Journal of Earth Sciences*, v. 3, p. 627-637.
- Middleton, G. V.**, 1970, Experimental studies related to problems of flysch sedimentation; *Geological Society of Canada Special Paper 7*, p. 253-272.
- Middleton, G. V.**, 1993, Sediment deposition from turbidity currents; *Annual Review of Earth and Planetary Sciences*; v. 21, p. 89-114.
- Mullins, H. T. and van Buren, H. M.**, 1979, Modern modified carbonate grain flow deposits; *Journal of Sedimentary Petrology*, v. 49, p. 747-752.
- Postma, G., Nemec, W., Kleinspehn, K.L.**, 1988, Large floating clasts in turbidites – a mechanism for their emplacement; *Sedimentary Geology*, v. 58 (1), p. 47-61.
- Postma, G., Cartigny, M. J. B., Kleverlaan, K.**, 2009, Structureless, coarse-tail graded Bouma Ta formed by internal hydraulic jump of the turbidity current?; *Sedimentary Geology*, v. 219 (1-4), p. 1-6.
- Sohn, Y. K.**, 1997, On traction carpet sedimentation; *Journal of sedimentary research*, v. 67, p. 502-509.
- Stauffer, P. H.**, 1967, Grain-flow deposits and their implications, Santa Ynez Mountains, California; *Journal of Sedimentary Petrology*, v. 37, p. 487-508.
- Sumner, E. J., Lawrence, A. A., Talling, P. J.**, 2008, Deposit structure and processes of sand deposition from decelerating sediment suspensions; *Journal of Sedimentary Research*, v. 78, p. 539-547.

Völtz, C., Schröter, M., Iori, G., Betat, A., Lange, A., Engel, A. and Rehberg, I., 2000, Finger-like patterns in sedimenting water–sand suspensions; Physics Reports, v. 337, p. 117-138.

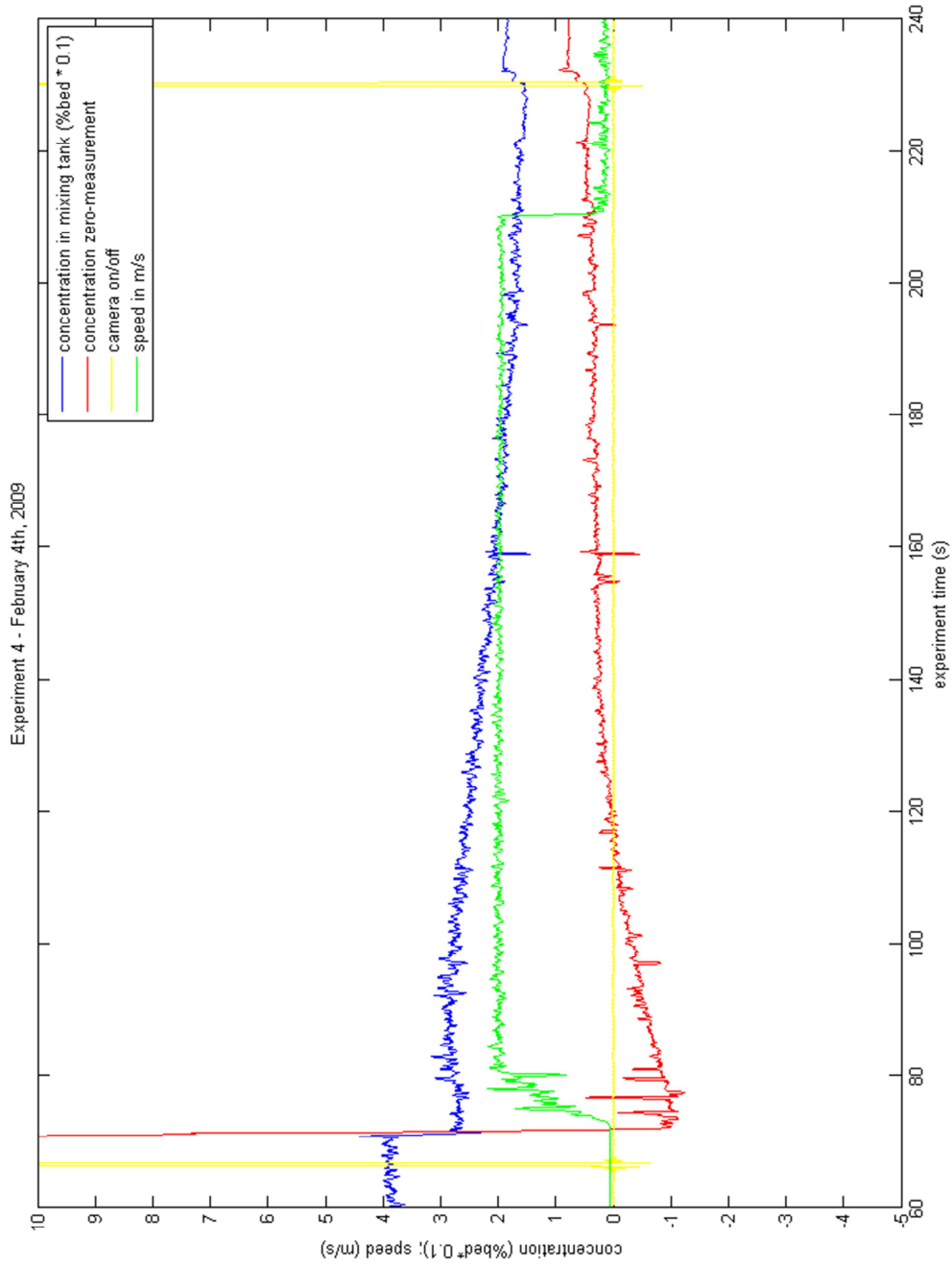
Walker, R. G., 1967, Turbidite sedimentary structures and their relationship to proximal and distal environments; Journal of Sedimentary Petrology, v. 37, p. 25-43

APPENDICES

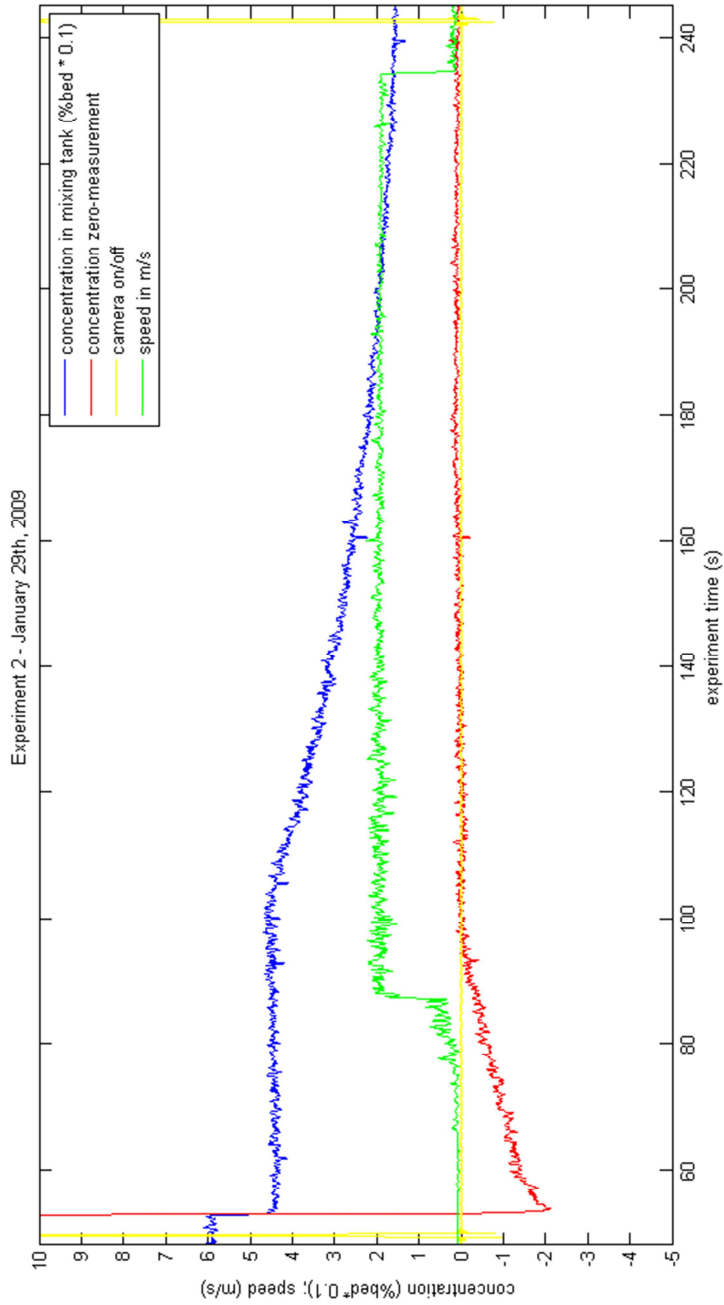
APPENDIX A1: RUN 1, EXP1_: MEASURED DATA



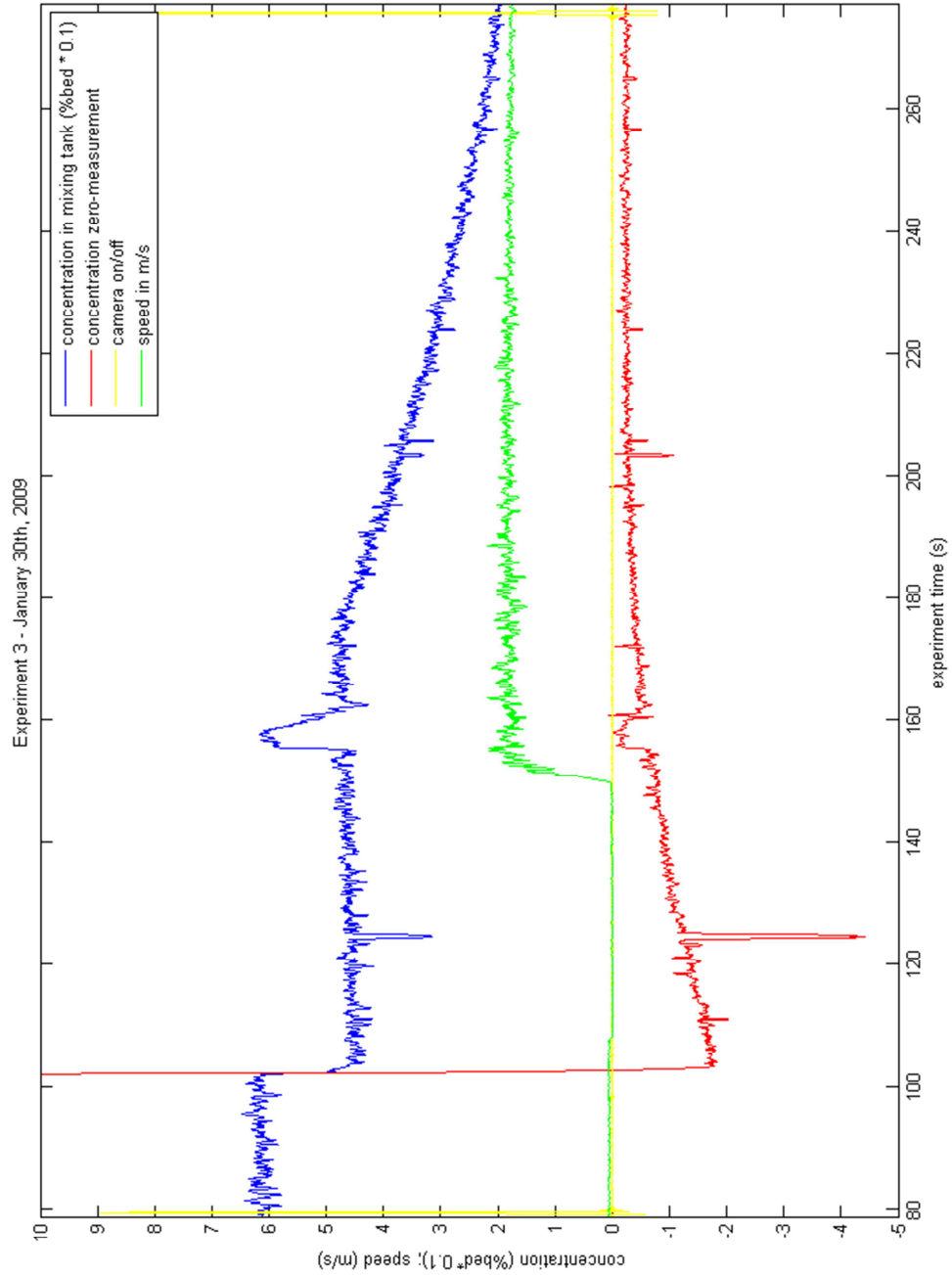
APPENDIX A2: RUN 2, EXP4: MEASURED DATA



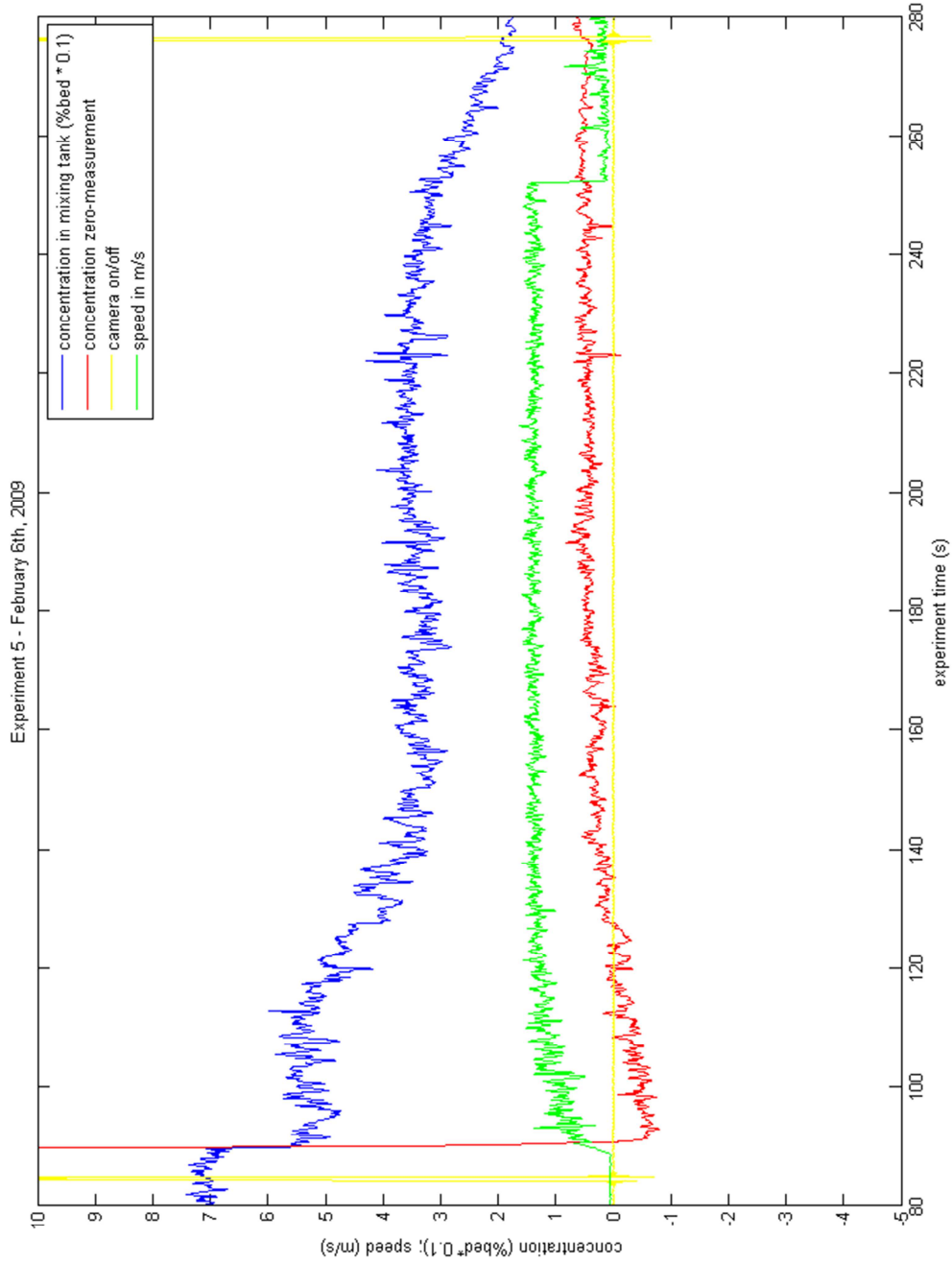
APPENDIX A3: RUN 3, EXP2_: MEASURED DATA



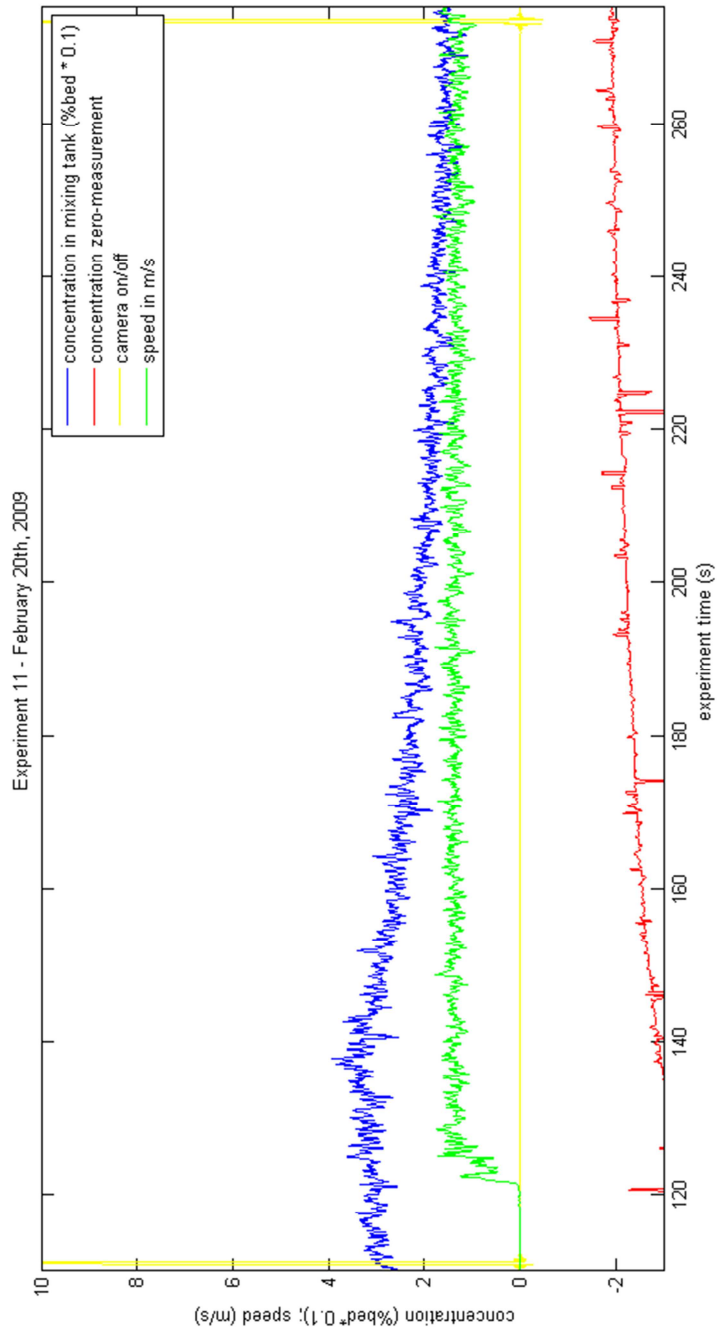
APPENDIX A4: RUN 4, EXP3: MEASURED DATA



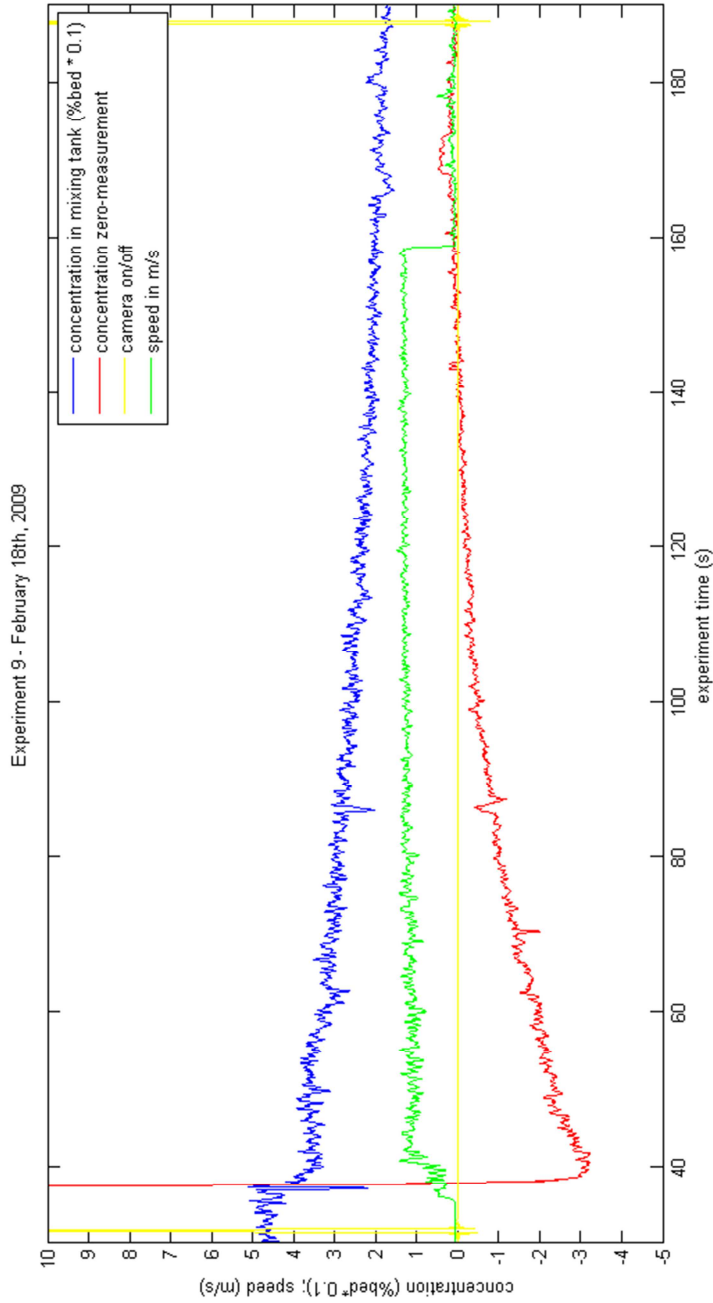
APPENDIX A5: RUN 5, EXP5: MEASURED DATA



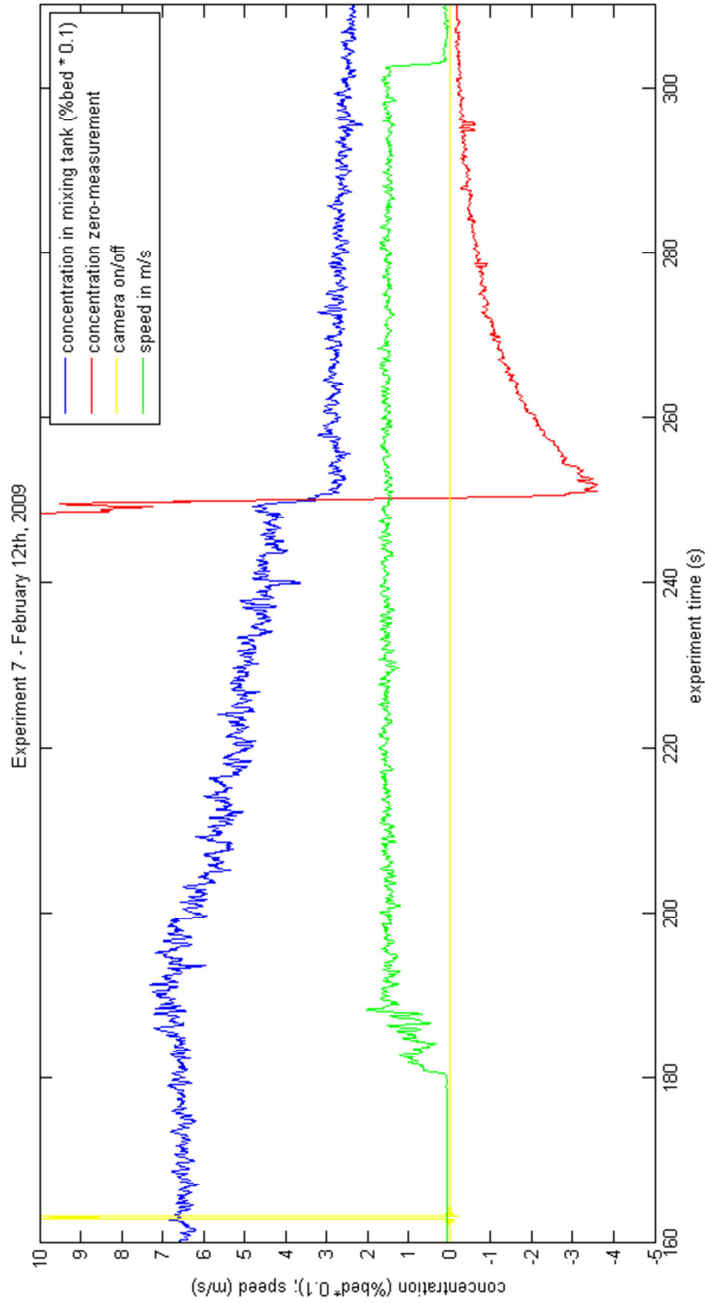
APPENDIX A6: RUN 6, EXP11: MEASURED DATA



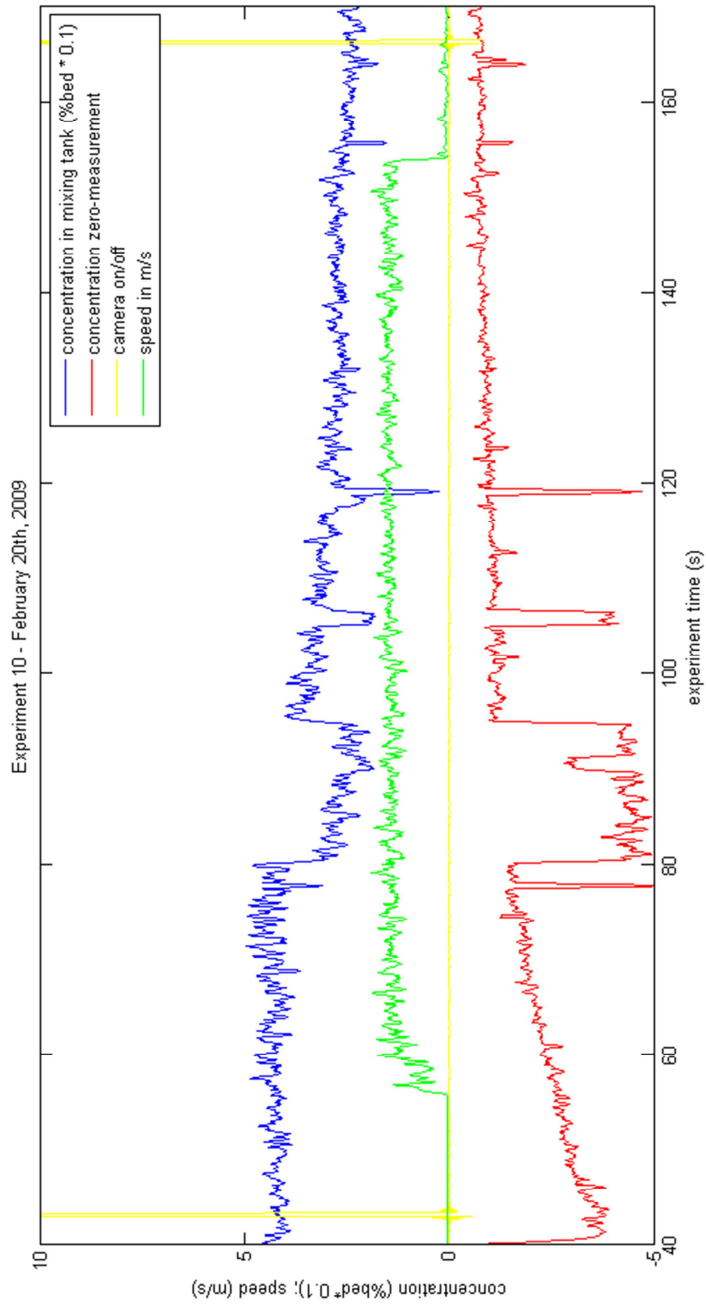
APPENDIX A7: RUN 7, EXP9_: MEASURED DATA



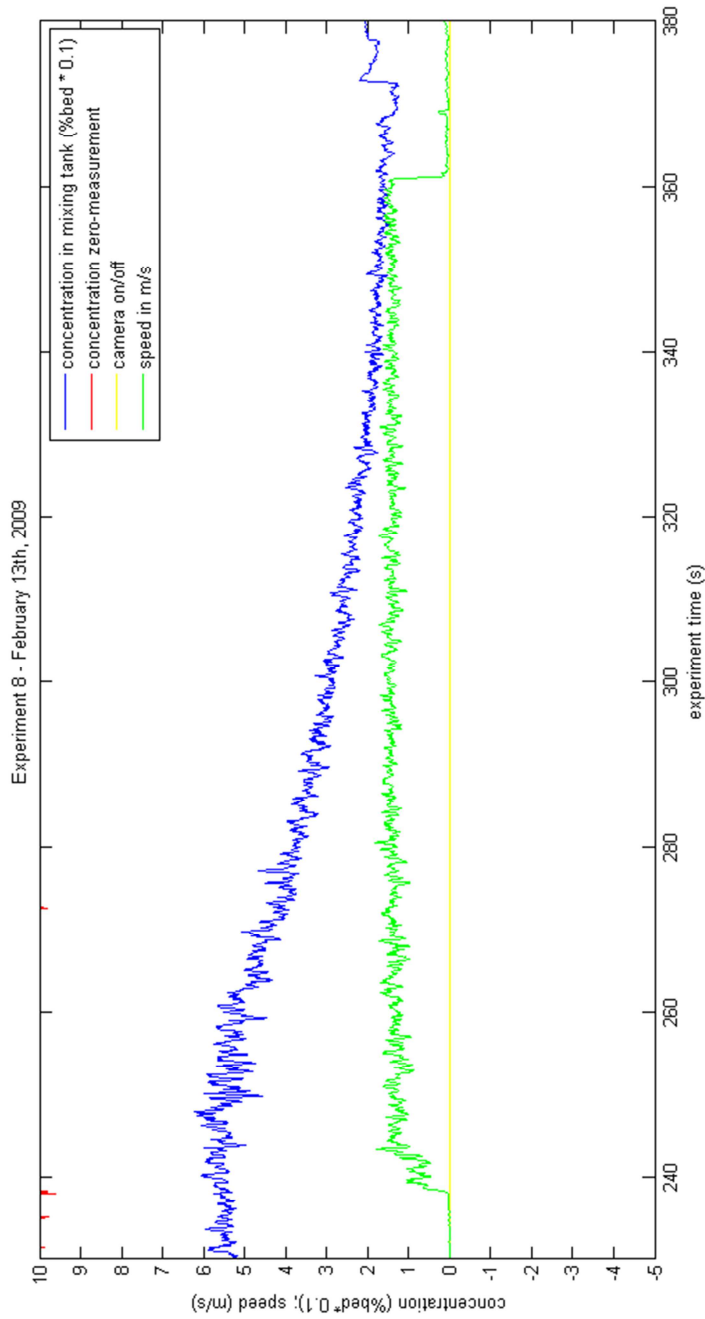
APPENDIX A8: RUN 8, EXP7: MEASURED DATA



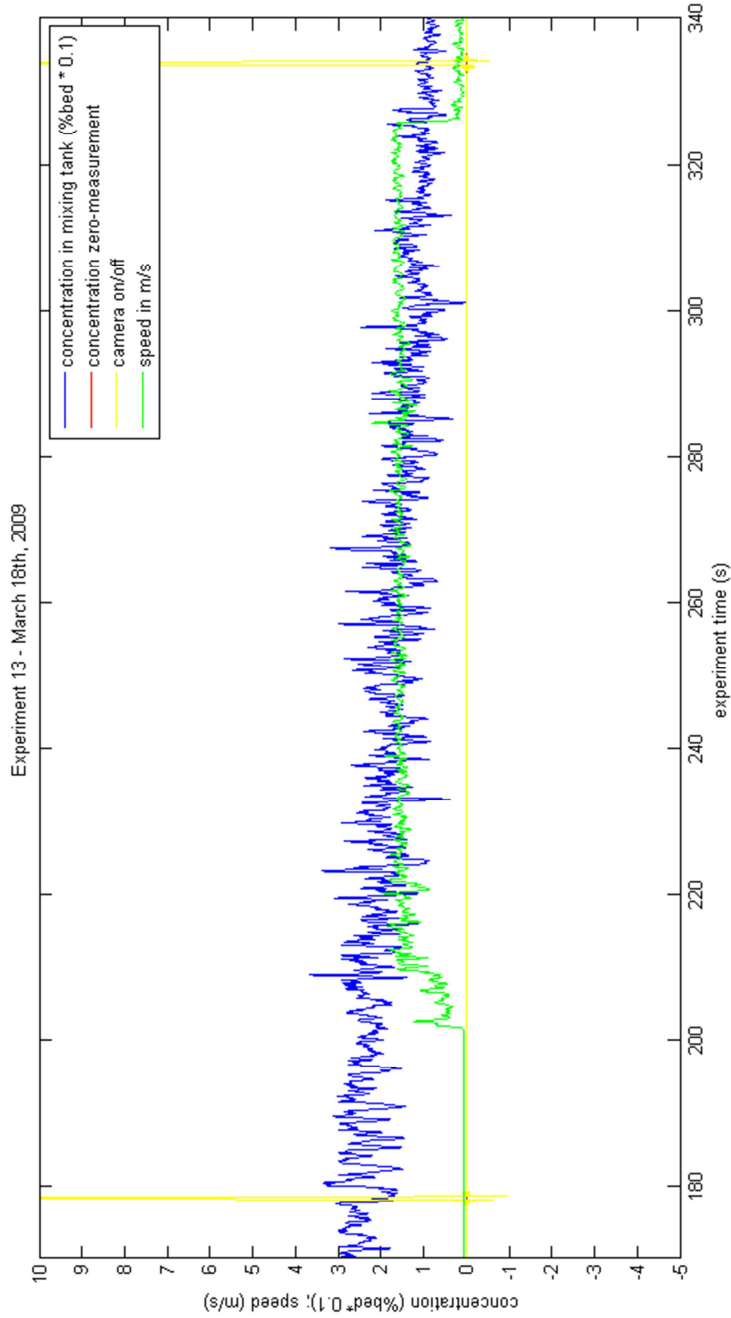
APPENDIX A9: RUN 9, EXP10: MEASURED DATA



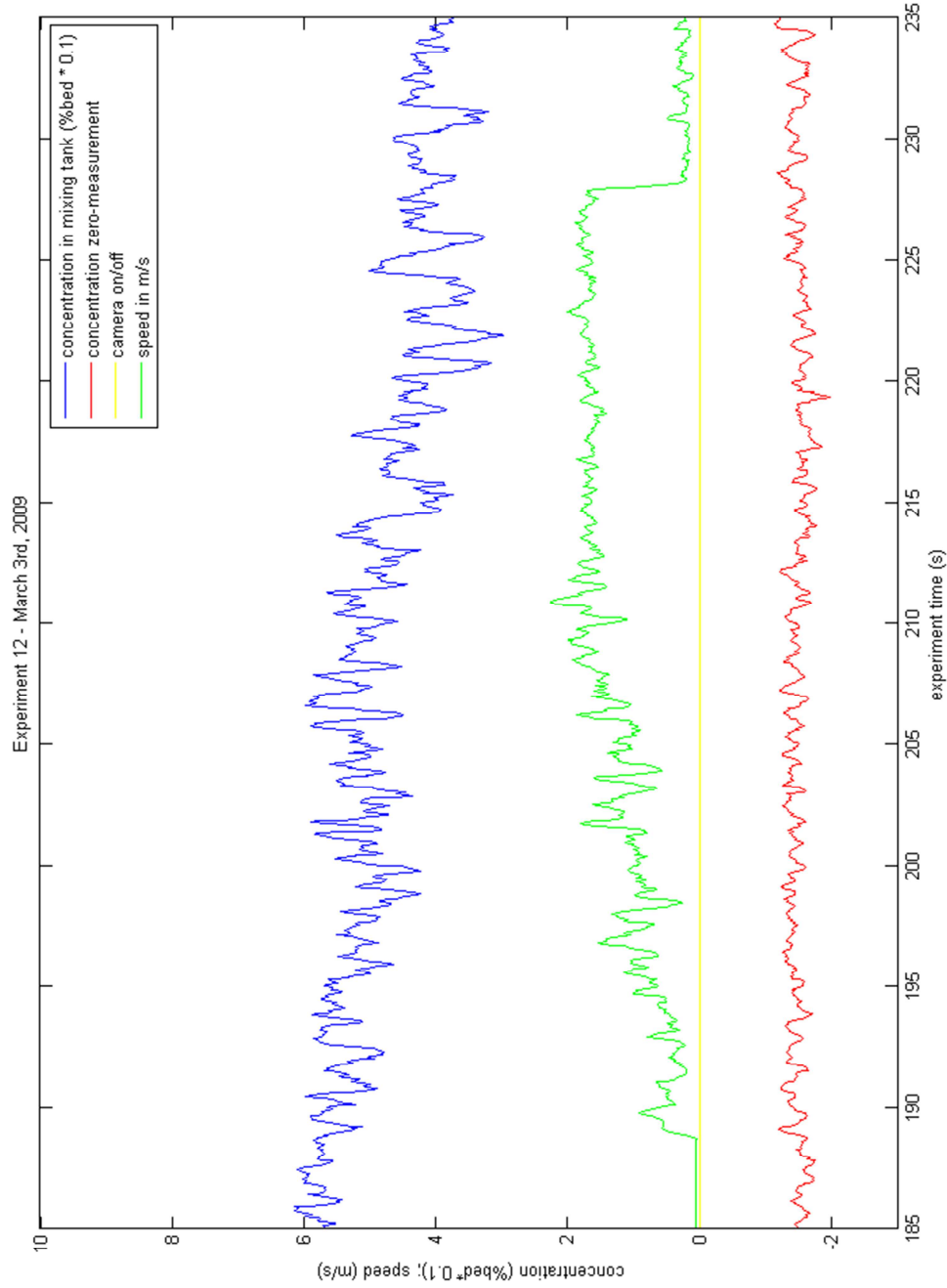
APPENDIX A10: RUN 10, EXP8: MEASURED DATA



APPENDIX A11: RUN 11, EXP13: MEASURED DATA



APPENDIX A12: RUN12, EXP12: MEASURED DATA



APPENDIX B: MATLAB SCRIPT FOR DATA RETRIEVAL AND PRESENTATION

```
clear all

% BHE = nulmeting 26
% BHN = mixtankmeting 24
% BHZ = voetpedaal camera
% WDI = output 1 EMS
% WKI = output 2 EMS

filename1='exp13';
filename2='2009.077.162838';

BHEdata=strcat(filename1,'.NR.BHE.',filename2,'.n.a');
BHNdata=strcat(filename1,'.NR.BHN.',filename2,'.n.a');
BHZdata=strcat(filename1,'.NR.BHZ.',filename2,'.n.a');
WDIdata=strcat(filename1,'.NR.WDI.',filename2,'.n.a');
WKIdata=strcat(filename1,'.NR.WKI.',filename2,'.n.a');

BHE = importdata(BHEdata);
BHN = importdata(BHNdata);
BHZ = importdata(BHZdata);
WDI = importdata(WDIdata);
WKI = importdata(WKIdata);

a=size(BHE);

for i = 1:a;
    sec(i)= i/20;
end;

BHEvolt=BHE * 0.00002341;
windowSize = 6;
BHEsmooth=filter(ones(1,windowSize)/windowSize,1,BHEvolt);

BHNvolt=BHN * 0.00002341;
windowSize = 6;
BHNsmooth=filter(ones(1,windowSize)/windowSize,1,BHNvolt);

BHZvolt=BHZ * 0.00002341;

speed=(sqrt((WDI.^2)+(WKI.^2)));
speedvolt=speed * 0.00002341;
speedms=speedvolt*0.25;
windowSize = 6;
speedmssmooth=filter(ones(1,windowSize)/windowSize,1,speedms);

plot(sec,BHNsmooth,'b')
hold on
plot(sec,BHEsmooth,'r')
plot(sec,BHZvolt,'y')
plot(sec,speedmssmooth,'g')
legend('concentration in mixing tank (%bed * 0.1)', 'concentration zero-measurement', 'camera on/off', 'speed in m/s')
xlim([50 225])
ylim([-5 10])
set(gca,'yTick',[-5 -4 -3 -2 -1 0 1 2 3 4 5 6 7 8 9 10])
xlabel('experiment time (s)')
ylabel('concentration (%bed* 0.1); speed (m/s)')
title('Experiment 13 - March 18th, 2009')
hold off
```